Molecular Therapy
Original Article

A Synthetic Mammalian Therapeutic Gene Circuit for Sensing and Suppressing Inflammation

Anže Smole,[1] Duško Lainšček,[1] Urban Bezeljak,[1,2,5] Simon Horvat,[1,3,4] and Roman Jerala[1,3]

[1]Department of Synthetic Biology and Immunology, National Institute of Chemistry, Hajdrihova 19, 1000 Ljubljana, Slovenia; [2]Faculty of Chemistry and Chemical Technology, University of Ljubljana, 1000 Ljubljana, Slovenia; [3]EN-FIST Centre of Excellence, 1000 Ljubljana, Slovenia; [4]Biotechnical Faculty, University of Ljubljana, 1000 Ljubljana, Slovenia

Inflammation, which is a highly regulated host response against danger signals, may be harmful if it is excessive and deregulated. Ideally, anti-inflammatory therapy should autonomously commence as soon as possible after the onset of inflammation, should be controllable by a physician, and should not systemically block beneficial immune response in the long term. We describe a genetically encoded anti-inflammatory mammalian cell device based on a modular engineered genetic circuit comprising a sensor, an amplifier, a "thresholder" to restrict activation of a positive-feedback loop, a combination of advanced clinically used biopharmaceutical proteins, and orthogonal regulatory elements that linked modules into the functional device. This genetic circuit was autonomously activated by inflammatory signals, including endogenous cecal ligation and puncture (CLP)-induced inflammation in mice and serum from a systemic juvenile idiopathic arthritis (sIJA) patient, and could be reset externally by a chemical signal. The microencapsulated anti-inflammatory device significantly reduced the pathology in dextran sodium sulfate (DSS)-induced acute murine colitis, demonstrating a synthetic immunological approach for autonomous anti-inflammatory therapy.

INTRODUCTION

Inflammation is a complex widespread response of multi-cellular organisms that is activated by the innate immune system upon detection of danger signals emanating from pathogenic microorganisms or from a damaged tissue.[1] Inflammation is generally beneficial for the organism because it alerts the immune system to eliminate the underlying cause and to restore homeostasis. However, deregulated and excessive inflammation is harmful and may become chronic due to positive feedback mediated by inflammatory cytokines. The immune response is one of the most complex biological subsystems with regulation involving various receptors, mediators, complex feedback mechanisms, and different effector molecules, which orchestrate the appropriate fine-tuning of the response to danger.[2,3] The rapid production of pro-inflammatory cytokines, such as tumor necrosis factor alpha (TNF-α), interleukin 1 beta (IL-1β), IL-6, and several others, is characteristic of autoimmune diseases, including inflammatory bowel disease (IBD), rheumatoid arthritis (RA), systemic juvenile idiopathic arthritis (sJIA), multiple sclerosis, psoriasis, and lupus erythematosus, as well as of autoinflammatory diseases, such as cryopyrin-associated periodic syndrome.[4] The prevalence of inflammatory diseases associated with excessive and harmful inflammation is 5%–7%, even in societies with an advanced health care system.[5]

Non-steroidal anti-inflammatory drugs (NSAIDs) and corticosteroids are widely used and effective anti-inflammatory therapies, yet they can have adverse side effects. Currently, the most advanced clinically used therapies for inflammatory diseases are neutralizers of TNF-α (adalimumab, etanercept, and infliximab) and endogenous cytokine antagonists, such as anakinra (an IL-1β antagonist) that specifically and effectively inhibit the activity of pro-inflammatory cytokines.[4] As inflammation is an essential component of the host defense system, long-term systemic suppression can cause adverse side effects, such as a decreased host immune response against infections and an increased risk of cancer development.[4] Anti-inflammatory therapy that could match the responsiveness and tunability of the natural cellular response, but could be controlled externally, represents both a challenge and an opportunity for synthetic biology. The strategy according to the principles of synthetic biology is to construct biological systems that are orthogonal to the existing signaling components yet are able to read the inputs from the cellular processes or external signals and produce the physiologically relevant outputs. The modular construction of interacting components allows this type of systems to be adapted to the selected applications. Progress has already been made in this direction, such as engineering of the bacterium *Lactococcus lactis* to secrete IL-10[6] or anti-TNF-α nanobody,[7] which has been used in situ to locally treat murine colitis. *Escherichia coli* that autonomously detect gut inflammation through nitric oxide sensing has been reported,[8] suggesting the feasibility of more sophisticated inflammation management strategies.

Received 27 May 2016; accepted 21 October 2016;
http://dx.doi.org/10.1016/j.ymthe.2016.10.005.

[5]Present address: Institute of Science and Technology Austria, Am Campus 1, 3400 Klosterneuburg, Austria

Correspondence: Roman Jerala, Department of Synthetic Biology and Immunology, National Institute of Chemistry, Hajdrihova 19, 1000 Ljubljana, Slovenia.
E-mail: roman.jerala@ki.si

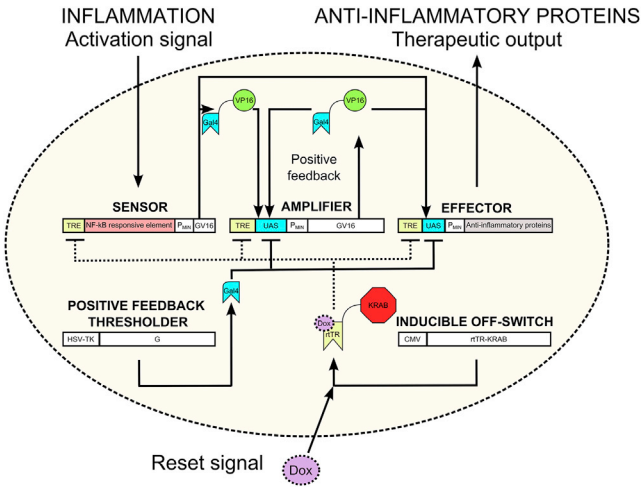

Figure 1. Schematic Design of the Synthetic Anti-inflammatory Device

The anti-inflammatory device comprises three basic modules (a sensor, an amplifier, and an effector), which are connected through the transcriptional activator Gal4-VP16 (GV16) and two supporting modules (an inducible OFF-switch and a thresholder). The latter allows additional control of the system performance.

Recently, synthetic biologists have demonstrated several innovative therapeutic strategies based on engineered mammalian cells designed to respond to a physiologically relevant signal in a highly predictable and controllable manner.[9] Using microencapsulation technology, such engineered cells could be implanted into a host.[10,11] These cells can act as prosthetic devices, which do not require any host genome modification. Of particular interest are sensor-effector designs that can autonomously detect and treat various pathological conditions, such as a malfunction in urate homeostasis,[12] diet-induced obesity,[13] and diabetic ketoacidosis.[14] Recently, an innovative designer cell device to treat experimental psoriasis by converting the disease-relevant inputs into the therapeutic output was presented.[15]

The therapeutic challenge in therapy of inflammatory diseases is to detect and suppress inflammatory flare-ups as soon as possible before they are amplified through positive-inflammatory-feedback loops and cause damage. Early intervention could clearly contribute to beneficial clinical outcomes in Crohn's disease[16,17] or sIJA.[18] As a safety and regulatory feature, implantable therapeutic cellular device aimed at treating inflammation should be amenable to external control and capability to rest into the standby state once the inflammation has been resolved. Additionally, autonomous activation of the device could also serve as a sensor of inflammation, reporting the previous inflammatory episode.

The inflammatory response is coordinated by highly complex regulatory networks, which consist of multiple, to some degree redundant inducers, sensors, mediators, and effectors.[1] In this study, we constructed a gene regulatory network that captured the required functionalities of a fine-tuned therapeutic device aimed to provide support to the organism to cope with the dysregulated inflammatory response. The introduced regulatory elements comprise several interacting functional modules that form a functional genetic circuit, which can be integrated into and modulate the existing inflammatory response. The prototypic synthetic anti-inflammatory device autonomously detected inflammatory signals at physiologically relevant concentrations and responded by sustainable production of a combination of clinically used anti-inflammatory proteins that suppressed inflammation, namely an anti-hTNF-α antibody in combination with IL-10 or interleukin-1 receptor antagonist (IL-1RA). The anti-inflammatory device was activated upon encounter of inflammatory signals, including endogenous mouse inflammation induced by cecal ligation and puncture (CLP) as well as by a serum sample from sJIA patient, and reset by an external chemical inducer. The genetic device, implemented by implantation of alginate-poly-L-lysine-alginate (alginate-PLL-alginate) microencapsulated engineered cells into the peritoneal cavity of mice, reduced the pathological symptoms in dextran sodium sulfate (DSS)-induced acute murine colitis, demonstrating a novel route of designed immunological intervention.

RESULTS

Design of the Functional Modules of the Synthetic Anti-inflammatory Gene Circuit

To design an efficient therapeutic anti-inflammatory device, we aimed to combine the following characteristics: (1) real-time monitoring of physiologically relevant markers of inflammation; (2) an ability to switch to a therapeutically active (ON) state in response to physiologically relevant concentrations of an inflammatory marker; (3) efficient suppression of inflammation via sustained production of anti-inflammatory effectors triggered by the activation of the device; (4) control mechanism for preventing pre-mature inactivation of the device by the neutralization of inflammation markers by effectors in the immediate vicinity of the therapeutic cells; (5) and an ability to reset the device to the standby state by external signal (e.g., small-molecule inducer) that could potentially also be used in clinical applications applied by a physician.

To detect and respond to an inflammatory signal, we developed a biomolecular circuit, which comprises three basic modules: a sensor, an amplifier, and an effector (Figure 1). These modules were interconnected via the well-characterized transcriptional activator Gal4-VP16 (GV16),[19] which is orthogonal to mammalian intracellular signaling and transcriptional pathways. To demonstrate the concept of an anti-inflammatory device that could be used in patients with inflammatory diseases, we aimed to develop a system that could sense a common signal of inflammation. As a large fraction of signals from the danger-sensing receptors of the innate and adaptive immune system converge on the activation of the NF-κB transcription factor,[20] the NF-κB-responsive sensor was chosen to monitor the inflammatory status of tissue as reported by cellular receptors. To build and validate the sensor, two different NF-κB-responsive elements were first examined. We utilized a validated combination of the κB DNA elements,[21] which are specifically recognized by the NF-κB transcription factor, and used the luciferase reporter activity as a readout. Constructs pAS36 ($P_{NF-\kappa B1}$-P_{TAL}-Luc, Table S1) and pAS37 ($P_{NF-\kappa B2}$-P_{TAL}-Luc, Table S1) driving the respective $P_{NF-\kappa B}$-P_{TAL} luciferase

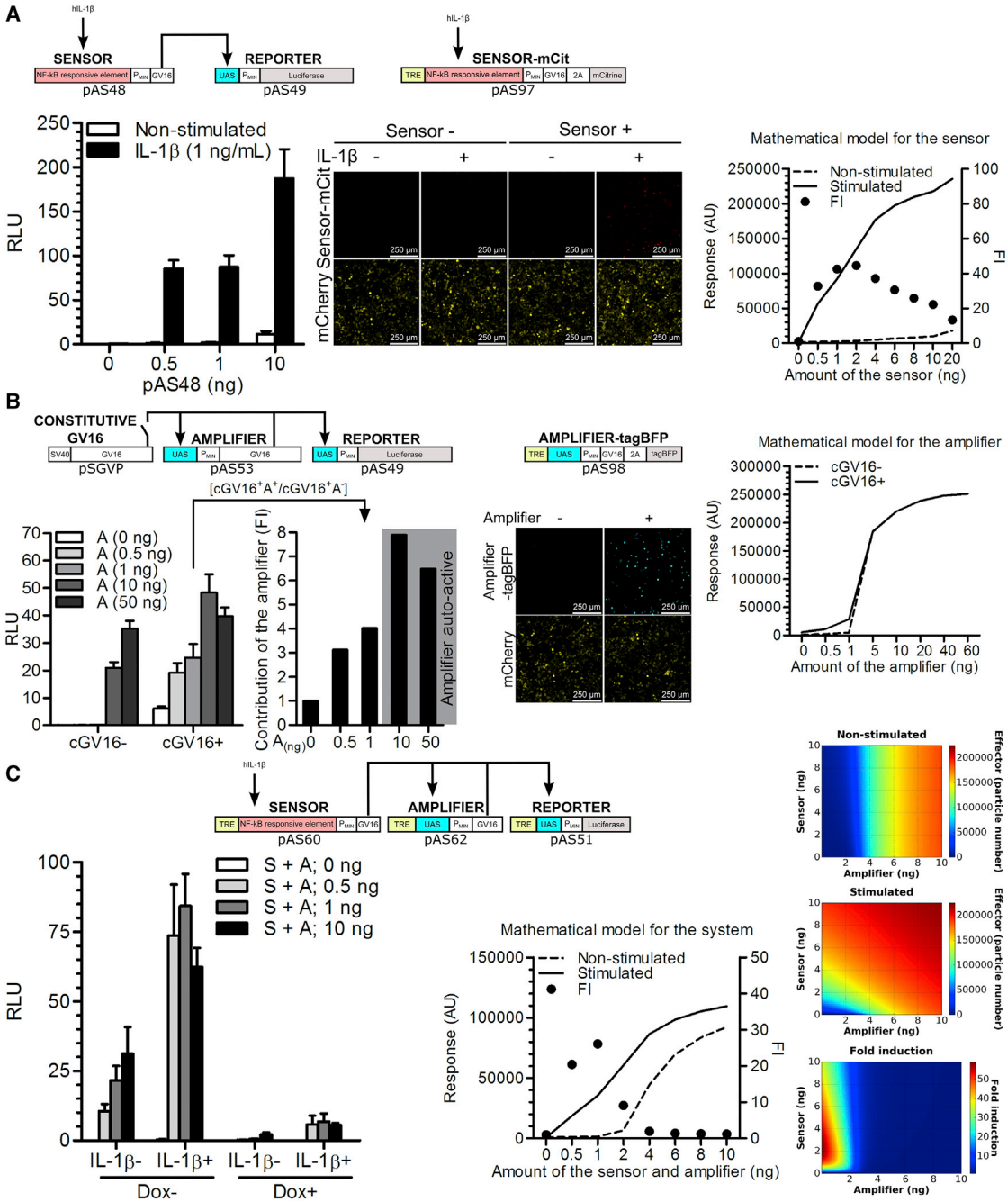

Figure 2. Characterization of the Functional Modules of the Synthetic Anti-inflammatory Gene Circuit

(A) Validation of the sensor construct (pAS48; $P_{NF\text{-}\kappa B2}$-P_{MIN}-GV16) in HEK293T cells. Left: Dual luciferase test. Middle: confocal fluorescence microscopy (mCherry represents a seeding/transfection control). Right: model simulation of the stimulated and non-stimulated sensor-reporter pairs with increasing sensor amounts 24 hr after stimulation. (B) Validation of the amplifier construct (pAS53; UAS-P_{MIN}-GV16) in HEK293T cells. Left: Dual luciferase test. Middle: confocal fluorescence microscopy (mCherry represents a seeding/transfection control). The amplifier autoactivates at higher amounts of transfected construct (cGV16− conditions and a confocal fluorescence image). Additionally, it amplifies an effect of constitutively expressed GV16 as observed in cGV16+ conditions and from FI calculated from the relative light units (RLU) for each amount of the transfected amplifier according the formula [$cGV16^+A^+/cGV16^+A^-$], where A^- represents constitutive expression of GV16 from the pSGVP in the absence of the amplifier ($A_{(0ng)}$ in the RLU graph). Right: model simulation of the amplifier-reporter pairs with increasing amplifier amounts after 24 hr. The effect of cGV16 was examined by setting the particle number of GV16 at t = 0 to 1×10^6 for the cGV16+ simulation. (C) Functional circuit, composed of all the basic elements, except for the thresholder,

(legend continued on next page)

expression were introduced into human embryonic kidney 293 T (HEK293T) cells, and construct pAS37 was selected as the sensor design that produced the highest fold induction (FI) upon stimulation with IL-1β or TNF-α (Figure S1A). The ectopic expression of the receptors for IL-1β and TNF-α was not required for the activation in HEK293T cells (Figure S1A), indicating that the endogenous levels were sufficient, similarly as observed in other studies in HEK293 cells.[22] Next, to decrease transcriptional leakage in the absence of stimulation, the P_{TAL} minimal promoter (derived from the pISRE-Luc vector; Clontech) was replaced with the P_{MIN} minimal promoter (derived from the pGL4.23[luc2/minP]; Promega) to build a pAS40 construct, which enabled $P_{NF\text{-}\kappa B2}$-P_{MIN}-driven expression of luciferase ($P_{NF\text{-}\kappa B2}$-P_{MIN}-Luc, Table S1). Apart from decreasing transcriptional leakage, this modification also increased the activation amplitude, which increased the FI in response to IL-1β stimulation from 25 to 150 (Figure S1B). Furthermore, the luciferase reporter gene from the pAS40 vector was replaced by a GV16 transcriptional activator to build pAS48 construct ($P_{NF\text{-}\kappa B2}$-P_{MIN}-GV16, Table S1) with an aim of testing whether GV16 could act as a module-connecting mediator. IL-1β stimulation of the HEK293T cells transfected with pAS48 resulted in the activation of the co-transfected reporter plasmid pAS49 (UAS-P_{MIN}-Luc, Table S1) that comprised five consecutive Gal4 binding sites (upstream activating sequence [UAS]), which enabled UAS-P_{MIN}-driven luciferase expression (Figure 2A, left). To guide the experimental work by predicting the responsiveness of the device to stimuli and to determine the optimal transfection amounts, a deterministic model based on the ordinary differential equations (ODEs) was constructed using CellDesigner 4.4 software.[23] The mathematical model that used the parameters derived from the experimentally determined values is represented by a constructed state transition diagram of the genetic circuit (Figure S2) and is explained in detail in Supplemental Materials and Methods. As predicted by the model (Figure 2A, right), in both stimulated and non-stimulated settings, the response increased with the increased amount of the transfected sensor. To visualize the activation of the sensor construct in the cells in situ, the mCitrine reporter gene was cloned in-frame with GV16 via the 2A peptide to build the construct pAS97 (TRE-$P_{NF\text{-}\kappa B2}$-P_{MIN}-GV16-myc-2A-mCit, Table S1), which was monitored by confocal fluorescence microscopy. Activation was observed only in the IL-1β-stimulated cells transfected with the respective construct (Figure 2A, middle). Therefore, the sensor construct enabled us to repurpose the endogenous inflammation-characteristic NF-κB signaling for the activation of the anti-inflammatory device.

Once the activation of the device was optimized, we then aimed to achieve sustained high-level production of anti-inflammatory proteins. This production should be persistent even after the input signal from the sensor, delivered by the inflammatory cytokines in the close proximity of the sensing cells, had decreased. The sustainability is important to prevent pre-mature shutdown of the production of anti-inflammatory therapeutics that neutralize the inflammatory cytokines (i.e., the input signal) in the immediate vicinity of the device. The sustainability of the system activation was achieved by incorporation of the positive-feedback amplifier module involving the transcriptional activator GV16, which activates its own transcription by binding to the UAS located upstream of the P_{MIN} (Figure 1). The mathematical model predicted that the amplifier switches to an activated state once a certain level of GV16 has been achieved due to the positive-feedback loop (Figure 2B, right). To test the functionality of the amplifier construct, HEK293T cells were transfected with increasing amounts of the pAS53 construct (UAS-P_{MIN}-GV16, Table S1). Based on the mathematical model predictions, we reasoned that, when the leakage surpasses the certain level, auto-activation would be observed. By monitoring pAS49 reporter activity, this turned out to be in the interval between 1 and 10 ng of pAS53 per well, which is in accordance with the mathematical model. We have also demonstrated that the amplifier augmented the low-level signal of the constitutively expressed GV16 (plasmid pSGVP) up to 4-fold in the relevant range where the amplifier itself was not yet auto-active (Figure 2B, left). The auto-activation of the amplifier-2A-tagBFP construct was also observed directly by confocal fluorescence microscopy (pAS98; TRE-UAS-P_{MIN}-GV16-myc-2A-tagBFP, Table S1) (Figure 2B, middle). Notably, the 2A fusion of mCitrine or tagBFP did not affect the activity of the respective constructs (Figure S1C). Therefore, by including a positive-feedback amplifier module, our device gained the ability to sustain high-level synthesis of therapeutic anti-inflammatory proteins.

To enable the external control over the activity of the device, an inducible OFF-switch, implemented as the rtTR-KRAB repressor,[24] was introduced. This switch reset the device by external chemical signal and shut down production of the anti-inflammatory effectors when they were no longer required. The orthogonal repressor binds to the Tet-binding sites (Tet-responsive element [TRE]) and silences gene expression only in the presence of doxycycline (Dox). The repression effect of KRAB domain spreads several kilobases upstream and downstream of its binding site.[25] Thus, we positioned the TRE into all three modules upstream of the other regulatory elements to avoid disrupting the existing transcriptional architecture, which could potentially impair the function of the fine-tuned constructs. The constitutively expressed rtTR-KRAB (pAS58; P_{CMV}-rtTR-NLS-KRAB, Table S1) repressed the reporter construct pAS51 carrying the TRE-UAS-P_{MIN}-driven luciferase expression unit (TRE-UAS-P_{MIN}-Luc, Table S1), which was activated by the GV16 (plasmid pSGVP[19]). Efficient and dose-dependent repression was achieved, whereas in the absence of external reset signal the rtTR-KRAB (pAS58) alone did not significantly influence the system activation

tested in HEK293T cells. Left: dual luciferase test, reporter pAS51; TRE-UAS-P_{MIN}-Luc. Right: model simulation and parameter scan. The graph and heat maps depict the level of the device activation in stimulated and non-stimulated setting with increasing sensor and amplifier amounts after 24 hr. The amount of each respective construct was increased from 0 to 10 ng, in 0.1-ng increments. Fold induction was calculated by dividing the effector particle number after 24 hr of stimulation with the corresponding effector particle number of non-stimulated circuit after 24 hr for each simulation. S, sensor; A, amplifier; FI, fold induction. Error bars indicate SD (n = 4).

(Figure S1D, left). Similarly, we reset both the activated sensor and the amplifier circuit (Figure S1D, middle and right), suggesting a successful implementation of the inducible OFF-switch function.

After testing and optimizing all the modules, they were incorporated into a functional device. Based on the mathematical model of the genetic network, we predicted higher leakage of the system at the increased amounts of the transfected sensor and amplifier constructs (Figure 2C, middle and right). Based on those predictions, the ratio of the sensor construct pAS60 (TRE-$P_{NF\text{-}\kappa B2}$-P_{MIN}-GV16-myc, Table S1) encoding TRE-$P_{NF\text{-}\kappa B2}$-P_{MIN}-driven expression of GV16-myc and the amplifier construct pAS62 (pAS62; TRE-UAS-P_{MIN}-GV16-myc, Table S1) encoding TRE-UAS-P_{MIN}-driven GV16-myc expression together with the inducible OFF-switch pAS58 and reporter pAS51 was fine-tuned (Figure 2C, left). The lowest amounts of the sensor and the amplifier constructs were used in all further experiments. As a result, we observed a robust system induction triggered by IL-1β, which was efficiently repressed by the addition of Dox (Figure 2C, left).

Introduction of the "Thresholder" and Sustained System Activity by the Amplifier

It is important to restrict activation of the positive-feedback loop until the signal is sufficiently strong. To decrease the transcriptional leakage of the system and increase the FI, a thresholder module was introduced. The thresholder concept is based on competition between GV16 and the constitutively expressed Gal4 that lacks the VP16 activation domain, implemented as the construct pAS67 ($P_{HSV\text{-}TK}$-G-myc, Table S1; schematic representation in Figure 1), for binding to the UAS operator in the amplifier and effector constructs, which acts as a threshold for the system activation. Using model simulations, we predicted that the constitutively expressed thresholder, which provides the constant amount of the UAS binding domain, should prevent activation of the system until the signal from the sensor surpasses the selected level, defined by the amount of the expressed thresholder (Figure 3A, upper right and bottom). According to the model simulations, the thresholder decreased the unwanted background activity while retaining high amplification (Figure 3A, upper right). The mathematical simulations represented by the heat maps demonstrated the effect of increasing thresholder amounts on the level of the device activation with rising leaky transcription rates (k_l) (Figure 3A, bottom). Experimental testing of the thresholder demonstrated its function in agreement with the simulations, decreasing leaky transcription and consequently increasing the FI (Figure 3A, upper left and middle). Importantly, the activated state remained high even at thresholder amounts that strongly decreased the leakage of the unstimulated state. This made it possible to tune the thresholder amount that gave the highest FI of approximately 60 (Figure 3A, upper left and middle). To our knowledge, this is a novel approach for decreasing transcriptional leakage in mammalian cells, which could be applicable to other systems employing positive-feedback regulation.

Furthermore, we tested additional characteristics of the final circuit when both the amplifier and the thresholder constructs were present. To evaluate the contribution of the amplifier to the amplitude and kinetics of the response, the system was stimulated for 24 hr (or 4 hr, Figure S3A). The medium was then replaced to remove the inducer. The amplifier sustained the response, which remained increased as much as 5-fold after 72 hr, compared to the decreased response of the system without the amplifier (Figure 3B). Thus, the amplifier enabled sustained system activation, which is important to avoid pre-mature decrease of anti-inflammatory therapeutics production. Importantly, at the same time, the fine-tuned strength of the positive-feedback loop enabled us to retain concentration-dependent system activation supported by the sensor construct (shown later in the text).

Additionally, the response of the pAS97 and pAS98 constructs in the final device was monitored directly. As shown in Figure S3B, they were both activated only when an input signal was present, and they remained silent if Dox was also added. The amplifier construct should, in principle, switch to an ON state only after the sensor has been activated and the threshold level of Gal4 has been outcompeted by GV16 induced by the sensor. Thus, we verified whether the activated sensor and amplifier constructs were present in the same cell. This was demonstrated by colocalization of the fluorescently tagged activated sensor and amplifier (Figure S3C).

After the successful construction of the system, its activation capacity was investigated. Low amounts (Table S2) of transfected sensor and amplifier constructs in the fine-tuned system yielded a comparable output from the reporter pAS51 as triggered by the equal amount of the constitutive CMV-driven reporter (Figure S1C).

Activation of the Anti-Inflammatory Device Ex Vivo and In Vivo

Next, we investigated the responsiveness of the anti-inflammatory device to physiologically relevant inflammatory signals. As described in the previous sections, we fine-tuned the strength of the positive-feedback loop to retain concentration-dependent system activation. First, we stimulated the engineered cells with increasing amounts of IL-1β and TNF-α, and observed a gradual increase in activation (Figure 4A). Inflammatory cytokine (IL-1β, TNF-α, and IL-6) levels in healthy humans range between undetectable amounts to approximately 10 pg/mL,[26,27] whereas they are strongly elevated in patients with active inflammatory disease. For example, in RA patients, levels of as much as 109 pg/mL of TNF-α and 184 pg/mL of IL-6 were detected.[28] Because IL-1β has a short half-live in vivo,[29,30] its secretion is often investigated indirectly by stimulating cultured peripheral blood mononuclear cells (PBMCs). It was shown that serum from sIJA patients induced secretion of an approximately 100 pg/mL of IL-1β in healthy PBMCs.[31] As our aim was to design a system that could, in principle, function in humans, it was important that the anti-inflammatory device-engineered cells responded at physiologically relevant concentrations. Notably, the system was far less responsive to mouse cytokines, as human receptors are not activated by mouse cytokines as potently as by human cytokines (Figure 4A).

We further demonstrated the physiological relevance of the anti-inflammatory device by demonstrating that the serum of healthy

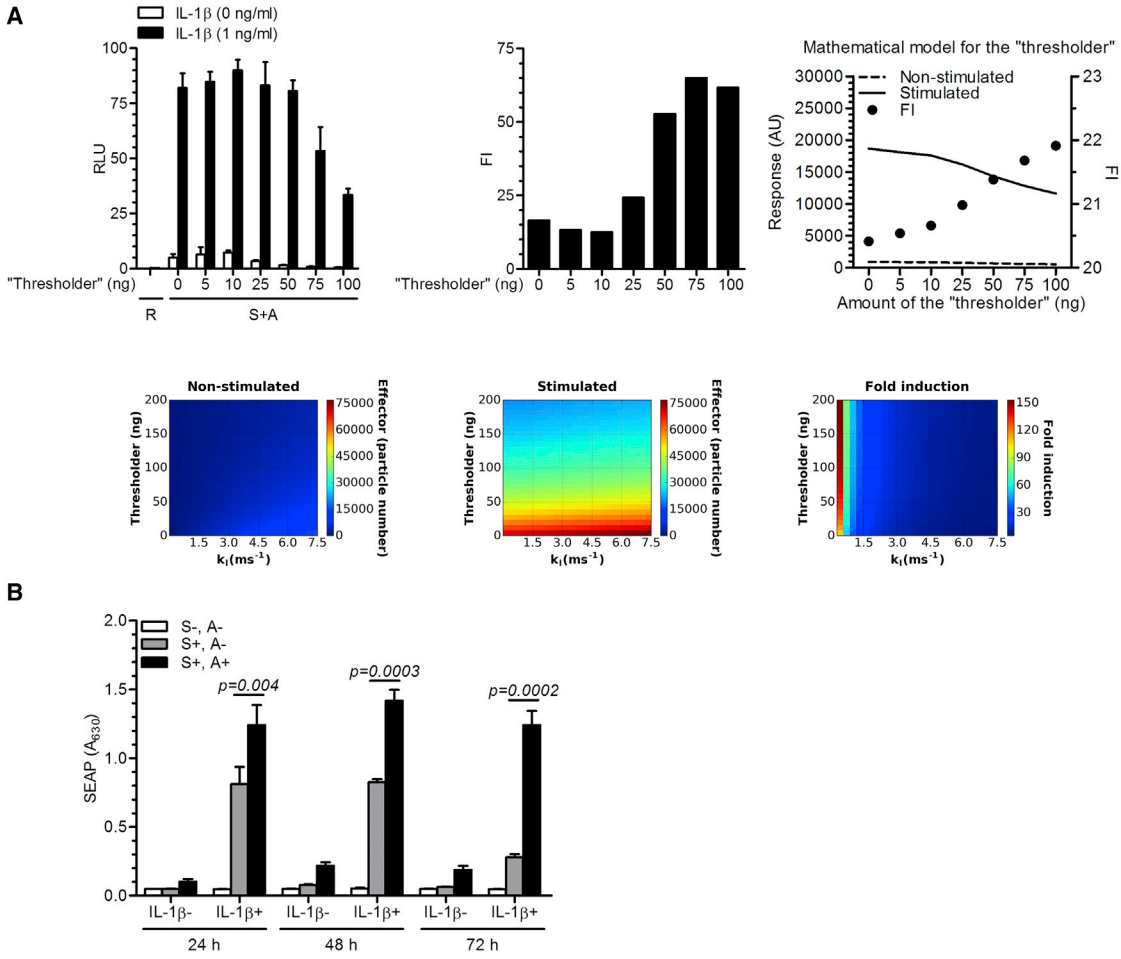

Figure 3. Introduction of the Thresholder and the Effect of the Amplifier

(A) Left: transcriptional leakage of the system was efficiently reduced by a thresholder (pAS67; $P_{HSV\text{-}TK}$-G-myc) tested in HEK293T cells. Right: model simulation and parameter scan. The graph depicts the level of the device activation in stimulated and non-stimulated setting with the increasing thresholder. Bottom panels: heat maps represent the effect of increasing thresholder amounts on the level of the device activation with rising leaky transcription rates (k_l) after 24 hr. (B) Anti-inflammatory device-engineered HEK293T cells (reporter pAS72; TRE-UAS-P_{MIN}-SEAP) were stimulated with hIL-1β for 24 hr, and then the input signal was removed by exchanging the medium. SEAP production was quantified in the culture supernatants every 24 hr along with a medium exchange to observe the kinetics of the system activation. S, sensor; A, amplifier; R, reporter; FI, fold induction. Error bars indicate SD (n = 4).

human individuals did not activate the anti-inflammatory device, whereas the 1:1-diluted human serum from a sIJA patient activated the system approximately 3.5-fold (Figure 4B).

We also observed high ex vivo system activation using peritoneal lavage fluid collected 1 hr after an injection of human IL-1β and TNF-α (intraperitoneally [i.p.]) in mice (Figure 4C). The activation, however, strongly decreased when using peritoneal lavage fluid collected 6 hr after the injection and was undetectable when stimulating with the one, collected after 24 hr (Figure 4C), that highlights the short half-life of the injected cytokines (Figure S4A). To demonstrate activation of the anti-inflammatory device by endogenous inflammation in mice, CLP procedure, which is frequently utilized as an animal model of sepsis and is characterized by high level of inflammatory cytokines (Figure S4B), was performed.[32] Peritoneal lavage fluid collected 24 hr after the CLP procedure demonstrated ex vivo activation of the designed device transfected in HEK293T cells (Figure 4D).

To test the functionality of the implemented anti-inflammatory device in vivo, the engineered cells were microencapsulated in alginate-PLL-alginate beads and were implanted into the peritoneal cavity of mice. An intracellular luciferase reporter, present in the pAS51, was replaced by a secretory alkaline phosphatase (SEAP) to construct the pAS72 reporter plasmid (TRE-UAS-P_{MIN}-SEAP, Table S1). A significant increase in serum SEAP levels was observed 48 hr after i.p. injection of human IL-1β or TNF-α, whereas the device remained silent in the absence of cytokines (Figure 4E). A similar increase in the SEAP activity was detected in the serum after 24 hr and

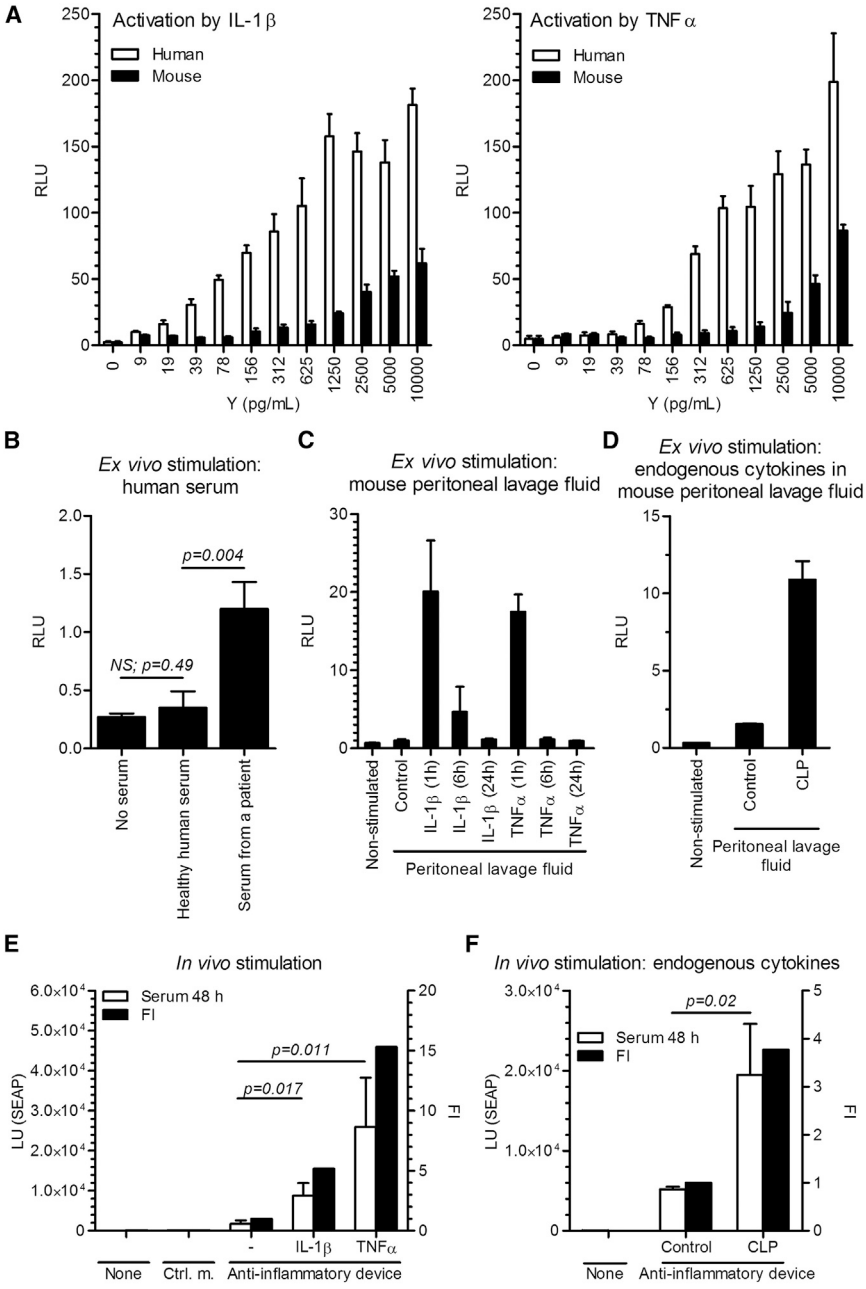

Figure 4. Activation of the Anti-inflammatory Device In Vitro and In Vivo

(A) The responsiveness of the system to recombinant human and mouse interleukin-1β (IL-1β) and tumor necrosis factor α (TNF-α) was tested in the anti-inflammatory device-engineered HEK293T cells by a dual luciferase test (reporter pAS51; TRE-UAS-P_{MIN}-Luc) after a 24-hr activation period. Error bars indicate SD (n = 4). (B) The responsiveness of the system to pooled healthy human serum (n = 4) and the serum of a patient with systemic juvenile idiopathic arthritis (sJIA). Error bars indicate SD (n = 4). (C) Activation of the anti-inflammatory device-engineered HEK293T cells ex vivo by a peritoneal lavage fluid of mice, injected i.p. with hIL-1β (300 ng/mice) or hTNF-α (250 ng/mice). The peritoneal lavage fluid was collected at different time points. Error bars indicate SD (n = 4). (D) Activation of the anti-inflammatory device-engineered HEK293T cells ex vivo by endogenous mouse cytokines in a peritoneal lavage fluid of mice that were subjected to the cecal ligation and puncture (CLP). The peritoneal lavage fluid was collected 24 hr after CLP procedure. Error bars indicate SD (n = 4). (E) The responsiveness of the system in vivo. The anti-inflammatory device-engineered HEK293T cells (reporter pAS72; TRE-UAS-P_{MIN}-SEAP) were microencapsulated and implanted i.p. An inflammatory signal was induced i.p. with an injection of hIL-1β (300 ng/mouse) or hTNF-α (250 ng/mouse) 1 and 24 hr post-implantation. Serum SEAP levels were profiled after 48 hr. Error bars indicate SD (n = 5). (F) The responsiveness of the implanted anti-inflammatory device to endogenous CLP-induced inflammation in mice. CLP procedure was performed 24 hr before microcapsules implantation, and SEAP levels were measured 48 hr post-implantation. Y, mass concentration; FI, fold induction; Ctrl. m., control microcapsules; Control, control mice. Error bars indicate SD (n = 5).

in the peritoneal lavage fluid after 48 hr (Figure S4C). The trend of in vivo studies was similar to that observed in parallel in vitro experiments (Figure S4D, left). As an internal control of the system, a construct for a secretory *Renilla* luciferase under the constitutive promoter, SR-Luc (pAS75; P_{CMV}-SR-Luc, Table S1), was designed and co-transfected along with the anti-inflammatory device. As seen in Figure S4D, right, the SR-Luc was comparable among the groups, indicating similar amounts of implanted microcapsules and similar microencapsulated cell viability. In a similar vein to ex vivo experiments, we have also demonstrated that the CLP procedure in mice resulted in elevated inflammatory cytokines, measured in the peritoneal lavage fluid and serum (Figure S4B), and led to an autonomous activation of the implanted anti-inflammatory device by the endogenous inflammation in vivo (Figure 4F).

These results therefore demonstrated that the microencapsulated anti-inflammatory device was able to respond reliably to an inflammatory signal in a complex biological environment when implanted into the peritoneal cavity of mice.

Design and Biological Activity of the Composite Anti-Inflammatory Therapeutic Proteins

Upon activation, a functional anti-inflammatory device should produce a therapeutically relevant output. For this purpose, we designed an advanced effector construct based on clinically used anti-inflammatory biopharmaceuticals, anti-human TNF-α antibody

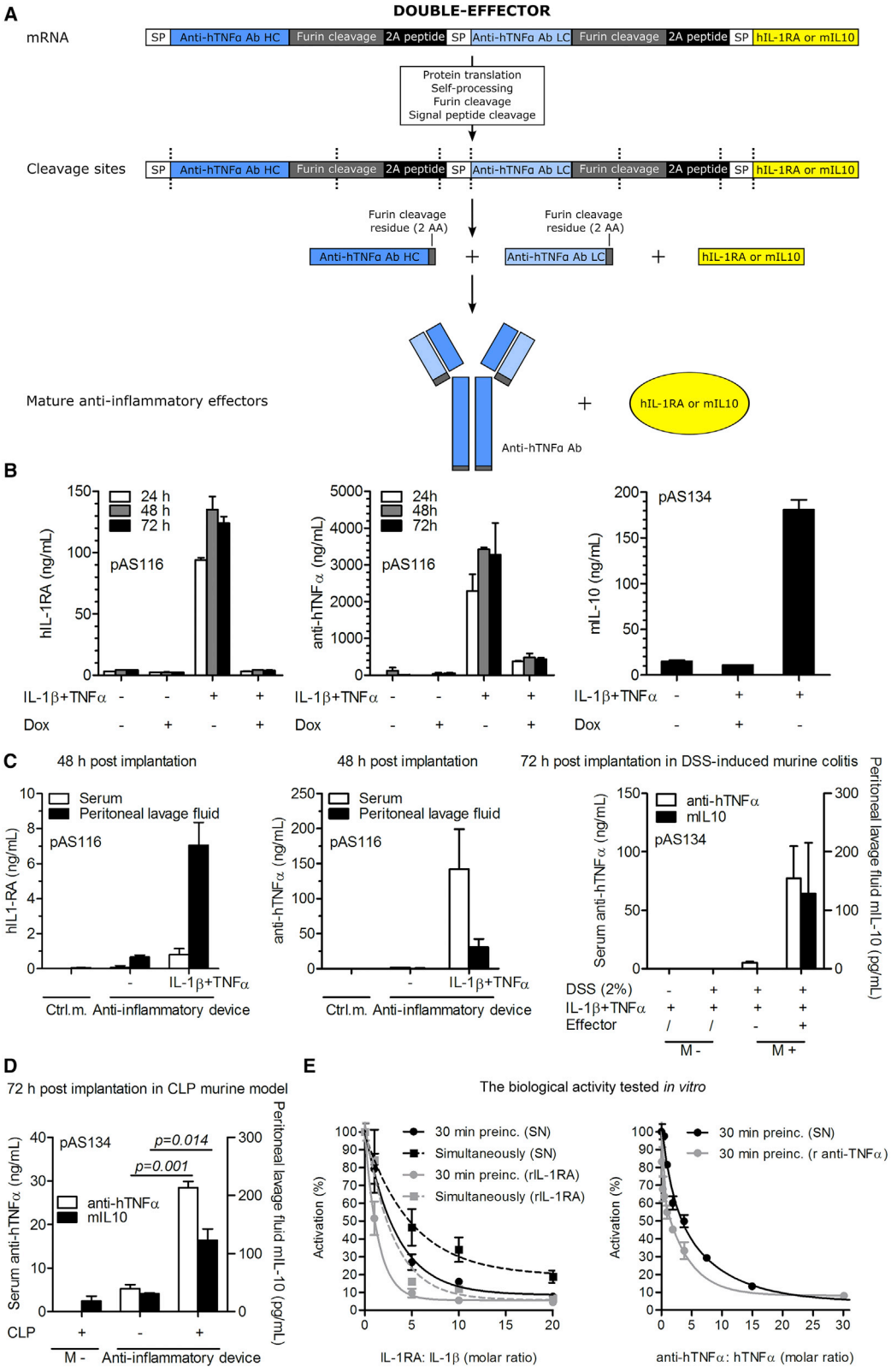

(legend on next page)

(anti-hTNF-α Ab with CDR from the adalimumab[33]), human IL-1β receptor antagonist (hIL-1RA), and mouse interleukin 10 (mIL-10). To produce a stoichiometric amount of the heavy and light antibody chain, the effector construct was designed as a single mRNA transcript comprising coding sequences for three polypeptide chains, an anti-hTNF-α antibody heavy chain, an anti-hTNF-α antibody light chain, and hIL-1RA or mIL-10. The polypeptide-coding chains were linked through the coding sequence for the 2A peptide, which interrupts the translation of the polypeptide chain, similar as described previously[34] (Figure 5A). These composite anti-inflammatory therapeutics were integrated in the final effector constructs pAS116 (TRE-UAS-P_{MIN}-anti-hTNF-α Ab-hIL-1RA) and pAS134 (TRE-UAS-P_{MIN}-anti-hTNF-α Ab-mIL-10, Table S1). The constitutive and inducible production of the anti-hTNF-α antibody and hIL-1RA separately, or coupled in the final effector construct, was validated by western blot analysis (Figure S5A). The ability and efficiency of the antibody molecules to traverse the membrane of the microcapsules was demonstrated (Figures S5B–S5D). Production of hIL-1RA, anti-hTNF-α, and mIL-10 from the pAS116 or pAS134-transfected microencapsulated cells was quantified by an ELISA. We determined the production of hIL-1RA, anti-hTNF-α antibody, and mIL-10 in the stimulated system (Figure 5B; see Figure S5E for SR-Luc). The unstimulated and the stimulated and subsequently Dox-reset system did not produce substantial amounts of anti-inflammatory effectors (Figure 5B; see Figure S5E for SR-Luc). Similar results were obtained in vitro with an inducible anti-hTNF-α (pAS113; TRE-UAS-P_{MIN}-anti-hTNF-α Ab, Table S1), mIL-10 in the setting with or without the effector construct pAS134, and constitutive hIL-1RA (pAS35; P_{cmv}-hIL-1RA-myc, Table S1) alone (Figure S5F).

The in vivo production of the effectors from the microencapsulated engineered cells implanted into the peritoneal cavity of mice was demonstrated. We detected 1 ng/mL of hIL-1RA and 150 ng/mL of anti-hTNF-α in the serum or 7 ng/mL of hIL-1RA and 30 ng/mL of anti-hTNF-α in the peritoneal lavage fluid 48 hr post-implantation only when the mice with implanted device were stimulated with human IL-1β and TNF-α. Mouse IL-10 was detected in the peritoneal lavage fluid at 200 pg/mL 72 hr post-implantation (Figure 5C; see Figure S5E for SR-Luc). Similar results were obtained for the constitutive in vivo production of hIL-RA (Figure S5G). Similarly as described above (Figure 4F), we have shown autonomous in vivo activation of the device by the CLP procedure, detected by anti-inflammatory therapeutics 72 hr post-implantation (Figure 5D). We speculate that the different concentration and distribution of therapeutic proteins between serum and peritoneal lavage fluid are due to the two factors. First, a longer serum half-life of human IgG1 antibody (approximately 3 days[35]) enables wide distribution of anti-hTNF-α and its accumulation in the serum, compared to the shorter-lived hIL-1RA and mIL-10 (serum half-life of an approximately 30 min[36,37] and 2 hr,[38] respectively), which results in the highest concentration in the vicinity of the implanted microcapsules. Second, the peritoneal lavage fluid-collecting procedure (see Materials and Methods) dilutes the local concentration of therapeutic proteins. In this way, the concentration of more evenly distributed anti-hTNF-α is higher in the serum than in the diluted peritoneal lavage fluid, whereas the concentration of hIL-1RA and mIL-10 is higher in peritoneal lavage fluid even after dilution, because their short circulating half-life compromises their accumulation in the serum.

The biological activity of hIL-1RA and anti-hTNF-α, produced in the HEK293T cells, was demonstrated in vitro by the inhibition of hIL-1β or hTNF-α signaling, respectively. Approximately 3-fold molar excess was required for 50% inhibition for both effectors, which was similar to the recombinant proteins used as controls (Figure 5E). Altogether, in this set of experiments, we were able to successfully construct and test composite anti-inflammatory therapeutic proteins.

Resetting of the Anti-Inflammatory Device In Vitro and In Vivo

Next, we demonstrated in vitro that, once activated, the device could be reset to the resting state by the addition of Dox after 24 hr. Complementary, when the device was initially reset by Dox, it could be reactivated by an inflammatory signal (Figures 6A and S6A). Furthermore, we wanted to recapitulate these results in vivo. First, we stimulated the implanted device for 1 hr to activate the circuit and then injected Dox, which prevented full system activation, as measured by SEAP release (Figure 6B; see Figure S6B for SR-Luc). Next, we

Figure 5. Design and Biological Activity of Composite Anti-inflammatory Therapeutics

(A) Schematic representation of the double effector construct. The construct was designed as a single mRNA transcript comprising coding sequences for the anti-hTNF-α antibody heavy chain, anti-hTNF-α antibody light chain, and mouse IL-10 (mIL-10) or human interleukin-1 receptor antagonist (hIL-1RA), linked through the coding sequence for the 2A peptide. Each coding sequence contains its own signal peptide (SP) and an additional furin cleavage site to truncate the length of 2A cleavage residues. After the protein translation, self-processing, and furin and signal peptide cleavage, the mature anti-inflammatory effectors were assembled, resulting in a mixture of proteins that counteracted inflammation. (B and C) In vitro (B) and in vivo (C) expression of the anti-inflammatory therapeutics from the effector constructs indicated in the figure. The anti-inflammatory device-engineered HEK293T cells were microencapsulated, and 700 μL of suspension was either incubated in vitro in 10 mL of media or implanted i.p. in mice. In vitro, the anti-inflammatory device was stimulated with a combination of interleukin-1β (IL-1β) (10 ng/mL) and tumor necrosis factor α (TNF-α) (10 ng/mL) or, in addition, subsequently shut down by doxycycline (Dox) (1 μg/mL). For in vivo expression, the mice were injected i.p. with a combination of 500 ng of hIL-1β and 250 ng of hTNF-α per mouse 1 hr after implantation. Serum and peritoneal lavage fluid were collected 48 or 72 hr post-implantation as indicated in the figure. The anti-hTNF-α antibody, mIL-10, and hIL-1RA concentrations were determined by an ELISA test. (D) The responsiveness of the implanted anti-inflammatory device to endogenous CLP-induced inflammation in mice. CLP procedure was performed 3 hr before microcapsules implantation, and SEAP levels were measured 72 hr post-implantation. (E) The biological activity of hIL-1RA and the anti-hTNF-α antibody was determined in vitro by competitive inhibition of hIL-1β and hTNF-α signaling via the NF-κB promoter (reporter pAS40; $P_{NF\text{-}κB2}$-P_{MIN}-Luc). We stimulated cells with 20 ng/mL hIL-1β or hTNF-α for 24 hr, to which we added (simultaneously or with 30-min preincubation) the titrated supernatant, containing anti-inflammatory proteins. SN, supernatant; Ctrl. m., control microcapsules; M−, without microcapsules; M+, with microcapsules. Error bars indicate SD (n = 4).

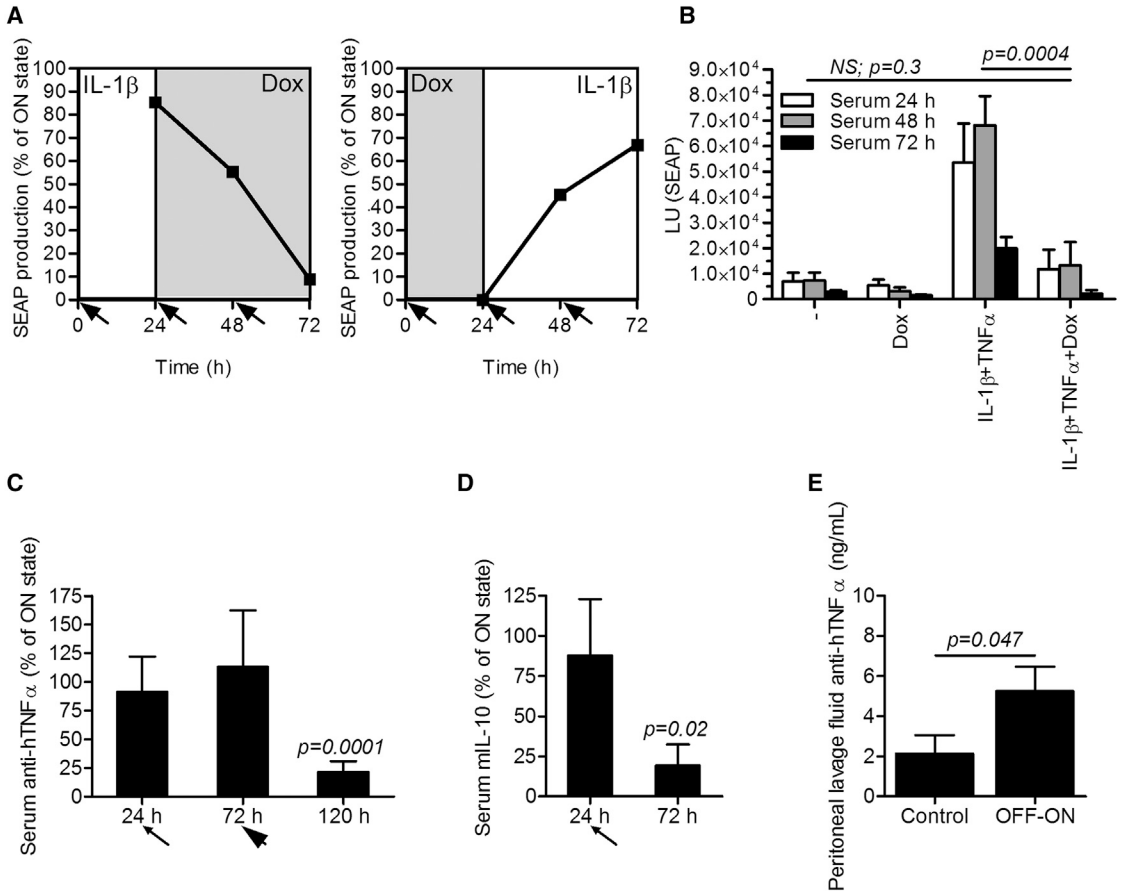

Figure 6. Reversibility of the Synthetic Anti-inflammatory Device In Vitro and In Vivo

(A) Reversibility of the synthetic anti-inflammatory device in vitro. Left: shutdown of the system. The anti-inflammatory device-engineered HEK293T cells (reporter pAS72; TRE-UAS-P_{MIN}-SEAP) were stimulated with hIL-1β (1 ng/mL) for 24 hr and then shut down by the addition of the doxycycline (Dox) (1 μg/mL) by exchanging the medium (indicated by the arrows). Right: rebooting of the initially shut down system. The anti-inflammatory device-engineered HEK293T cells (reporter pAS72; TRE-UAS-P_{MIN}-SEAP) were shut down by Dox (1 μg/mL) for 24 hr and then reactivated by the addition of hIL-1β (1 ng/ml) during medium exchange (indicated by the arrows). Error bars indicate SD (n = 4). (B) In vivo restraint of the full system activation. The anti-inflammatory device-engineered HEK293T cells (reporter pAS72; TRE-UAS-P_{MIN}-SEAP) were micro-encapsulated and implanted i.p. One hour after implantation, the mice were injected i.p. with a combination of 300 ng of hIL-1β and 250 ng of hTNF-α per mouse. After 1 hr and then every 24 hr, the device was shut down by an i.v. Dox injection (20 mg/kg). Serum was collected daily, and SEAP levels were measured. (C and D) In vivo shut down of the system. The anti-inflammatory device-engineered HEK293T cells (effector pAS134; TRE-UAS-P_{MIN}-anti-hTNF-α Ab-mIL-10) were microencapsulated, implanted i.p., and fully activated by injection of a combination of 300 ng of hIL-1β and 250 ng of hTNF-α per mouse. After 24 hr (thin arrow), the device was shut down by an i.v. Dox injection (20 mg/kg). (C) The device was additionally activated and shut down after 72 hr (thick arrow) to reach the relevant time span needed for an observation of the anti-hTNF-α antibody kinetics. Serum was collected at different time points, and (C) anti-hTNF-α antibody or (D) mIL-10 levels were measured. (E) Reactivation of the anti-inflammatory device in vivo. The anti-inflammatory device-engineered HEK293T cells (effector pAS134; TRE-UAS-P_{MIN}-anti-hTNF-α Ab-mIL-10) were microencapsulated and shut down by i.v. Dox injection (20 mg/kg) 1 hr after implantation. After 72 hr, the system was activated by a single application of 300 ng of hIL-1β and 250 ng of hTNF-α per mouse. Implanted anti-inflammatory device alone represented the control group. Anti-hTNF-α antibody concentration was profiled in the peritoneal lavage fluid 120 hr after implantation. Error bars indicate SD (n = 4).

wanted to demonstrate in vivo reset of the fully activated system by injecting Dox 24 hr after activation (thin arrow in Figure 6C) and measuring the anti-inflammatory therapeutics concentrations (pAS134; TRE-UAS-P_{MIN}-anti-hTNF-α Ab-mIL-10, Table S1). Considering a long half-life of human IgG1 antibody (approximately 3 days[35]) and likewise of the SEAP (approximately 1 day[39]) in vivo in mice and taking in account the kinetics of the reset switch shown in Figure 6A, there was no difference in the anti-hTNF-α antibody serum concentrations 48 hr after Dox injection, because the fully activated device secreted anti-hTNF-α antibody that accumulated in the circulation during that period (Figure 6C). Therefore, the experiment was prolonged and the device was additionally reset 72 hr after the first activation (thick arrow in Figure 6C). In this case, the device was activated simultaneously with the reset. This was done to ensure the full activity of the circuit receiving signals from the sensor and the amplifier constructs in the ON group throughout the time course of the experiment and to show the ability to keep the system shut down even in the presence of the inflammatory signal (i.e., the

dominant effect of the OFF-switch) in the OFF group. One hundred twenty hours after the implantation, the activity of the initially fully activated system dropped to around 20%, demonstrating an efficient reset in vivo (Figures 6C and S6C). Additionally, when mIL-10, which has a short serum half-life (approximately 2 hr[38]), was monitored, we demonstrated that one injection of Dox 24 hr after the system activation (thin arrow in Figure 6D) decreased the activity of fully activated system to around 20% after 48 hr (Figures 6D and S6D). Finally, we have shown in vivo that, if the system was initially reset by Dox injection 1 hr after implantation, it could be reactivated by a single application of human IL-1β and TNF-α 3 days after, as measured by the presence of anti-hTNF-α antibody in the peritoneal lavage fluid 120 hr after implantation (Figure 6E). However, the in vivo reactivation was low by means of capacity, presumably because of the transient nature of the system as shown in Figure S7A and possibly also due to the residual Dox in the bloodstream (half-life of an approximately 3 hr in mice[40]).

Application of the Anti-inflammatory Device In Vivo in the Acute Murine Colitis

The anti-inflammatory device was designed and optimized to function in humans. Here, we tested the robustness of the system and the efficiency of the composite anti-inflammatory therapeutics also in an animal disease model. We tested the in vivo physiological functionality of the implanted device in the amelioration of acute (8-day) DSS-induced murine colitis. Although we have shown activation of the anti-inflammatory device by endogenous mouse cytokines in the CLP model (Figures 4F and 5D), the DSS-induced murine colitis did not result in the sufficient increase of the endogenous systemic inflammatory cytokines to activate the system, as substantial amounts were detected only in the supernatants of colon biopsy samples (Figure S7B) and the receptors of human HEK293T cells are far more responsive to the human than mouse inflammatory cytokines as shown in Figure 4A. To mimic an inflammatory flare and to reach an optimal effect in a DSS-induced murine colitis, we stimulated the microencapsulated anti-inflammatory device by injecting human inflammatory cytokines. As a therapeutic output, a combination of anti-hTNF-α, which also inhibits mTNF-α,[33] and mIL-10 was used, because both anti-inflammatory therapeutics have previously shown efficiency in a mouse colitis model.[6,7] When the microencapsulated anti-inflammatory device was implanted on the fifth day of the experimental model (i.e., 5 days after the starting of the DSS exposure), a significantly reduced colon shortening was observed, when mice were sacrificed on the eighth day, in comparison to the control without microcapsules or the implants containing the engineered cells without the effector module (Figure 7A). The microencapsulated anti-inflammatory device clearly improved the intestinal morphology as observed at the end of the in vivo experiment, compared to that of the controls (Figure 7B), and significantly reduced the daily monitored disease activity index, defined by the stool form and stool blood (Figure 7C). Furthermore, the anti-inflammatory device improved the colon histopathology (Figure 7E) and consequently the histological score (Figure 7F), which was evaluated on the eighth day upon sacrifice of the mice. Colon from animals with the implanted anti-inflammatory device showed less infiltration of lymphocytes and neutrophil granulocytes, less crypt damage, and no formation of ulcers. In control animals, foci of hydropic degeneration were also observed in contrast to mice with implanted active device. When the anti-inflammatory device was implanted on the third day after DSS exposure, activated, and simultaneously restrained by Dox, a significant difference in the amount of body mass lost was measured on the fifth day (2 days after the implantation of the device), compared to the device that remained activated (Figure 7D). However, at later time points, the device was not able to reverse the body mass loss, presumably because of the severity of the damage to the gastrointestinal tract caused by DSS and possibly also because of the decrease of the circuit's therapeutic capacity at later time points due to the transient nature of the system (Figure S7A).

DISCUSSION

Several innovative concepts for a variety of medical applications have already been introduced employing the principles of synthetic biology.[41] One particularly promising strategy is the modification of mammalian cells by designed genetic therapeutic networks that autonomously sense pathological conditions (i.e., metabolites or other signature molecules) and respond by a therapeutic output.[9] When implanted into the host organism, such engineered cells act as therapeutic prosthetic devices. In this way, synthetic biology could contribute to the next generation of cell-based therapies for important medical problems, representing a new pillar of pharmacotherapy.[42]

Inflammatory processes are central to many widespread diseases such as IBD, which alone affects more than 2 million people in Europe.[43] As pro-inflammatory cytokines are the key pathophysiological components in the inflammatory disease manifestation,[44] biological drugs that interfere with those mediators represent an effective therapy.[45]

The anti-inflammatory device developed in this study enabled a prompt detection of inflammatory signals requiring only 4 hr of stimulation (Figure S3A) and the initiation of an in vivo localized therapeutic response designed to be strengthened by the amplifier device. In addition to its inflammatory signal-induced rapid response, a major advantage of the therapeutic device compared to established biological therapies, such as TNF-α and other inflammatory cytokine neutralizers, is the avoidance of long-term systemic blockage of beneficial inflammatory reactions. Upon future developments of the therapeutic systems, the main medical conditions that might benefit from the anti-inflammatory device are chronic inflammatory diseases or medical conditions with high risk of acute inflammatory flare-ups.

We demonstrated that the sensor module enabled dose-dependent activation of the device at physiologically relevant concentrations of inflammatory mediators both in vitro and in vivo in mice (Figures 4 and 5). Similarly as in other studies,[13] the dynamic range of the genetic circuit in the in vivo conditions did not fully recapitulate the in vitro setting, but nevertheless we have demonstrated that the device

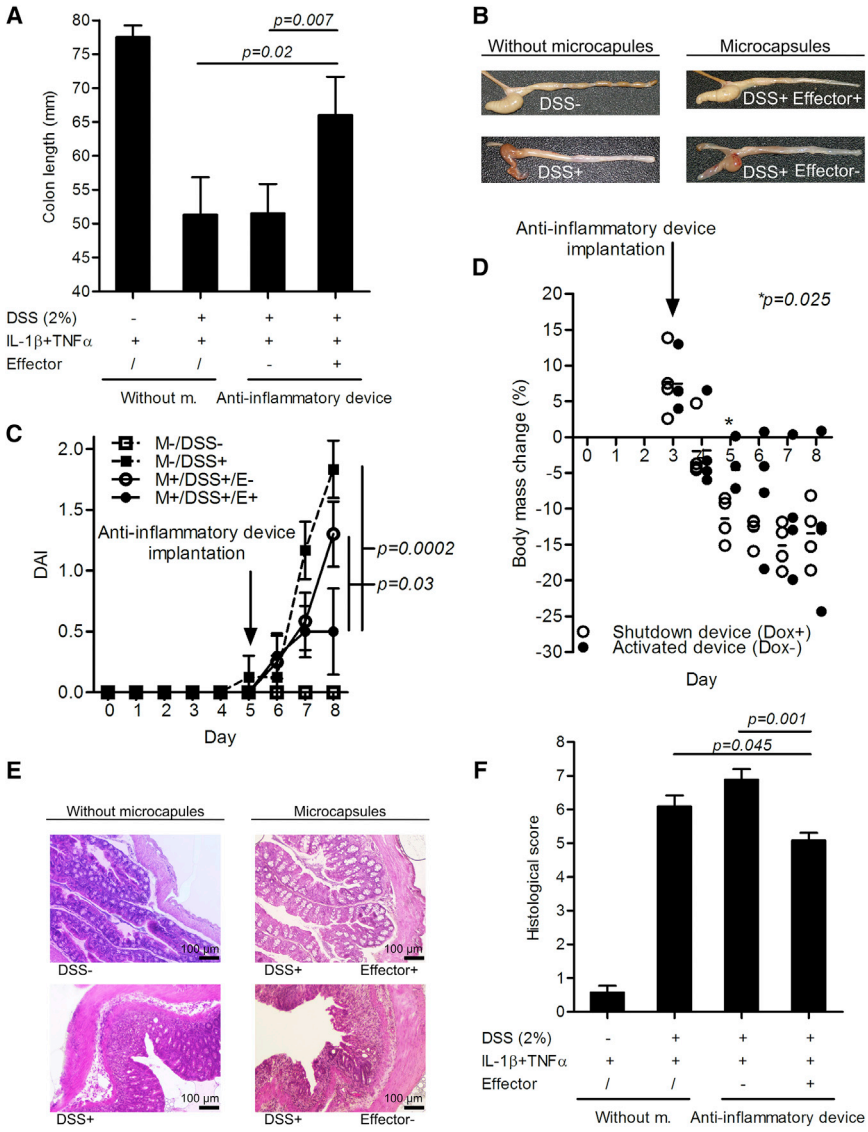

Figure 7. Anti-inflammatory Device Demonstrates Efficacy by Reducing the Symptoms in the Acute Murine Colitis

The anti-inflammatory device-engineered HEK293T cells (double effector pAS134; TRE-UAS-P_{MIN}-anti-hTNF-α Ab-mIL-10) were microencapsulated and implanted i.p. into mice with DSS-induced acute murine colitis on the fifth day (except for D) of the experimental model (i.e., 5 days after exposing mice to DSS). One hour after implantation, the device was activated by a combined inflammatory signal (an i.p. injection containing a combination of 300 ng of hIL-1β and 250 ng of hTNF-α per mouse). (A) The anti-inflammatory device blocked colon shortening induced by DSS (the mean ± SD is shown) and (B) improved the intestinal morphology as validated at the end of the in vivo experiment; (C) reduced daily monitored disease activity index, defined by the combined scores of stool consistency and stool blood (two-tailed Student's t test assuming unequal variances; mean ± SEM is shown); (D) temporarily reduced daily monitored body mass loss (each data point represents the body mass measurement of one mouse); and, as measured upon the sacrifice of the mice, (E) improved colon histopathology, and (F) the histological score (Mann-Whitney U test; mean ± SEM is shown). Without m., without microcapsules.

enabled a reasonable FI with a relatively low leakage when measuring SEAP as an output (Figures 4E and 4F). When therapeutic proteins were profiled in the serum or peritoneal lavage fluid of mice, a better dynamic range was observed, which was attributed to the lower background (Figures 5C and 5D). Additionally, ex vivo activation by human serum from a sIJA patient was demonstrated (Figure 4B). sJIA is an auto-inflammatory disease affecting 250,000 children in the United States alone.[31] Anakinra has been previously shown to have a beneficial effect on the disease outcome, when administered early in the disease progression before arthritis has become well established.[18] That is exactly what the described anti-inflammatory device enables and anakinra as a therapeutic output was also validated in this study (Figures 5B, 5C, and 5E). The activation of the system by the human serum from sIJA patient was lower than in the in vitro titration experiment. This is in part due to the dilution of the serum used in this experiment, but also due to a very short half-life of hIL-1β in the human serum.[29,30] Considering these limitations, a 3.5-fold induction is probably an underestimation of what the systems' response would be in a hypothetical in vivo setting, where the circulating hIL-1β would fuel the activity of the implanted device. Nevertheless, it remains to be investigated, whether this level of activation would suffice for the therapeutic efficacy in the in vivo setting, which clearly depends on the particular inflammatory disease being targeted. Although the anti-inflammatory device was optimized for a human setting, activation by endogenous mouse cytokines was shown in the CLP model of sepsis in vivo (Figures 4F and 5D).

The notion and application of a threshold for regulation has already been established in DNA nanotechnology, where in vitro DNA strand displacement enabled a construction of neural networks by linear threshold circuits.[46] The novelty of our designed circuit is introduction of the thresholder, which decreases the transcriptional leakage in the mammalian cell system. This was achieved by a competition between transcriptionally active and inactive proteins for the same DNA binding site (Figure 3A). This principle contributes to the synthetic biology toolbox for mammalian cell engineering and could be applied in genetic circuits that are prone to a transcriptional leakage. It has been demonstrated by others[47,48] that repeated DNA sequences containing transcription factor binding sites that are not coupled to

system activation can act as decoys. In this way, by sequestering transcriptional activator, decoy binding sites can influence the properties of the circuit by increasing its ultra-sensitivity. On the other hand, when designing complex gene circuits by joining several modules, decoy DNA binding sites can apply a load to a system and negatively influence circuit function, which was alleviated by a designed load driver device.[49] However in this study, we did not test how the thresholder affected ultra-sensitivity of the system, because our primary goal was to decrease the transcriptional leakage of the circuit. Upon introduction of the thresholder, our circuit retained graded response, which depended on the concentration of the input inflammatory signals (Figure 4A).

The activated device produced sufficient amounts of biologically active anti-inflammatory therapeutic proteins in vitro (Figure 5B) and in vivo (Figures 5C and 5D) to impair the excessive inflammation and its pathological effects. Sustained production of effector proteins was achieved by incorporation of the positive-feedback amplifier module (Figure 3B), bypassing device inactivation by sequestration of the inflammatory signals in the immediate vicinity of the implant. The production of therapeutic proteins with this device can be terminated by the administration of a clinically licensed chemical mediator Dox. Dox, acting via a repressor module, resets the therapeutic device into the standby state as demonstrated in vitro (Figures 2C and 6A) and in vivo (Figures 6B–6D). At the same time, the integrated OFF-switch does not prevent the recurrent system activation as shown in vitro (Figure 6A) and in vivo (Figure 6E).

The designed synthetic strategies against inflammation have already been reported and included orally administered *L. lactis* secreting IL-10[6] or anti-TNF-α nanobody[7] and adenoviral IL-10 gene therapy,[50] which constitutively produce anti-inflammatory proteins. These approaches demonstrated efficacy in the murine colitis models. The production capacity of the anti-inflammatory device, which was activated autonomously upon encountering inflammatory signals, was similar to these studies. As an example, we demonstrated the in vivo efficacy of the microencapsulated anti-inflammatory device in a DSS-induced acute murine colitis model evaluated by several physiological parameters (Figure 7).

From an engineering perspective, the anti-inflammatory device in the present study can be considered a gene regulatory circuit, in which the active, therapeutic protein-producing state is triggered by an inflammatory signal and the OFF signal is provided by an external chemical signal. This setup allows for a rapid autonomous activation and the external control of the reset (e.g., when a physician decides that the therapeutic production of anti-inflammatory proteins is no longer required).

Recently, *E. coli* was engineered to detect and record the presence of anhydrotetracycline in the mammalian gut, serving as a living diagnostic device.[51] Detection of in vivo anti-inflammatory device activation (Figures 4E and 4F), representing an inflammatory episode, could serve as a diagnostic reporter of an ongoing inflammatory process or as a log of past inflammatory events, without having to frequently sample the body fluids of an organism.

The modular design of the device enables adaptation of a combination of effector proteins for the particular pathology and for an optimal effect. Changing the sensor module allows alternative endogenous signals to be detected. The latter ability of the device was demonstrated by introduction of the STAT3 responsive element, which enabled IL-6 detection (Figure S4E). Combining two or more input signals by an AND or similar logic could increase the specificity of the response to different combinations of inflammatory mediators. As this type of device would be used for patients diagnosed with chronic inflammatory diseases, we speculate that the activation of the device mediated by the NF-κB signal, activated also by other stimuli, such as bacterial or viral infection, should not cause a problem as also infection-triggered inflammation can aggravate or even initiate the disease.[52–54] Furthermore, the ability to switch off the production of anti-inflammatory therapeutics by applying a chemical signal would allow the anti-inflammatory action to be bypassed, if required.

Although the capacity of the system decreased with time due to the transient nature of the system, the device was still active also 6 days after transfection in vitro; however, the productivity decreased at later time points (Figure S7A). The underlying cause is probably a well-documented phenomena of the intracellular plasmid degradation, spontaneous loss, and dilution during cell divisions in transiently transfected cells.[55,56] We have demonstrated that the sensor and the amplifier constructs were present and activated in the same cell 48 hr after the transfection (Figure S3C). However, as expected, the plasmid copy number per cell dropped within 5 days after transfection, but nevertheless, the amplifier construct, which was introduced at the lowest amounts, and the inducible OFF-switch representing a safety mechanism, were still present at that time (Figure S7C). Importantly, the initial amounts of the inducible OFF-switch were much higher than the amounts of the sensor and amplifier, which are the drivers of the device activation, ensuring that the safety switch is functional for the duration of the device activity.

Although the reliability and robustness of the anti-inflammatory device were demonstrated in vitro and in vivo, it should be noted that, in this configuration, the device is a prototype that needs further refinements for clinical applications in human therapy. In particular, long-term stable cell lines would need to be established by genome integration of the device, either using autologous or validated safe cell lines.

Particularly for the translation of the system from mice to a human setting, the capacity to produce anti-inflammatory proteins and pharmacodynamics analysis of the local concentration in the affected organs will have to be taken into account for therapeutic applications. The results indicated that the production levels of the anti-inflammatory effectors were sufficient to suppress inflammatory reactions in mice (Figure 7) and that the engineered microencapsulated cells remained viable in the in vitro culture (Figure S7D) and, more importantly, in the peritoneal cavity of mice (Figure S7E).

Alginate microencapsulation has already been tested in clinical trials,[57,58] for example, microencapsulated human islets transplanted into a type 1 diabetic patient aided insulin independence for 9 months.[59] Besides alginate microencapsulation, there are alternative cell implantation technologies, such as biocompatible hollow fibers, which may enable an easy removal of the implanted device.[60] Advancing safety and efficacy of cell implantation technologies may foster the translation of the designed synthetic biology-inspired prosthetic devices into the clinic.

In conclusion, the concept of an autonomous anti-inflammatory device may provide an alternative to anti-inflammatory therapy and the emerging field of synthetic immunology[61] may significantly contribute to the development of novel therapeutic solutions for important medical problems.

MATERIALS AND METHODS

Plasmid Construction

The genetic constructs used and designed in this study are listed and explained in detail (including their architecture, construction methods, and annotated sequences of relevant elements) in Table S1. Key plasmids include the following: the sensor construct pAS60, encoding the TRE-$P_{NF\text{-}\kappa B2}$-P_{MIN}-driven GV16-myc expression unit (TRE-$P_{NF\text{-}\kappa B2}$-P_{MIN}-GV16-myc); the amplifier construct pAS62, encoding the TRE-UAS-P_{MIN}-driven GV16-myc expression unit (TRE-UAS-P_{MIN}-GV16-myc); the double effector construct pAS134, encoding the TRE-UAS-P_{MIN}-driven anti-hTNF-α antibody-mIL-10-myc double effector expression unit (TRE-UAS-P_{MIN}-anti-hTNF-α Ab-mIL-10; DE2); the positive-feedback thresholder construct pAS67, encoding the constitutive HSV-TK promoter-driven Gal4-myc expression unit ($P_{HSV\text{-}TK}$-G-myc); the inducible OFF-switch construct pAS58, encoding constitutive CMV-promoter-driven rtTR-NLS-KRAB expression (P_{CMV}-rtTR-NLS-KRAB); the luciferase reporter construct pAS51, encoding the TRE-UAS-P_{MIN}-driven luciferase expression unit (TRE-UAS-P_{MIN}-Luc); and the SEAP reporter construct pAS72, encoding the TRE-UAS-P_{MIN}-driven SEAP expression unit (TRE-UAS-P_{MIN}-SEAP).

Cell Culture and Transfection

The HEK293T cell line (American Type Culture Collection) was cultured in DMEM+GlutaMAX-I medium (Invitrogen) (supplemented with 10% fetal bovine serum) (BioWhittaker) at 37°C in a 5% CO_2 humidified atmosphere. At 50%–70% confluence, cells were transfected with a mixture of DNA and JetPEI (Polyplus-transfection) according to the manufacturer's instructions.

Inducer Molecules

For in vitro experiments, doxycycline hyclate (Sigma-Aldrich; D9891) was dissolved in MQ at a concentration of 0.1 mg/mL, sterile filtered, and used at a final concentration of 1 μg/mL. For in vivo experiments, doxycycline was dissolved in PBS at 5 mg/mL (pH 7.3), sterile filtered, and used at a final concentration of 20 mg/kg. Human IL-1β and human TNF-α (R&D Systems) were used at a final concentration of 1 ng/mL in the in vitro experiments and at 250 ng/mouse in the in vivo experiments, unless stated otherwise.

Transfection and Dual Luciferase Assay

The HEK293T cells (2×10^4 cells per well) were seeded into CoStar White 96-well plates (Corning). At a confluence of 50%–70%, cells were transfected with a mixture of DNA and JetPEI (Polyplus-transfection) according to the manufacturer's instructions. Detailed information about the transfected plasmids and their amount in a specific experiment are provided in Table S2. After 24 hr, cells were activated as stated in the specific experiment. After 24 or 48 hr, cells were harvested and lysed with 30 μL of 1× passive lysis buffer (Promega). Firefly luciferase and *Renilla* luciferase expression were measured using a dual luciferase assay (Promega) and an Orion II microplate reader (Berthold Technologies). The relative luciferase activity was calculated by normalizing each sample's firefly luciferase activity to the constitutive *Renilla* luciferase activity determined in the same sample.

Stimulation with Human Serum

Human serum was collected from four healthy individuals and from a patient with a sJIA. Pooled serum samples (n = 4) from healthy individuals were tested along with the serum from a patient in a 1:1 dilution for the anti-inflammatory device activation according to the protocol described in Transfection and Dual Luciferase Assay (for information about the transfected plasmids, see Table S2). Written informed consent for obtaining blood samples from healthy controls and from a patient was obtained. Principles of the Declaration of Helsinki were followed, and the Slovenian National Medical Ethics Committee approved the study (decree number 29_2_13).

SEAP Detection

Human placental SEAP levels were determined in cell culture supernatants using a QUANTI-Blue assay (InvivoGen) according to the manufacturer's instructions. Briefly, 30 μL of supernatant was added to 200 μL of pre-warmed (37°C), sterile-filtered QUANTI-Blue reagent solution. After 15 min, the absorbance was measured at 630 nm using a Synergy Mx automated microplate reader (BioTec). The SEAP levels in blood samples and peritoneal lavage fluid of the mice were quantified using a chemiluminescence-based assay (Great EscAPe SEAP Chemiluminescence Kit 2.0; Clontech) according to the manufacturer's instructions, with a few adaptations. Briefly, 5 μL of serum or 15 μL of peritoneal lavage fluid was mixed with 95 or 85 μL of a 1× dilution buffer, respectively, and incubated for 30 min at 65°C to heat inactivate endogenous phosphatases. After cooling to room temperature (22°C), 100 μL of substrate solution was added. After 10 min, the samples were centrifuged (2 min, 20,000 × *g*), and 100 μL of the supernatant was transferred to CoStar White 96-well plates (Corning). Thirty minutes after the addition of the substrate solution, the luminescence was measured with an Orion II microplate reader (Berthold Technologies). As an internal control, the activity of the constitutive secretory *Renilla* luciferase SR-Luc (pFLAG-CMV3-R-Luc; pAS75, Table S1) was measured in 50 μL of the same sample.

Microencapsulation

The cells were microencapsulated in 400-μm alginate-PLL-alginate microcapsules (approximately 200 cells/microcapsule) using the Encapsulator Biotech (Büchi), according to the manufacturer's protocol and as previously described.[62] The following settings were applied: a 200 μM single nozzle, a 20-mL syringe with a flow of 19 mL/min, a vibration frequency of 1,200 Hz, an electrostatic dispersion of 1,300 V, and a stirrer speed of 200 rpm. We used 1.4% ultrapure alginate (PRONOVA UP LVG; Novamatrix) and 0.04% poly-L-lysine hydrobromide (molecular weight [mol wt], 15.000-30.000 PLL; Sigma-Aldrich; P7890). The microencapsulated cells were used for in vitro or in vivo experiments.

Confocal Fluorescence Microscopy

To directly observe the system's performance in vitro, HEK293T cells were seeded onto eight-well microscopic chambers (Ibidi) at a density of 5×10^4 cells per well. Cells were transfected with the constructs pAS97 (to observe the sensor's activity) and/or pAS98 (to observe the amplifier's activity), pAS72, pAS67, pAS58, pAS75, and pmCherry-C1 (Table S1). Twenty-four hours after transfection, the system was stimulated with human IL-1β (R&D Systems) at a final concentration of 1 ng/mL. Four hours after stimulation, the medium was removed and the cells were washed three times using fresh medium to remove input signal. After 24 hr, the responsiveness of the system was visualized, and microscopic images were acquired using a Leica TCS SP5 inverted laser-scanning microscope on a Leica DMI 6000 CS module equipped with a HCX PL Fluotar L (20×; numerical aperture, 0.4) (Leica Microsystems).

Quantification and Biological Activity of Anti-inflammatory Proteins

Supernatants from cell cultures or in vivo samples (the preparation of the serum and peritoneal lavage fluid was as described in Animal Models) were collected, and protein levels were measured with a sandwich ELISA (eBioscience). hIL-1RA was detected with a human IL-1RA Platinum ELISA (eBioscience; BMS2080), anti-hTNF-α antibody was detected with a human IgG1 Platinum ELISA (eBioscience; BMS2092TWO), and mouse IL-10 was detected with a mouse IL-10 ELISA Ready-SET-Go! (2nd Generation) (eBioscience; 88-7105-22). The biological activity of the hIL-1RA and anti-hTNF-α antibody was determined by competitive inhibition of hIL-1β and hTNF-α signaling through the NF-κB promoter. First, hIL-1RA and anti-hTNF-α antibody were produced in supernatants of HEK293T cells, transfected with constitutive promoter-driven expression form pAS35 and pAS114 (Table S1), respectively. We transfected the reporter cell line HEK293T with pAS40 and phRL-TK (Table S1) to observe NF-κB-driven luciferase activity. The cells were stimulated with 20 ng/mL hIL-1β or hTNF-α for 24 hr, to which we added (simultaneously or with 30-min preincubation) the titrated supernatant, containing anti-inflammatory proteins to observe the molar ratio-dependent decrease in luciferase activity. Recombinant human IL-1RA (Sigma-Aldrich; SRP3084) and anti-hTNF-α-hIgG1 (InvivoGen; htnfa-mab1) were used as controls.

Animal Models

For the all in vivo experiments, 8- to 10-week-old C57BL/6JOlaHsd mice of mixed sexes (evenly distributed between the groups) were used. The numbers of mice are stated in the figure captions.

The microcapsules were produced as described in Microencapsulation. A 1:1 suspension of microcapsules with MOPS buffer (10 mM MOPS, 0.85% NaCl) was prepared and 700 μL were injected i.p. into the mice using a 20G needle (10,000 microcapsules per mouse, 200 cells per microcapsule), as described previously.[62]

To determine the responsiveness of the synthetic anti-inflammatory device to an inflammatory signal in vivo (for information on the transfected plasmids, see Table S2), we injected mice i.p. with 300 ng of hIL-1β per mouse or 250 ng of hTNF-α per mouse 1 and 24 hr after implantation. Serum was collected using Multivette 600 (Sarstedt; 3,000 rpm, 30 min) 24 and 48 hr later, and peritoneal lavage fluid was collected after 48 hr (5 mL of PBS). We tested the peritoneal lavage fluid for system activation ex vivo.

To demonstrate activation of the anti-inflammatory device by endogenous mouse cytokines, we performed CLP model following the described method.[32,63] In Figure 4A, we collected peritoneal lavage fluid 24 hr after CLP procedure; in Figure 4F, we performed CLP 1 day before, and in Figure 5D, 3 hr before microcapsules implantation.

For the in vivo restraint (Figure 6B) (see Table S2 for information on the transfected plasmids used in the study), the mice were first injected i.p. with a combination of 300 ng of hIL-1β and 250 ng of hTNF-α per mouse 1 hr after implantation. After 1 hr and every 24 hr, 20 mg/kg of Dox was injected intravenously (i.v.).

For the in vivo shut down (Figures 6C and 6D) (see Table S2 for information on the transfected plasmids used in the study), the mice were first injected i.p. with a combination of 300 ng of hIL-1β and 250 ng of hTNF-α per mouse 1 hr after implantation. After 24 hr (Figures 6C and 6D) and in addition after 72 hr (Figure 6C), 20 mg/kg of Dox was injected i.v. In the case of Figure 6C, at 72-hr time point, the mice in ON and OFF groups were injected i.p. also with a combination of 300 ng of hIL-1β and 250 ng of hTNF-α per mouse simultaneously with Dox injection. Serum was collected, and anti-hTNF-α and mIL-10 concentrations were profiled. Control values were subtracted from the ON and OFF state, and results were represented as a percentage of a fully activated system (raw data are presented in Figures S6C and S6D).

For the in vivo reactivation (Figure 6E) (see Table S2 for information on the transfected plasmids used in the study), 20 mg/kg of Dox was injected i.v. into mice 1 hr after implantation. After 72 hr, the system was activated by a single application of 300 ng of hIL-1β and 250 ng of hTNF-α per mouse, and peritoneal lavage fluid was collected 120 hr after implantation.

To produce therapeutic anti-inflammatory proteins in vivo, the mice were injected i.p. with a combination of 500 ng of hIL-1β and 250 ng of hTNF-α per mouse 1 hr after implantation. After 48 hr, serum and peritoneal lavage fluid were collected.

The application of the anti-inflammatory device in vivo was then demonstrated in an acute murine colitis model.[64] The mice were given either water or 2% DSS (T*dB* Consultancy, DB001-31) for 8 days as previously described, and on the fifth day (Figure 7, except for D) of this time-course experimental model, the microcapsules containing anti-inflammatory device-engineered cells were implanted i.p. The control groups without microcapsules received 700 μL of MOPS buffer. One hour after implantation and then daily, the mice were injected i.p. with a combination of 300 ng of hIL-1β and 250 ng of hTNF-α per mouse. Weight, stool blood, and stool consistency were monitored daily. Disease activity index (DAI) was determined by combining the stool blood and stool consistency scores. Each score was determined as follows: stool blood, 0–2 (0, no blood; 1, hemoocult bleeding; 2, gross bleeding); and stool consistency, 0–2 (0, normal stool; 1, soft stool; 2, diarrhea). Upon the sacrifice of the mice, the colon length was measured from the body of the caecum to the distal part of the rectum. Histological samples of the sacrificed mice were fixated overnight in 10% neutral buffered formalin (Sigma-Aldrich; HT501128) and then embedded in paraffin (Leica; Paraplast; 39601006). The paraffin blocks were cut 7 μm thick with a rotation microtome RM 2245 (Leica; 1492245UL01) and stained with hematoxylin and eosin (Sigma-Aldrich; MHS32; HT110332). The histological score was determined as previously described: formation of ulcus, 0–4; epithelium morphology, 0–4; immune cell infiltration, 0–4; and lymph follicles, 0–4.[65] Alternatively, the microcapsules were implanted on the third day after DSS exposure (Figure 7D). In this case, the control group comprised full anti-inflammatory system that was initially activated by injecting the mice with a combination of 300 ng of hIL-1β and 250 ng of hTNF-α per mouse, and the activation of the circuit was simultaneously restrained by a daily i.v. Dox injection (20 mg/kg). All of the animal experiments were performed according to the directives of the EU 2010/63, approved by the Ministry of Agriculture, Forestry, and Foods, Republic of Slovenia (no. U34401-55/2013/6).

Mathematical Model and Simulations

The mathematical model and simulations are explained in detail in Supplemental Mathematical Model. Briefly, the mathematical model was generated using CellDesigner 4.4 software[23] by first constructing a state transition diagram and describing the transitions with ODEs according to mass action kinetics. The initial quantities of genetic constructs were approximated by estimating the efficiency of transient transfection. The input signal for the modeled genetic device was the NF-κB particle number, and the output signal was the effector protein particle number. The simulations were run with the CellDesigner 4.4 software using an integrated SBML ODE Solver.[66]

Statistics

Representative experiments are shown. All values are represented as the mean ± SD, except for in Figures 7C and 7F, where the mean ± SEM is shown. The data were analyzed with two-tailed Student's t test assuming unequal variances, except in Figure 7F, where a Mann-Whitney U test was used. p values are shown for each comparison of interest.

SUPPLEMENTAL INFORMATION

Supplemental Information includes Supplemental Materials and Methods, seven figures, five tables, and can be found with this article online at http://dx.doi.org/10.1016/j.ymthe.2016.10.005.

AUTHOR CONTRIBUTIONS

R.J. conceived and supervised the study. A.S. and R.J. designed the experiments, with the help of D.L., U.B., and S.H. A.S., D.L., and U.B. performed the experimental work. A.S., D.L., U.B., S.H., and R.J. analyzed and discussed the results. D.L. and S.H., with the assistance of A.S., performed the in vivo experimental work. U.B. designed the mathematical model and performed the simulations. A.S. and R.J. wrote the manuscript, with help from D.L., U.B., and S.H. A.S., D.L., U.B., S.H., and R.J. discussed and commented on the manuscript before submission.

CONFLICTS OF INTEREST

The authors declare no conflicts of interest.

ACKNOWLEDGMENTS

We thank the Slovenian Research Agency (grants P4-0176 and J1-6740) and EN-FIST Centre of Excellence for their financial support. We thank Luka Smole for help with introducing microencapsulation technology in our laboratory. We thank Dr. Mojca Benčina and Dr. Jelka Pohar for help with the confocal fluorescence microscopy. We thank Lucija Kadunc for help with preparing the implant membrane hollow fibers. We thank Professor Dr. Martin Fussenegger (Institute of Biotechnology, Swiss Federal Institute of Technology), Dr. Rok Gaber, Dr. Jelka Pohar, Dr. Slavko Čeru, and Jan Lonzarić for fruitful discussions. We thank Karen Butina for suggestions with the statistical analysis and Robert Bremšak, Darija Oven, and Irena Škraba for technical support. We thank Vesna Mrak for maintenance of the mouse colony. We thank Professor Dr. Tadej Avčin, MD (University Children's Hospital, University Medical Centre Ljubljana, Department of Allergology, Rheumatology and Clinical Immunology; Faculty of Medicine, University of Ljubljana), and Professor Dr. Uroš Potočnik (Faculty of Medicine, Centre for Human Molecular Genetics and Pharmacogenomics, University of Maribor; Faculty for Chemistry and Chemical Engineering, Laboratory for Biochemistry, Molecular Biology and Genomics, University of Maribor) for providing human blood samples.

REFERENCES

1. Medzhitov, R. (2008). Origin and physiological roles of inflammation. Nature *454*, 428–435.

2. Dempsey, P.W., Vaidya, S.A., and Cheng, G. (2003). The art of war: innate and adaptive immune responses. Cell. Mol. Life Sci. *60*, 2604–2621.

3. Clark, R., and Kupper, T. (2005). Old meets new: the interaction between innate and adaptive immunity. J. Invest. Dermatol. *125*, 629–637.

4. Dinarello, C.A. (2010). Anti-inflammatory agents: present and future. Cell *140*, 935–950.
5. El-Gabalawy, H., Guenther, L.C., and Bernstein, C.N. (2010). Epidemiology of immune-mediated inflammatory diseases: incidence, prevalence, natural history, and comorbidities. J. Rheumatol. Suppl. *85*, 2–10.
6. Steidler, L., Hans, W., Schotte, L., Neirynck, S., Obermeier, F., Falk, W., Fiers, W., and Remaut, E. (2000). Treatment of murine colitis by *Lactococcus lactis* secreting interleukin-10. Science *289*, 1352–1355.
7. Vandenbroucke, K., de Haard, H., Beirnaert, E., Dreier, T., Lauwereys, M., Huyck, L., Van Huysse, J., Demetter, P., Steidler, L., Remaut, E., et al. (2010). Orally administered *L. lactis* secreting an anti-TNF Nanobody demonstrate efficacy in chronic colitis. Mucosal Immunol. *3*, 49–56.
8. Archer, E.J., Robinson, A.B., and Süel, G.M. (2012). Engineered *E. coli* that detect and respond to gut inflammation through nitric oxide sensing. ACS Synth. Biol. *1*, 451–457.
9. Ye, H., Aubel, D., and Fussenegger, M. (2013). Synthetic mammalian gene circuits for biomedical applications. Curr. Opin. Chem. Biol. *17*, 910–917.
10. Ausländer, S., Wieland, M., and Fussenegger, M. (2012). Smart medication through combination of synthetic biology and cell microencapsulation. Metab. Eng. *14*, 252–260.
11. Murua, A., Portero, A., Orive, G., Hernández, R.M., de Castro, M., and Pedraz, J.L. (2008). Cell microencapsulation technology: towards clinical application. J. Control. Release *132*, 76–83.
12. Kemmer, C., Gitzinger, M., Daoud-El Baba, M., Djonov, V., Stelling, J., and Fussenegger, M. (2010). Self-sufficient control of urate homeostasis in mice by a synthetic circuit. Nat. Biotechnol. *28*, 355–360.
13. Rössger, K., Charpin-El-Hamri, G., and Fussenegger, M. (2013). A closed-loop synthetic gene circuit for the treatment of diet-induced obesity in mice. Nat. Commun. *4*, 2825.
14. Ausländer, D., Ausländer, S., Charpin-El Hamri, G., Sedlmayer, F., Müller, M., Frey, O., Hierlemann, A., Stelling, J., and Fussenegger, M. (2014). A synthetic multifunctional mammalian pH sensor and CO_2 transgene-control device. Mol. Cell *55*, 397–408.
15. Schukur, L., Geering, B., Charpin-El Hamri, G., and Fussenegger, M. (2015). Implantable synthetic cytokine converter cells with AND-gate logic treat experimental psoriasis. Sci. Transl. Med. *7*, 318ra201.
16. Miyoshi, J., Hisamatsu, T., Matsuoka, K., Naganuma, M., Maruyama, Y., Yoneno, K., Mori, K., Kiyohara, H., Nanki, K., Okamoto, S., et al. (2014). Early intervention with adalimumab may contribute to favorable clinical efficacy in patients with Crohn's disease. Digestion *90*, 130–136.
17. Fascì Spurio, F., Aratari, A., Margagnoni, G., Doddato, M.T., and Papi, C. (2012). Early treatment in Crohn's disease: do we have enough evidence to reverse the therapeutic pyramid? J. Gastrointestin. Liver Dis. *21*, 67–73.
18. Nigrovic, P.A., Mannion, M., Prince, F.H.M., Zeft, A., Rabinovich, C.E., van Rossum, M.A.J., Cortis, E., Pardeo, M., Miettunen, P.M., Janow, G., et al. (2011). Anakinra as first-line disease-modifying therapy in systemic juvenile idiopathic arthritis: report of forty-six patients from an international multicenter series. Arthritis Rheum. *63*, 545–555.
19. Sadowski, I., Ma, J., Triezenberg, S., and Ptashne, M. (1988). GAL4-VP16 is an unusually potent transcriptional activator. Nature *335*, 563–564.
20. Ruland, J. (2011). Return to homeostasis: downregulation of NF-κB responses. Nat. Immunol. *12*, 709–714.
21. Chen, F.E., Huang, D.B., Chen, Y.Q., and Ghosh, G. (1998). Crystal structure of p50/p65 heterodimer of transcription factor NF-kappaB bound to DNA. Nature *391*, 410–413.
22. Hellweg, C.E., Arenz, A., Bogner, S., Schmitz, C., and Baumstark-Khan, C. (2006). Activation of nuclear factor κ B by different agents: influence of culture conditions in a cell-based assay. Ann. N Y Acad. Sci. *1091*, 191–204.
23. Funahashi, A., Morohashi, M., Kitano, H., and Tanimura, N. (2003). CellDesigner: a process diagram editor for gene-regulatory and biochemical networks. Biosilico *1*, 159–162.
24. Szulc, J., Wiznerowicz, M., Sauvain, M.O., Trono, D., and Aebischer, P. (2006). A versatile tool for conditional gene expression and knockdown. Nat. Methods *3*, 109–116.
25. Groner, A.C., Meylan, S., Ciuffi, A., Zangger, N., Ambrosini, G., Dénervaud, N., Bucher, P., and Trono, D. (2010). KRAB-zinc finger proteins and KAP1 can mediate long-range transcriptional repression through heterochromatin spreading. PLoS Genet. *6*, e1000869.
26. Kleiner, G., Marcuzzi, A., Zanin, V., Monasta, L., and Zauli, G. (2013). Cytokine levels in the serum of healthy subjects. Mediators Inflamm. *2013*, 434010.
27. Lyke, K.E., Burges, R., Cissoko, Y., Sangare, L., Dao, M., Diarra, I., Kone, A., Harley, R., Plowe, C.V., Doumbo, O.K., and Sztein, M.B. (2004). Serum levels of the proinflammatory cytokines interleukin-1 beta (IL-1beta), IL-6, IL-8, IL-10, tumor necrosis factor alpha, and IL-12(p70) in Malian children with severe *Plasmodium falciparum* malaria and matched uncomplicated malaria or healthy controls. Infect. Immun. *72*, 5630–5637.
28. Manicourt, D.H., Triki, R., Fukuda, K., Devogelaer, J.-P., Nagant de Deuxchaisnes, C., and Thonar, E.J. (1993). Levels of circulating tumor necrosis factor α and interleukin-6 in patients with rheumatoid arthritis. Relationship to serum levels of hyaluronan and antigenic keratan sulfate. Arthritis Rheum. *36*, 490–499.
29. Lopez-Castejon, G., and Brough, D. (2011). Understanding the mechanism of IL-1β secretion. Cytokine Growth Factor Rev. *22*, 189–195.
30. Kudo, S., Mizuno, K., Hirai, Y., and Shimizu, T. (1990). Clearance and tissue distribution of recombinant human interleukin 1 beta in rats. Cancer Res. *50*, 5751–5755.
31. Pascual, V., Allantaz, F., Arce, E., Punaro, M., and Banchereau, J. (2005). Role of interleukin-1 (IL-1) in the pathogenesis of systemic onset juvenile idiopathic arthritis and clinical response to IL-1 blockade. J. Exp. Med. *201*, 1479–1486.
32. Dejager, L., Pinheiro, I., Dejonckheere, E., and Libert, C. (2011). Cecal ligation and puncture: the gold standard model for polymicrobial sepsis? Trends Microbiol. *19*, 198–208.
33. Abbott Biotechnology, Ltd. July 2000. Human antibodies that bind human TNFα. U.S. patent 6,090,382.
34. Fang, J., Qian, J.-J., Yi, S., Harding, T.C., Tu, G.H., VanRoey, M., and Jooss, K. (2005). Stable antibody expression at therapeutic levels using the 2A peptide. Nat. Biotechnol. *23*, 584–590.
35. Dall'Acqua, W.F., Woods, R.M., Ward, E.S., Palaszynski, S.R., Patel, N.K., Brewah, Y.A., Wu, H., Kiener, P.A., and Langermann, S. (2002). Increasing the affinity of a human IgG1 for the neonatal Fc receptor: biological consequences. J. Immunol. *169*, 5171–5180.
36. Liu, M., Huang, Y., Hu, L., Liu, G., Hu, X., Liu, D., and Yang, X. (2012). Selective delivery of interleukine-1 receptor antagonist to inflamed joint by albumin fusion. BMC Biotechnol. *12*, 68.
37. Petrasek, J., Bala, S., Csak, T., Lippai, D., Kodys, K., Menashy, V., Barrieau, M., Min, S.Y., Kurt-Jones, E.A., and Szabo, G. (2012). IL-1 receptor antagonist ameliorates inflammasome-dependent alcoholic steatohepatitis in mice. J. Clin. Invest. *122*, 3476–3489.
38. Li, L., Elliott, J.F., and Mosmann, T.R. (1994). IL-10 inhibits cytokine production, vascular leakage, and swelling during T helper 1 cell-induced delayed-type hypersensitivity. J. Immunol. *153*, 3967–3978.
39. Salucci, V., Scarito, A., Aurisicchio, L., Lamartina, S., Nicolaus, G., Giampaoli, S., Gonzalez-Paz, O., Toniatti, C., Bujard, H., Hillen, W., et al. (2002). Tight control of gene expression by a helper-dependent adenovirus vector carrying the rtTA2(s)-M2 tetracycline transactivator and repressor system. Gene Ther. *9*, 1415–1421.
40. Böcker, R., Estler, C.J., Maywald, M., and Weber, D. (1981). Comparison of distribution of doxycycline in mice after oral and intravenous application measured by a high-performance liquid chromatographic method. Arzneimittelforschung *31*, 2116–2117.
41. Ruder, W.C., Lu, T., and Collins, J.J. (2011). Synthetic biology moving into the clinic. Science *333*, 1248–1252.
42. Fischbach, M.A., Bluestone, J.A., and Lim, W.A. (2013). Cell-based therapeutics: the next pillar of medicine. Sci. Transl. Med. *5*, 179ps7.
43. Molodecky, N.A., Soon, I.S., Rabi, D.M., Ghali, W.A., Ferris, M., Chernoff, G., Benchimol, E.I., Panaccione, R., Ghosh, S., Barkema, H.W., and Kaplan, G.G.

(2012). Increasing incidence and prevalence of the inflammatory bowel diseases with time, based on systematic review. Gastroenterology *142*, 46–54.e42, quiz e30.

44. Strober, W., and Fuss, I.J. (2011). Proinflammatory cytokines in the pathogenesis of inflammatory bowel diseases. Gastroenterology *140*, 1756–1767.

45. Ford, A.C., Sandborn, W.J., Khan, K.J., Hanauer, S.B., Talley, N.J., and Moayyedi, P. (2011). Efficacy of biological therapies in inflammatory bowel disease: systematic review and meta-analysis. Am. J. Gastroenterol. *106*, 644–659, quiz 660.

46. Qian, L., Winfree, E., and Bruck, J. (2011). Neural network computation with DNA strand displacement cascades. Nature *475*, 368–372.

47. Lee, T.-H.H., and Maheshri, N. (2012). A regulatory role for repeated decoy transcription factor binding sites in target gene expression. Mol. Syst. Biol. *8*, 576.

48. Lu, M.S., Mauser, J.F., and Prehoda, K.E. (2013). Ultrasensitive synthetic protein regulatory networks using mixed decoys. ACS Synth Biol. *16*, 65–72.

49. Mishra, D., Rivera, P.M., Lin, A., Del Vecchio, D., and Weiss, R. (2014). A load driver device for engineering modularity in biological networks. Nat. Biotechnol. *32*, 1268–1275.

50. Sasaki, M., Mathis, J.M., Jennings, M.H., Jordan, P., Wang, Y., Ando, T., Joh, T., and Alexander, J.S. (2005). Reversal of experimental colitis disease activity in mice following administration of an adenoviral IL-10 vector. J. Inflamm. (Lond.) *2*, 13.

51. Kotula, J.W., Kerns, S.J., Shaket, L.A., Siraj, L., Collins, J.J., Way, J.C., and Silver, P.A. (2014). Programmable bacteria detect and record an environmental signal in the mammalian gut. Proc. Natl. Acad. Sci. USA *111*, 4838–4843.

52. Navaneethan, U., Venkatesh, P.G.K., and Shen, B. (2010). *Clostridium difficile* infection and inflammatory bowel disease: understanding the evolving relationship. World J. Gastroenterol. *16*, 4892–4904.

53. Shih, D.Q., and Targan, S.R. (2008). Immunopathogenesis of inflammatory bowel disease. World J. Gastroenterol. *14*, 390–400.

54. Mann, E.A., and Saeed, S.A. (2012). Gastrointestinal infection as a trigger for inflammatory bowel disease. Curr. Opin. Gastroenterol. *28*, 24–29.

55. Kichler, A., Leborgne, C., Coeytaux, E., and Danos, O. (2001). Polyethylenimine-mediated gene delivery: a mechanistic study. J. Gene Med. *3*, 135–144.

56. Oh, Y.-K., Suh, D., Kim, J.M., Choi, H.-G., Shin, K., and Ko, J.J. (2002). Polyethylenimine-mediated cellular uptake, nucleus trafficking and expression of cytokine plasmid DNA. Gene Ther. *9*, 1627–1632.

57. Jacobs-Tulleneers-Thevissen, D., Chintinne, M., Ling, Z., Gillard, P., Schoonjans, L., Delvaux, G., Strand, B.L., Gorus, F., Keymeulen, B., and Pipeleers, D.; Beta Cell Therapy Consortium EU-FP7 (2013). Sustained function of alginate-encapsulated human islet cell implants in the peritoneal cavity of mice leading to a pilot study in a type 1 diabetic patient. Diabetologia *56*, 1605–1614.

58. Buder, B., Alexander, M., Krishnan, R., Chapman, D.W., and Lakey, J.R. (2013). Encapsulated islet transplantation: strategies and clinical trials. Immune Netw. *13*, 235–239.

59. Soon-Shiong, P., Heintz, R.E., Merideth, N., Yao, Q.X., Yao, Z., Zheng, T., Murphy, M., Moloney, M.K., Schmehl, M., Harris, M., et al. (1994). Insulin independence in a type 1 diabetic patient after encapsulated islet transplantation. Lancet *343*, 950–951.

60. Krishnan, R., Alexander, M., Robles, L., Foster, C.E., 3rd, and Lakey, J.R.T. (2014). Islet and stem cell encapsulation for clinical transplantation. Rev. Diabet. Stud. *11*, 84–101.

61. Geering, B., and Fussenegger, M. (2015). Synthetic immunology: modulating the human immune system. Trends Biotechnol. *33*, 65–79.

62. Weber, W., Fux, C., Daoud-el Baba, M., Keller, B., Weber, C.C., Kramer, B.P., Heinzen, C., Aubel, D., Bailey, J.E., and Fussenegger, M. (2002). Macrolide-based transgene control in mammalian cells and mice. Nat. Biotechnol. *20*, 901–907.

63. Rittirsch, D., Huber-Lang, M.S., Flierl, M.A., and Ward, P.A. (2009). Immunodesign of experimental sepsis by cecal ligation and puncture. Nat. Protoc. *4*, 31–36.

64. Wirtz, S., Neufert, C., Weigmann, B., and Neurath, M.F. (2007). Chemically induced mouse models of intestinal inflammation. Nat. Protoc. *2*, 541–546.

65. Kojouharoff, G., Hans, W., Obermeier, F., Männel, D.N., Andus, T., Schölmerich, J., Gross, V., and Falk, W. (1997). Neutralization of tumour necrosis factor (TNF) but not of IL-1 reduces inflammation in chronic dextran sulphate sodium-induced colitis in mice. Clin. Exp. Immunol. *107*, 353–358.

66. Machné, R., Finney, A., Müller, S., Lu, J., Widder, S., and Flamm, C. (2006). The SBML ODE Solver Library: a native API for symbolic and fast numerical analysis of reaction networks. Bioinformatics *22*, 1406–1407.

YMTHE, Volume *25*

Supplemental Information

A Synthetic Mammalian Therapeutic Gene Circuit for Sensing and Suppressing Inflammation

Anže Smole, Duško Lainšček, Urban Bezeljak, Simon Horvat, and Roman Jerala

SUPPLEMENTARY FIGURES

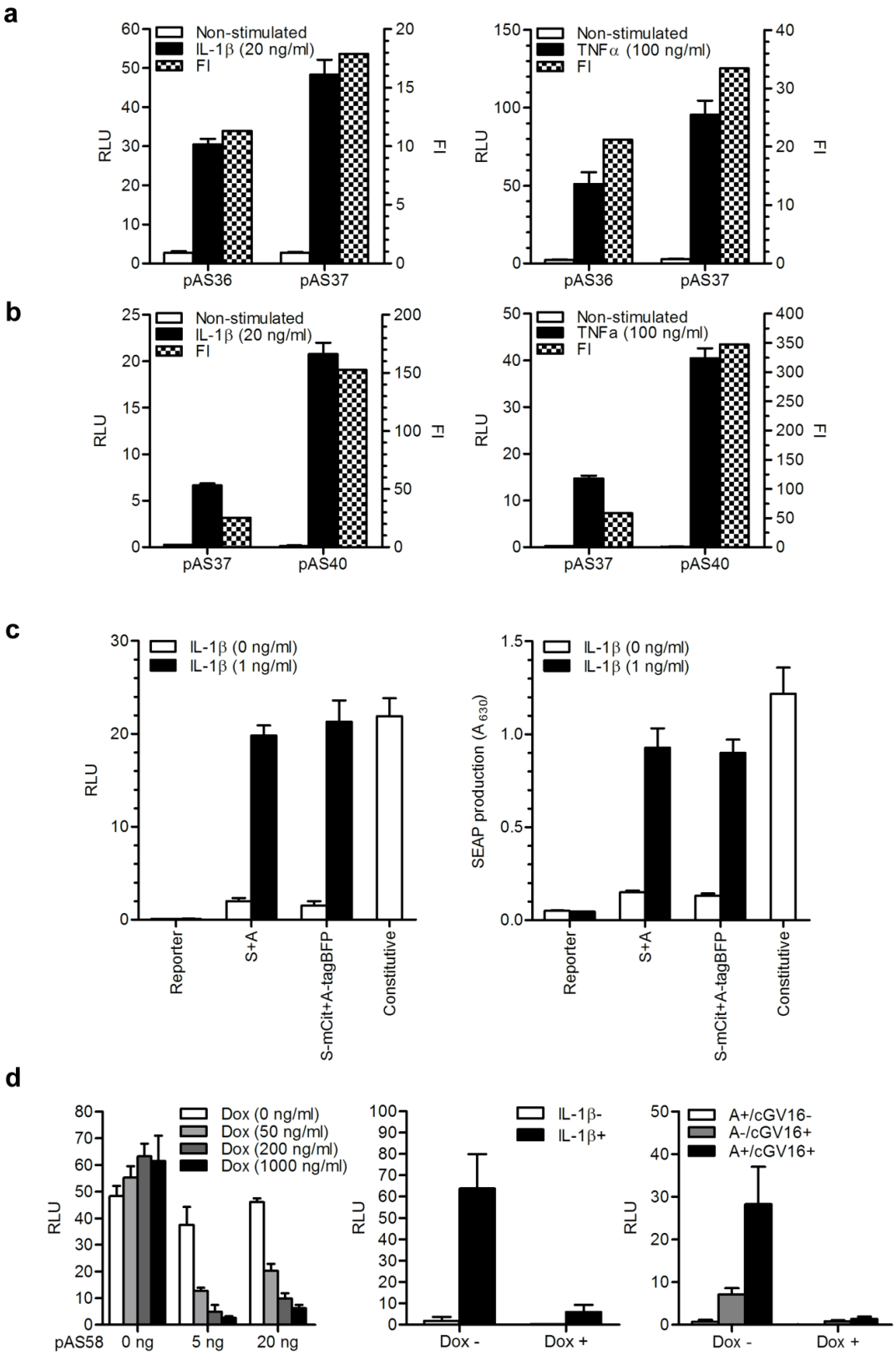

Supplementary Figure 1 Related to Figure 2

Tuning the elements used for constructing the anti-inflammatory device

(**a**) Optimization of NF-κB responsive element. HEK 293T cells were transfected with pAS36 or pAS37 and stimulated with 20 ng/mL IL-1β (left) or 100 ng/mL TNFα (right). After 24 h luciferase activity was measured by dual luciferase test.

(**b**) Optimization of a minimal promoter. HEK 293T cells were transfected with pAS37 or pAS40 and stimulated with 20 ng/mL IL-1β (left) or 100 ng/mL TNFα (right). After 24 h luciferase activity was measured by dual luciferase test.

(**c**) The capacity of system activation. Activated anti-inflammatory device supports comparable reporter expression level to the constitutively expressed control (pAS108; P_{CMV}-Luc or pAS109; P_{CMV}-SEAP) as measured by luciferase (left) or SEAP (right). Similarly, sensor and amplifier constructs with 2A peptide-fluorescent protein fusions (pAS97; TRE-$P_{NF\text{-}κB2}$-P_{MIN}-GV16-myc-2A-mCit and pAS98; TRE-UAS-P_{MIN}-GV16-myc-2A-tagBFP) support comparable system activation to the basic sensor and amplifier. For detailed information about transfected plasmids and their amounts in each specific experiment, see Supplementary table 1 and 2, respectively. Error bars indicate s.d. (*n*=4).

(**d**) Validation of the rtTR-KRAB reset repressor. The constitutively expressed rtTR-KRAB (pAS58; P_{hCMV}-rtTR-NLS-KRAB) represses Gal4-VP16 (plasmid pSGVP)-induced activation of the reporter construct (pAS51; TRE-UAS-P_{MIN}-Luc) in the presence of the increasing concentrations of doxycycline (Dox). In the absence of Dox, pAS58 alone did not significantly influence system activation (left). Activated sensor (middle) and amplifier (right) can also be shut down efficiently.

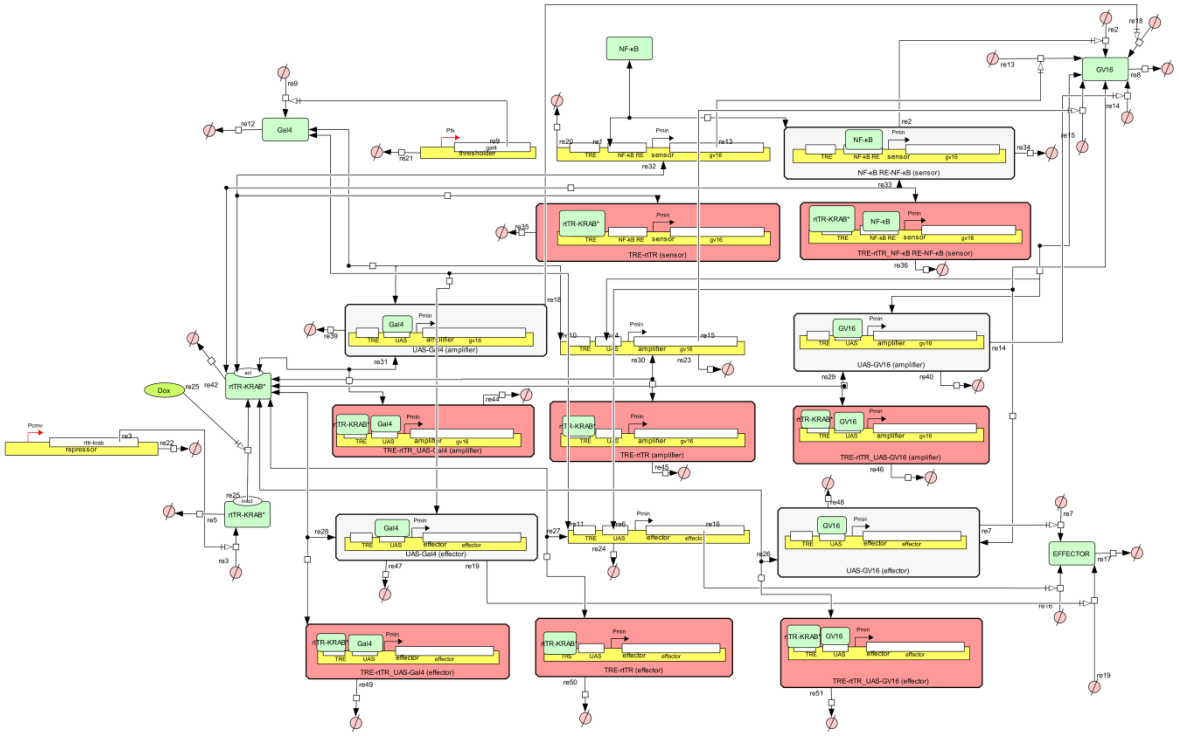

Supplementary Figure 2 Related to the Matematical ODE model

State transition diagram of the genetic circuit.

The state transition diagram of the genetic circuit was constructed using CellDesigner 4.4 software[13]. The state transitions were described with reactions listed in Supplementary Table 5.

a

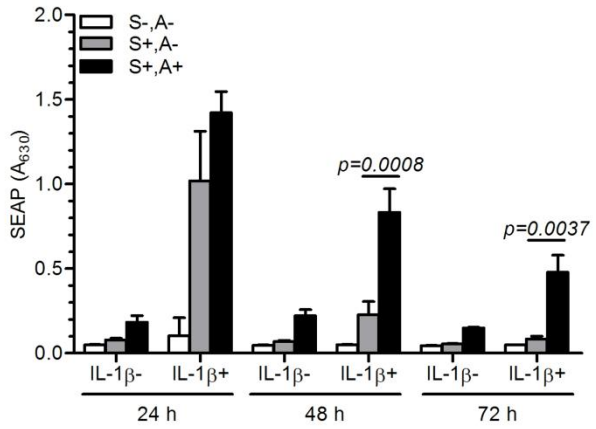
S-,A-
S+,A-
S+,A+
SEAP (A_{630})
2.0
1.5
1.0
0.5
0.0
p=0.0008
p=0.0037
IL-1β-
IL-1β+
IL-1β-
IL-1β+
IL-1β-
IL-1β+
24 h
48 h
72 h

b

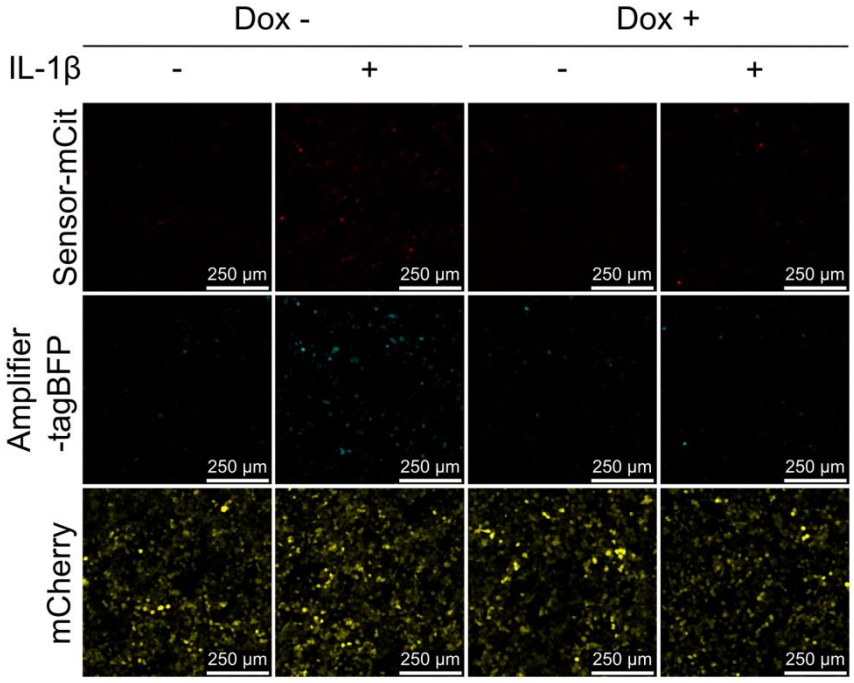
Dox -
Dox +
IL-1β
-
+
-
+
Sensor-mCit
Amplifier -tagBFP
mCherry
250 µm

c

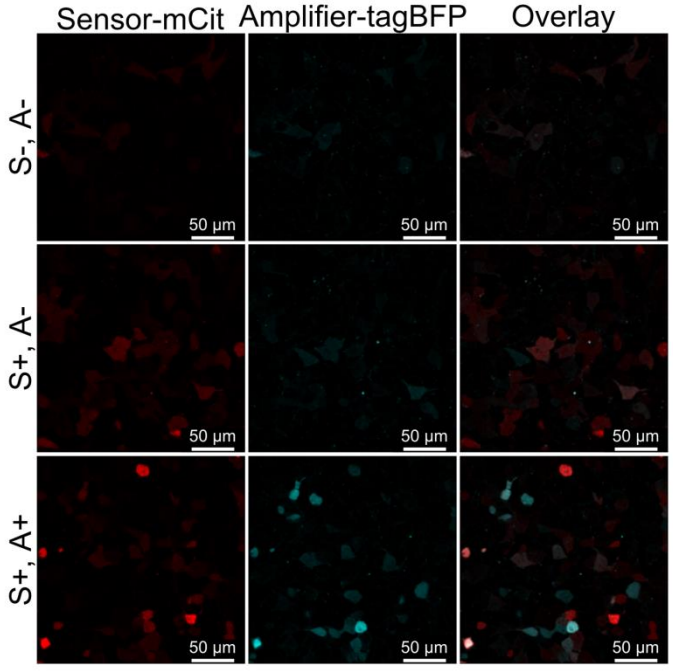
Sensor-mCit
Amplifier-tagBFP
Overlay
S-, A-
S+, A-
S+, A+
50 µm

Supplementary Figure 3 Related to Figure 3

(**a**) Anti-inflammatory device-engineered HEK 293T cells (reporter pAS72; TRE-UAS-P_{MIN}-SEAP) were stimulated with hIL-1β for 4 h and then input signal was removed by medium exchange. SEAP production was quantified in the culture supernatants every 24 h along with a medium exchange to observe kinetics of a system activation. Compared to sensor alone (grey bars), setup which included also amplifier construct (black bars) yielded stronger system activation at the later time points indicating its role in the sustained system activation. For detailed information about transfected plasmids and their amounts in each specific experiment, see the Tables S1 and S2, respectively. Error bars indicate s.d. (*n*=4).

(**b**) Demonstration of the system performance by a confocal fluorescence microscopy of anti-inflammatory device-engineered HEK 293T cells. Sensor and amplifier constructs were observed directly by in frame fusion via 2A peptide with mCitrine and tagBFP reporter genes, respectively (pAS97; TRE-$P_{NF\text{-}\kappa B2}$-P_{MIN}-GV16-myc-2A-mCit and pAS98; TRE-UAS-P_{MIN}-GV16-myc-2A-tagBFP). Twenty-four hours after stimulation, mCitrine and tagBFP positive cells were observed only in the presence of interleukin-1β (IL-1β) and absence of doxycycline (Dox). mCherry was used as a transfection control.

(**c**) System functionality is dependent on intracellular Gal4-VP16 transcriptional activator (GV16) meaning it is inevitable that sensor and enhancer are activated in the same cell. Cells were stimulated with IL-1β for 24 h and then observed by a confocal fluorescence microscopy to demonstrate the simultaneous activation of both constructs in the same cell. For detailed information about transfected plasmids and their amounts in each specific experiment, see the Supplementary Table 1 and 2, respectively. Error bars indicate s.d. (*n*=4).

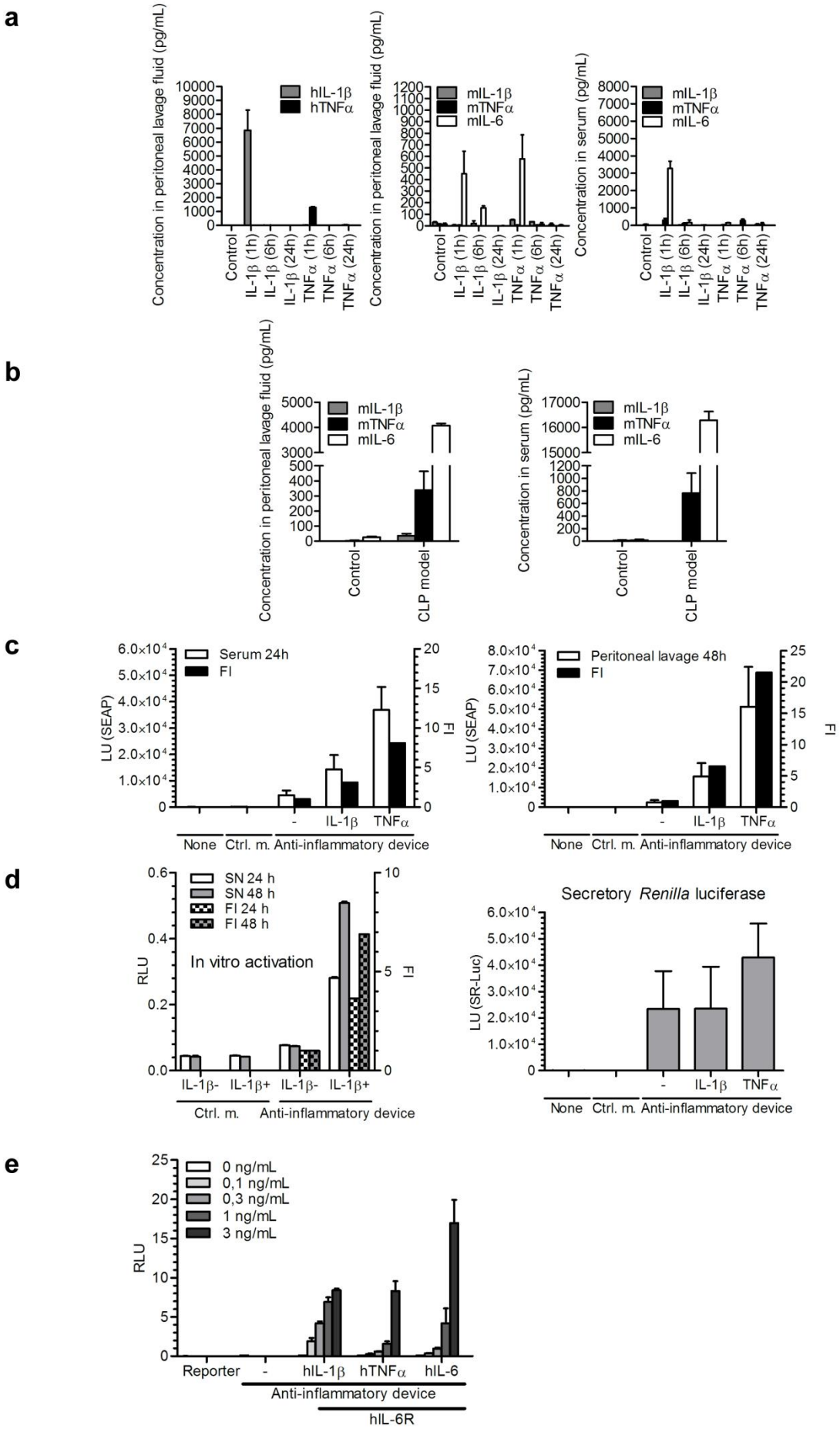
a
Concentration in peritoneal lavage fluid (pg/mL)
hIL-1β
hTNFα
Control
IL-1β (1h)
IL-1β (6h)
IL-1β (24h)
TNFα (1h)
TNFα (6h)
TNFα (24h)
Concentration in peritoneal lavage fluid (pg/mL)
mIL-1β
mTNFα
mIL-6
Concentration in serum (pg/mL)
b
Concentration in peritoneal lavage fluid (pg/mL)
Concentration in serum (pg/mL)
Control
CLP model
c
Serum 24h
FI
LU (SEAP)
Peritoneal lavage 48h
None
Ctrl. m.
Anti-inflammatory device
-
IL-1β
TNFα
d
SN 24 h
SN 48 h
FI 24 h
FI 48 h
In vitro activation
RLU
IL-1β-
IL-1β+
Secretory Renilla luciferase
LU (SR-Luc)
e
0 ng/mL
0,1 ng/mL
0,3 ng/mL
1 ng/mL
3 ng/mL
Reporter
hIL-1β
hTNFα
hIL-6
hIL-6R

Supplementary Figure 4 Related to Figure 4

(**a**) Concentration of human IL-1β and TNFα in peritoneal lavage fluid (left), mouse IL-1β, TNFα and IL-6 in peritoneal lavage fluid (middle) or serum (right) of mice, which were injected i.p. with human IL-1β (300 ng/mouse) or human TNFα (250 ng/mouse) and then sacrificed at different time points.

(**b**) Concentration of mouse IL-1β, TNFα and IL-6 in peritoneal lavage fluid (left) and serum (right) of mice 72 h after CLP procedure.

(**c**) SEAP levels in serum 24 h post implantation and in the peritoneal lavage fluid 48 h post implantation. For detailed information about transfected plasmids and their amounts in each specific experiment, see Supplementary table 1 and 2, respectively. Error bars indicate s.d.

(**d**) The response of the microencapsulated anti-inflammatory device *in vitro* prior to implantation in mice (left) and secretory *Renilla* luciferase (pAS75; SR-Luc) in peritoneal lavage fluid 48 h after microcapsules implantation. SR-Luc was co-transfected along with the anti-inflammatory device but not with the control microcapsules. SR-Luc is comparable among all groups (right).

(**e**) Validation of the chimeric NF-κB-STAT3 sensor. Cells were transfected with the constructs for the anti-inflammatory device, except for the sensor, where pAS60 (TRE-$P_{NF\text{-}\kappa B2}$-P_{MIN}-GV16-myc) was replaced by pAS132 (TRE-$P_{NF\text{-}\kappa B2\text{-}STAT3}$-$P_{MIN}$-GV16-myc). Cells were also transfected with hIL-6 receptor (hIL-6R) where indicated to enable responsiveness to human IL-6. For detailed information about transfected plasmids and their amounts in each specific experiment, see Supplementary table 1 and 2, respectively. Error bars indicate s.d. (n=4).

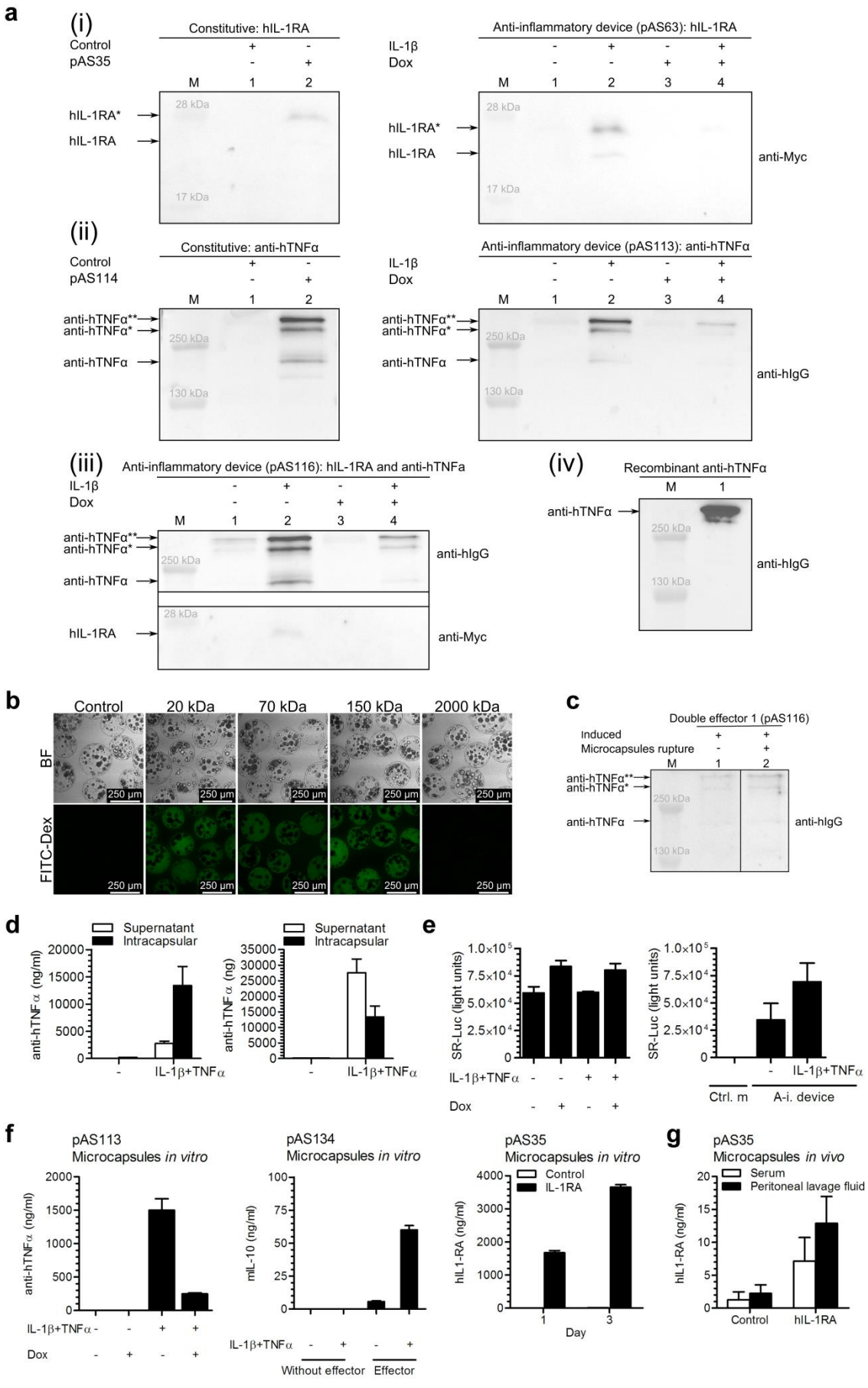
a
(i)
Constitutive: hIL-1RA
Control
pAS35
M 1 2
hIL-1RA*
hIL-1RA
28 kDa
17 kDa
Anti-inflammatory device (pAS63): hIL-1RA
IL-1β
Dox
M 1 2 3 4
anti-Myc
(ii)
Constitutive: anti-hTNFα
Control
pAS114
anti-hTNFα**
anti-hTNFα*
anti-hTNFα
250 kDa
130 kDa
Anti-inflammatory device (pAS113): anti-hTNFα
anti-hIgG
(iii)
Anti-inflammatory device (pAS116): hIL-1RA and anti-hTNFa
(iv)
Recombinant anti-hTNFα
b
Control
20 kDa
70 kDa
150 kDa
2000 kDa
BF
FITC-Dex
250 μm
c
Double effector 1 (pAS116)
Induced
Microcapsules rupture
d
Supernatant
Intracapsular
anti-hTNFα (ng/ml)
anti-hTNFα (ng)
IL-1β+TNFα
e
SR-Luc (light units)
Dox
Ctrl. m
A-i. device
f
pAS113
Microcapsules in vitro
pAS134
Microcapsules in vitro
mIL-10 (ng/ml)
Without effector
Effector
pAS35
Microcapsules in vitro
Control
IL-1RA
hIL1-RA (ng/ml)
Day
g
pAS35
Microcapsules in vivo
Serum
Peritoneal lavage fluid
Control
hIL-1RA

Supplementary Figure 5 Related to Figure 5

(**a**) Western blot analysis of anti-inflammatory effectors from cell culture. (i) Left: Constitutive (pAS35; P_{cmv}-hIL-1RA-myc); and right: inducible (pAS63; TRE-UAS-P_{MIN}-hIL-1RA) production of human interleukin-1 receptor antagonist (hIL-1RA). (ii) Left: Constitutive (pAS114; P_{CMV}-anti-hTNFα Ab); and right: inducible (pAS113; TRE-UAS-P_{MIN}-anti-hTNFα Ab) production of anti-hTNFα antibody (anti-hTNFα). (iii) Anti-inflammatory device-derived (pAS116; TRE-UAS-P_{MIN}-anti-hTNFα Ab-hIL-1RA) production of hIL-1RA and anti-hTNFα. (iv) Recombinant anti-hTNFα used as a control. Amounts of effectors produced from the anti-inflammatory device are comparable to the amounts from a constitutive expression. Putative glycosylation of hIL-1RA is marked as an asterisk. Anti-hTNFα produced in our system has a putative glycosylation at a heavy chain, resulting in tree bands observed (none, only one or both heavy chains glycosylated, marked as an asterisk). Recombinant control, produced from CHO cells however, shows only one substantial band, implicating that biological activity could not be exactly the same. For detailed information about the transfected plasmids and their amounts in each specific experiment, see Supplementary table 1 and 2, respectively.

(**b**) MWCO of the microcapsules. MWCO was determined by FITC-Dextrane (FITC-Dex) of different molecular weights (20 kDa, 70 kDa, 150 kDa, 2000 kDa). Alginate-PLL-alginate microcapsules were incubated overnight at 37 °C with the FITC-Dex solution (20 μg/mL) and then they were washed 3 x using MOPS buffer. Immediately after that, we acquired images using confocal fluorescence microscopy.

(**c**) All forms of anti-hTNFα are able to cross the membrane of microcapsules as observed by western blot analysis, where all bands are present in both, ruptured and unruptured microcapsules. Microcapsules were ruptured by injecting the suspension through 23G needle.

(**d**) Intracapsular amount of anti-hTNFα produced from double effector (pAS116; TRE-UAS-

P_{MIN}-anti-hTNFα Ab-hIL-1RA). Concentration, determined in 10 mL of supernatant or in 1 mL suspension of the same, but previously ruptured microcapsules (left) and total amount of anti-hTNFα (right). For detailed information about transfected plasmids and their amounts in each specific experiment, see Supplementary table 1 and 2, respectively. Error bars indicate s.d. (*n*=3).

(**e**) Secretory *Renilla* luciferase (SR-Luc) control for the *in vitro* (left) and *in vivo* (right) production of anti-inflammatory proteins. SR-Luc was measured either in ruptured microcapsules for *in vitro* assay or in the peritoneal lavage fluid 48 h after microcapsules implantation. SR-Luc is comparable among all groups. For detailed information about transfected plasmids and their amounts in each specific experiment, see Supplementary table 1 and 2, respectively. Error bars indicate s.d. (*n*=4).

(**f**) Production of anti-inflammatory effectors from different constructs and different regimes as indicated in the figure. For detailed information about transfected plasmids and their amounts in each specific experiment, see Supplementary table 1 and 2, respectively. Error bars indicate s.d. (*n*=4).

(**g**) Constitutive *in vivo* production of hIL-RA from the construct pAS35; P_{cmv}-hIL-1RA-myc. For detailed information about transfected plasmid and its amount see Supplementary table 1 and 2, respectively. Error bars indicate s.d. (*n*=4).

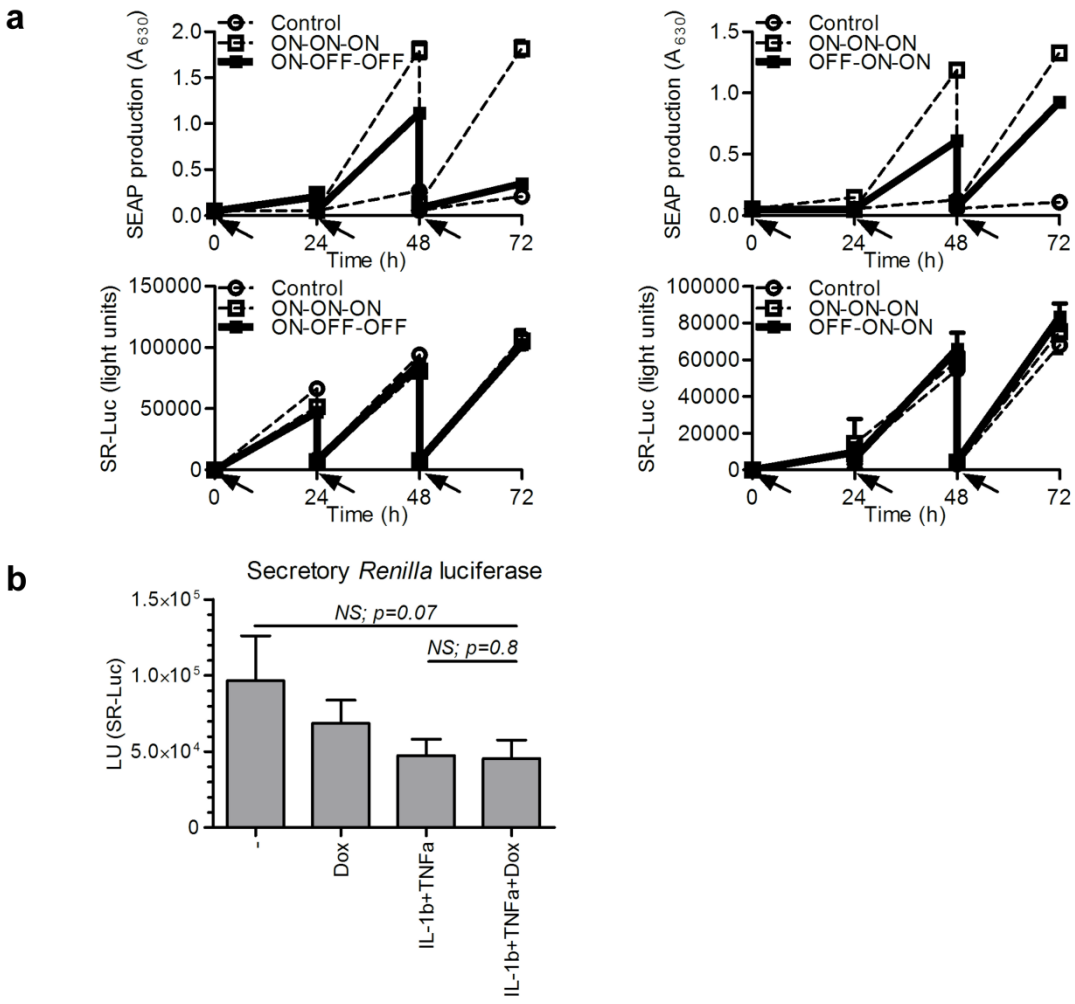
a
SEAP production (A630)
Control
ON-ON-ON
ON-OFF-OFF
OFF-ON-ON
Time (h)
SR-Luc (light units)
b
Secretory Renilla luciferase
LU (SR-Luc)
NS; p=0.07
NS; p=0.8
-
Dox
IL-1b+TNFa
IL-1b+TNFa+Dox
c
Serum anti-hTNFα (ng/mL)
IL-1β+TNFα
IL-1β+TNFα+Dox
p=0.0001
24 h
72 h
120 h
d
Serum mIL-10 (pg/mL)
p=0.03

Supplementary Figure 6 Related to Figure 6

(**a**) The reversibility of the synthetic anti-inflammatory device. Upper left panel: Raw SEAP measurements for *in vitro* shutdown of the system. Anti-inflammatory device-engineered HEK 293T cells (reporter pAS72; TRE-UAS-P_{MIN}-SEAP) were stimulated with interleukin-1β (IL-1β, 1 ng/mL) 6 h after transfection (marked as ON) or left unstimulated (marked as control). 24 h after first stimulation, supernatant containing SEAP was collected and medium was exchanged (indicated by arrows) or in addition, cells were stimulated with IL-1β (1 ng/mL) (marked as ON) or shut down by doxycycline (Dox, 1 μg/mL) (marked as OFF). 48 h and 72 h after first stimulation, procedure was repeated. Upper right panel: Raw SEAP measurements for *in vitro* rebooting of the system shutdown. Anti-inflammatory device-engineered HEK 293T cells (reporter pAS72; TRE-UAS-P_{MIN}-SEAP) were stimulated with IL-1β (1 ng/mL) 6 h after transfection (marked as ON), shut down by Dox (1 μg/mL) (marked as OFF) or left unstimulated (marked as control). 24 h after first stimulation, supernatant containing SEAP was collected and medium was exchanged (indicated by arrows) or in addition, cells were stimulated with IL-1β (1 ng/mL) (marked as ON) or left unstimulated (Control). Lower panel: Secretory *Renilla* luciferase (SR-Luc) used for an internal control. Secretory *Renilla* luciferase is comparable among all groups at any time point in *in vitro* reversibility test.

(**b**) SR-Luc corresponding to the *in vivo* restraint of the full system activation

(**c, d**) Shut down of the anti-inflammatory device *in vivo*. The data represent concentrations corresponding to the results represented in Fig. 6c and 6d. The anti-inflammatory device-engineered HEK 293T cells (effector pAS134; TRE-UAS-P_{MIN}-anti-hTNFα Ab-mIL-10) were microencapsulated, implanted i.p. and fully activated by injection of a combination of 300 ng of hIL-1β and 250 ng of hTNFα per mouse. After 24 h (thin arrow) the device was shut down by an i.v. Dox injection (20 mg/kg). (c) The device was additionally activated and

shut down after 72 h (thick arrow) to reach the relevant time span needed for an observation of the anti-hTNFα antibody kinetics. Serum was collected at different time points and anti-hTNFα antibody or mIL-10 levels were measured.

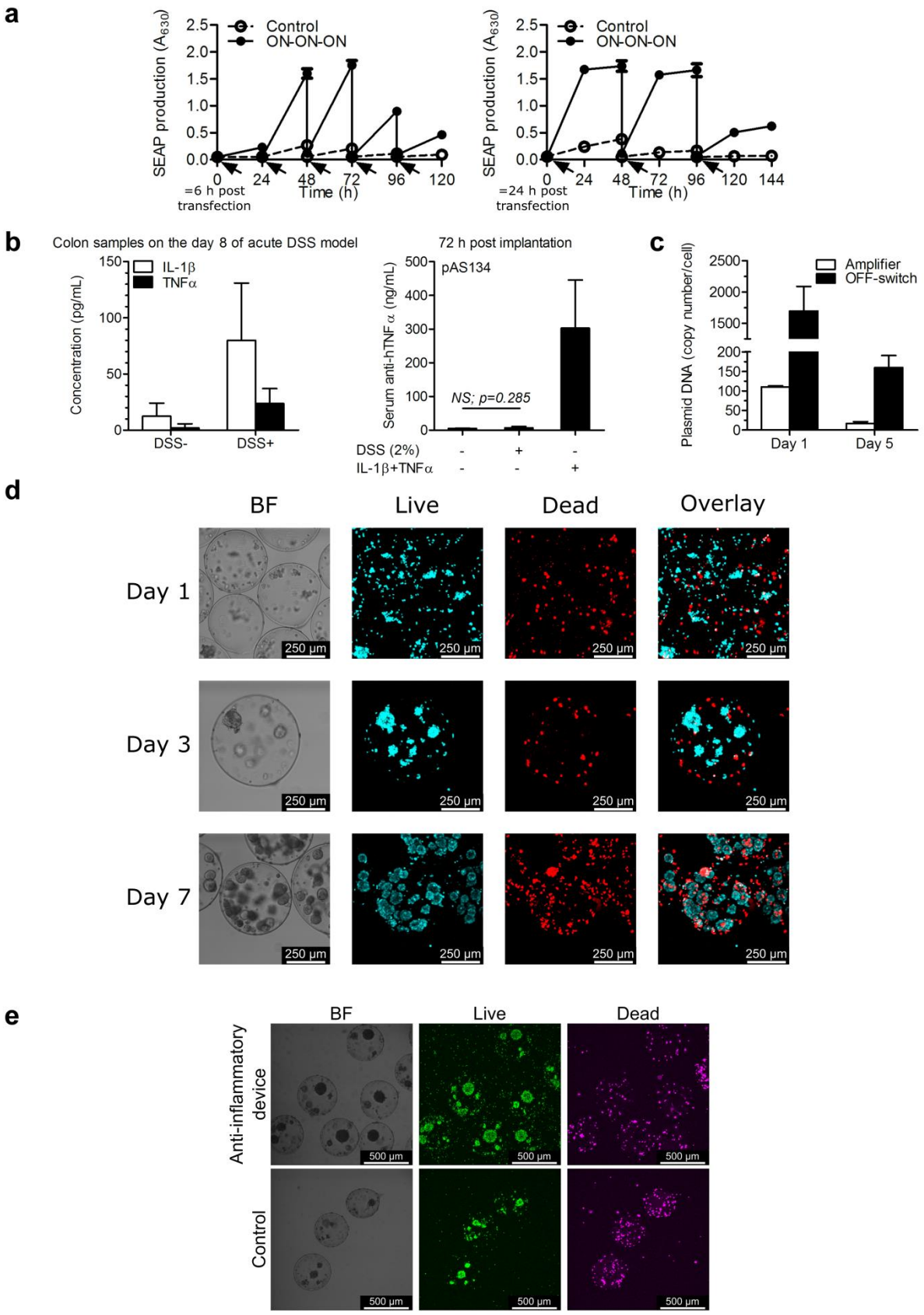
a
SEAP production (A_{630})
Control
ON-ON-ON
Time (h)
=6 h post transfection
=24 h post transfection
b
Colon samples on the day 8 of acute DSS model
IL-1β
TNFα
Concentration (pg/mL)
DSS-
DSS+
72 h post implantation
pAS134
Serum anti-hTNFα (ng/mL)
NS; p=0.285
DSS (2%)
IL-1β+TNFα
c
Amplifier
OFF-switch
Plasmid DNA (copy number/cell)
Day 1
Day 5
d
BF
Live
Dead
Overlay
Day 1
Day 3
Day 7
250 µm
e
BF
Live
Dead
Anti-inflammatory device
Control
500 µm

Supplementary Figure 7 Related to Figure 7

(**a**) A decrease in the system's capacity due to the transient nature of the system. Left: The anti-inflammatory device-engineered HEK 293T cells (reporter pAS72; TRE-UAS-P_{MIN}-SEAP) were stimulated with hIL-1β (1 ng/mL) every 24 h by exchanging the medium (indicated by the arrows). The experiment was started 6 h post transfection, which was represented by 0 h time point. The kinetics of SEAP production was measured every 24 h. Right: The anti-inflammatory device-engineered HEK 293T cells (reporter pAS72; TRE-UAS-P_{MIN}-SEAP) were stimulated with hIL-1β (1 ng/mL) every 48 h by exchanging the medium (indicated by the arrows). The experiment was started 24 h post transfection, which was represented by 0 h time point. The kinetics of SEAP production was measured every 24 h to observe a cumulative SEAP production. Error bars indicate s.d. (*n*=4).

(**b**) DSS-induced colitis increased endogenous inflammatory cytokines in the supernatants of colon biopsy samples but does not activate the device. Left: Concentration of endogenous mIL-1β and mTNFα in the supernatants of colon biopsy samples on the 8^{th} day of DSS-induced acute colitis (*n*=6 biopsy samples per mouse, 2 mice per group) Right: The activation of the implanted anti-inflammatory device by DSS. The mice were given either water or 2 % DSS for 8 days and on the 5^{th} day of this time-course experimental model, the microcapsules containing anti-inflammatory device-engineered cells (effector construct pAS134; TRE-UAS-P_{MIN}-anti-hTNFα Ab-mIL-10, Supplementary Table 1) were implanted i.p. Positive control group was stimulated with a combination of 300 ng of hIL-1β and 250 ng of hTNFα per mouse 1 h post implantation. Concentration of anti-hTNFα was measured 72 h post implantation (on the 8^{th} day of the experimental colitis model) (*n*=3).

(**c**) A decrease in the system's capacity due to the transient nature of the system. HEK 293T cells were transfected according to the Supplementary Table 2 and lysed after 1 or 5 days. Samples were analyzed by real-time quantitative PCR using the primers to specifically

amplify the amplifier or the inducible OFF-switch constructs. The plasmid copy number in the samples was estimated from the standard curves of the known amounts of the respective constructs spiked into the lysate and recalculated per cell (n = 2 biological replicates tested at 2 different dilutions of the respective lysate).

(**d**) Confocal fluorescence microscopy of the microcapsules in the *in vitro* culture as observed 1, 3 or 7 days after microencapsulation procedure. A large majority of the microencapsulated cells remained viable and divided as observed by aggregates formed. Live and dead cells were stained with Hoechst and propidium iodide, respectively.

(**e**) Confocal fluorescence microscopy of the microcapsules after having been implanted in peritoneal cavity of mice for 3 days. Cells remain viable during the course of the experiments, conducted in this study. Live and dead cells were stained with Hoechst and propidium iodide, respectively.

EXTENDED EXPERIMENTAL PROCEDURES

The ability of antibody molecules to transverse the alginate-PLL-alginate membrane

Anti-hTNFα antibody is a glycosylated, 150 kDa molecule and since the ability of antibody molecules to transverse the alginate-PLL-alginate membrane is somewhat controversial[1,2], we investigated whether the anti-hTNFα is able to cross the membrane of microcapsules in our system. First, we have shown that 20 kDa, 70 kDa and also 150 kDa, but not 2000 kDa FITC-Dextrane molecules are able to cross the membrane (Supplementary Fig. 5b). Next, we have shown that glycosylated, higher molecular mass forms of the antibody are secreted from the microcapsules, since we detected corresponding bands in the western blot analysis of either intact or ruptured microcapsules (Supplementary Fig. 5c). The intracapsular concentration of anti-hTNFα was somewhat higher than the concentration in the supernatant, nevertheless, the majority of anti-hTNFα was released into the supernatant (Supplementary Fig. 5d).

Confocal fluorescence microscopy related to Supplementary Fig. 3b, 3c, 5b and 7

For the *in vitro* direct observation of the system's performance, HEK 293T cells were seeded onto 8-well microscopic chambers (Ibidi) at a density of 5 x 10^4 cells per well. Cells were transfected with the constructs pAS97 (observation of the sensor activity) and/or pAS98 (observation of the amplifier activity), pAS72, pAS67, pAS58, pAS75 and pmCherry-C1 (detailed description in the Supplementary Table 1). 4 h after transfection, doxycycline (1 μg/mL) was added to the samples, which we wanted to shut down. 24 h after transfection, the system was stimulated with human IL-1β (R&D Systems, Inc., Minneapolis, USA) at a final concentration of 1 ng/mL. 4 h after stimulation, medium was removed and cells were washed 3 x using fresh medium to remove an input signal. After 24 h, the responsiveness of the system was visualized and microscopic images were acquired using the Leica TCS SP5 inverted laser-scanning microscope on a Leica DMI 6000 CS module equipped with a HCX PL Fluotar L 20 x, numerical aperture 0.4 (Leica Microsystems, Wetzlar, Germany). A 514-

nm laser line of a 100-mW argon laser with 25 % laser power was used for mCitrine excitation, and the emitted light was detected between 520 and 580 nm. A 50-mW 405-nm diode laser was used for tagBFP excitation and the emitted light was detected between 420 and 460 nm. A 1-mW 543-nm HeNe laser was used for mCherry excitation and the emitted light was detected between 560 and 630 nm. Leica LAS AF software was used for acquisition and ImageJ software was used for image processing.

To determine an approximate MWCO of the microcapsules, we observed the permeability of microcapsules for fluorescein isothiocyanate-dextran (FITC-Dex, Sigma Aldrich) of different molecular weights (20 kDa, 70 kDa, 150 kDa and 2000 kDa). Alginate-PLL-alginate microcapsules were incubated overnight at 37 °C with the FITC-Dex solution (20 μg/mL) and then they were washed 3 x using MOPS buffer. Immediately after that, we acquired images using confocal fluorescence microscopy. A 488 Argon laser was used for FITC-Dex excitation and the emitted light was detected between 502 and 553 nm.

To observe integrity of microcapsules and viability of cells after 3 day *in vivo* experiment we made peritoneal lavage and collected microcapsules. We stained microcapsules with Hoechst at a final concentration of 1 μg/mL (ImmunoChemistry Technologies, LLC, 639) for live cells and propidum iodide at a final concentration of 0.6 μg/mL (Sigma Aldrich, P4864) for dead cells. After 30 min incubation at 37 °C, images were acquired. A 1-mW 543-nm HeNe laser was used for propidium iodide excitation and the emitted light was detected between 600 and 670 nm. A 405 Diode laser was used for Hoechst excitation and the emitted light was detected between 429 and 509 nm. The same procedure was followed for the visualization of the microencapsulated cells after 1, 3 and 7 days in the *in vitro* culture.

Cytokine detection related to Supplementary Fig. 4a, 4b and 7b

Serum and peritoneal lavage fluid of mice were collected as described in the Materials and Methods section (Animal Models) in the main article. Colon biopsy samples were prepared by following the described[3] "Full-thickness organ culture" method to determine a concentration of inflammatory cytokines in the supernatants. Inflammatory cytokine levels were measured by a sandwich ELISA according to the manufacturer's instructions (eBioscience) as follows: human IL-1β was detected by human IL-1 beta ELISA Ready-SET-Go! (eBioscience, 88-7010), human TNF-α by human TNF alpha ELISA Ready-SET-Go! (eBioscience, 88-7346), mouse IL-1β by mouse IL-1 beta ELISA Ready-SET-Go! (eBioscience, 88-7013), mouse TNFα by mouse TNF alpha ELISA Ready-SET-Go! (eBioscience, 88-7324), mouse IL-6 by mouse IL-6 ELISA Ready-SET-Go! (eBioscience, 88-7064).

Western blotting related to Supplementary Fig. 5a and 5c

Supernatants from pAS35 (CMV promoter-driven hIL-1RA-myc production), pAS113 (NF-κB-driven anti-hTNFα antibody expression), pAS114 (CMV promoter-driven anti-hTNFα antibody) and pAS116 (NF-κB-driven anti-hTNFα antibody-hIL-1RA-myc double effector expression unit) (detailed description in the Supplementary Table 1) were analyzed for hIL-RA-myc and anti-hTNFα antibody expression. 30 μL of a cell culture supernatant, expressing certain protein was mixed with 4xSDS buffer without reducing agent, boiled for 5 min at 95 °C and centrifuged at 14000g for 3 min. Proteins were resolved on 12 % SDS-PAGE and analyzed by a standard western blotting procedure. hIL-1RA-myc was detected by rabbit anti-myc IgG primary antibody (1: 500) (Sigma Aldrich, C3956) and goat polyclonal to rabbit IgG (HRP) secondary antibody (1: 3000) (Abcam, ab6721), while anti-hTNFα antibody was detected by rabbit polyclonal secondary antibody to human IgG – H and L (HRP) (1: 3000) (Abcam, ab 6759). Recombinant anti-hTNF-α-hIgG1 (InvivoGen, htnfa-mab1) and an empty vector pcDNA3.1 were used as controls.

Estimation of the plasmid copy number per cell related to Supplementary Fig. 7c

A decrease in the system's capacity due to the transient nature of the transfection was estimated by real-time quantitative PCR analysis. HEK 293T cells were seeded in 10 cm tissue culture petri dish (TPP), transfected at 50-70 % confluency according to the Supplementary Table 2, washed with PBS twice, trypsinized and collected by centrifugation (1400 rpm, 8 min) 1 or 5 days post transfection. The number of cells was determined by Trypan blue staining. Cell lysis was performed by resuspending the pellet in 500 μL MQ, incubation at 4 °C for 12 h, freezing at -70 °C, boiling at 95 °C for 10 min and centrifugation (12000 rpm, 20 min). Supernatants were transferred to fresh tubes and stored for analysis at -20 °C. Samples were diluted 1000-fold or 10000-fold and analyzed by real-time quantitative PCR using the primers to specifically amplify the plasmid encoding the amplifier (F: 5'-ACTGTCCTCCGAGAGATCTTAGAGGG-3' R: 5'-GCGACACTCCCAGTTGTTCTTCAG-3') or the inducible OFF-switch (F: 5'-GGCGGTGGTGCTTTGTCTCC-3' R: 5'-CTCCAGCATCACATTTCTGTACACG-3') constructs. Real-time PCR was performed using Power SYBR Green PCR Master Mix (Roche) in a Roche LightCycler® 480. Known amounts of the corresponding plasmids were spiked into the 1000-fold or 10000-fold diluted lysate of the non-transfected cells (prepared as described above) to obtain the standard curves (C_t plotted against log plasmid copy number) under the same cycling conditions. The plasmid copy number in the samples was estimated from the standard curves and recalculated per cell.

Supplementary Table 1. Genetic constructs used and designed in this study

Name of the plasmid	Description of gene construct	Reference
pISRE-Luc	Mammalian expression vector encoding P_{ISRE}-P_{TAL}-driven luciferase expression unit (P_{ISRE}-P_{TAL}-Lucuferase-pA). pISRE-Luc contains five copies of the ISRE-binding sequence, located upstream of the TATA-like promoter (P_{TAL}) region from the herpes simplex virus thymidine kinase (HSV-TK) promoter.	Clontech
pcDNA3.1	Mammalian expression vector (P_{CMV}-MCS-pA)	Life Technologies
pFLAG-CMV3	Mammalian expression vector for secretory proteins (P_{CMV}-preprotrypsin leader sequence-flag-tag-MCS-pA)	Sigma Aldrich
pMF208	Mammalian expression vector encoding SV40-PIR3-driven SEAP expression (P_{PIR}ON-SEAP- pA)[4]	Kindly provided by Professor Dr. Martin Fussenegger (Institute of Biotechnology, Swiss Federal Institute of Technology, ETH Zürich)[4]
phRL-TK	Mammalian expression vector for constitutive HSV-TK-promoter-driven renilla luciferase expression (phRL-TK-rLuc)	Promega
pSGVP	Mammalian expression vector for constitutive SV40 promoter-driven GV16 expression (GV16 is Gal4-VP16 transcriptional activator).	Kindly provided by Professor Dr Mark Ptashne (Memorial Sloan Kettering Cancer Center, New York, NY,

		USA)[5]
pLVPT-rtTR-KRAB-2SM2	Lentiviral vector containing rtTR-NLS-KRAB (reverse tetracycline repressor fused to nuclear localization signal and KRAB transcription repression domain)	(plasmid 11652, Addgene)[6]
pMF111	Mammalian expression vector pTBC1 encoding tetracycline-responsive element TetO7-driven SEAP expression.	Kindly provided by Professor Dr. Martin Fussenegger (Institute of Biotechnology, Swiss Federal Institute of Technology, ETH Zürich)[7]
pmCherry-C1	Mammalian expression vector encoding constitutive CMV promoter-driven expression of pmCherry-C1 (Clontech). Plasmid ensures constitutive expression of mCherry, and was used to normalize levels of transfection in confocal microscopy experiments.	Clontech
pORF9-hIL06Ra	Mammalian expression vector for constitutive hEF1/HTLV promoter-driven human IL6R (IL-6 receptor, isoform 1) expression.	InvivoGen
pAS34	Mammalian expression vector encoding constitutive HSV-TK promoter-driven hIL-1RA-myc expression unit (P_{HSV-TK}-hIL-1RA-myc). hIL-1RA was PCR amplified from pORF9-hIL1RNa (InvivoGen, commercially available vector) (5'-caggaagcttggcattccggtactgttggtaaagccaccATGGAAATCTGCAGAGGCCTCCGC-3', 5'-ggcctctagaattacagatcctcttcagagatgagtttctgctcCTCGTCCTCCTGGAAGTAGAATTTGGTGACC-3') adding C-terminal myc-tag and cloned into the corresponding sites (HindIII/XbaI) of phRL-TK, replacing chimeric intron-renilla luciferase cassette.	This work
pAS35	Mammalian expression vector encoding constitutive CMV promoter-driven hIL-1RA-myc expression unit (P_{cmv}-hIL-1RA-myc). hIL-1RA was PCR amplified from pORF9-hIL1RNa (InvivoGen, commercially available vector) (5'-caggaagcttCGACCCTCTGGGAGAAAATCCAGC-3', 5'-ggcctctagaattacagatcctcttcagagatgagtttctgctcCTCGTCCTCCTGGAAGTAGAATTTGGTG	This work

	ACC-3') omitting signal sequence but adding C-terminal myc-tag and cloned into the corresponding sites (HindIII/XbaI) of pFLAG-CMV3, creating secretory of hIL-1RA (preprotrypsin leader sequence).	
pAS36	Mammalian expression vector encoding $P_{NF\text{-}\kappa B1}$-P_{TAL}-driven luciferase expression unit ($P_{NF\text{-}\kappa B1}$-P_{TAL}-Luc). The NF-κB responsive element (sequence: GGGAATTTCCGGGAATTTCCGGGAATTTCCGGGAATTTCC) was cloned into the corresponding sites (NheI/BglII) of the pISRE-Luc vector, replacing the P_{ISRE}.	This work
pAS37	Mammalian expression vector encoding $P_{NF\text{-}\kappa B2}$-P_{TAL}-driven luciferase expression unit ($P_{NF\text{-}\kappa B2}$-P_{TAL}-Luc). The NF-κB responsive element (sequence: GGGAATTTCCGGGGACTTTCCGGGAATTTCCGGGGACTTTCCGGGAATTTCC) was cloned into the corresponding sites (NheI/BglII) of the pISRE-Luc vector, replacing the P_{ISRE}.	This work
pAS40	Mammalian expression vector encoding $P_{NF\text{-}\kappa B2}$-P_{MIN}-driven luciferase expression unit ($P_{NF\text{-}\kappa B2}$-P_{MIN}-Luc). We excised P_{TAL} from pAS37 with BglII/HindIII and replaced it with P_{MIN} minimal promoter (sequence: TAGAGGGTATATAATGGAAGCTCGACTTCCAG).	This work
pAS44	Mammalian expression vector encoding $P_{NF\text{-}\kappa B2}$-P_{MIN}-driven GV16-myc expression unit (GV16-myc, Gal4-VP16 transcriptional activator with C-terminal myc-tag,) ($P_{NF\text{-}\kappa B2}$-P_{MIN}-GV16-myc). GV16 was PCR amplified from pSGVP vector adding C-terminal myc-tag with the reverse primer (5'-cagg<u>aagcttg</u>gcattccggtactgttggtaaagccaccATGAAGCTACTGTCTTCTATCGAACAAGC-3' and 5'-ggcc<u>tctaga</u>attacagatcctcttcagagatgagtttctgctcCCCACCGTACTCGTCAATTCCAAGGGC-3') and cloned into the corresponding sites (HindIII/XbaI) of pAS40, replacing the luciferase expression unit.	This work
pAS48	Mammalian expression vector encoding $P_{NF\text{-}\kappa B2}$-P_{MIN}-driven GV16 expression unit (GV16, Gal4-VP16 transcriptional activator) ($P_{NF\text{-}\kappa B2}$-P_{MIN}-GV16). GV16 was PCR amplified from pSGVP vector (5'-cagg<u>aagcttg</u>gcattccggtactgttggtaaagccaccATGAAGCTACTGTCTTCTATCGAACAAGC-3' and 5'-ggcc<u>tctaga</u>aTTACCCACCGTACTCGTCAATTCCAAGGGC-3') and cloned into the corresponding sites (HindIII/XbaI) of pAS40, replacing the luciferase expression	This work

	unit.	
pAS49	Mammalian expression vector encoding UAS-P_{MIN}-driven luciferase expression unit. Luciferase is expressed only in the presence of GV16, which binds to UAS sequence (5 consecutive Gal4 binding sites), placed directly upstream P_{MIN} (UAS-P_{MIN}-Luc, UAS, upstream activatory sequence). UAS (sequence: CGGAGTACTGTCCTCCGAGCGGAGTACTGTCCTCCGAGCGGAGTACTGTCCTC CGAGCGGAGTACTGTCCTCCGAGCGGAGTACTGTCCTCCGAG) was cloned into the corresponding sites (NheI/BglII) of pAS40, replacing the $P_{NF\text{-}\kappa B2}$.	This work
pAS51	Mammalian expression vector encoding TRE-UAS-P_{MIN}-driven luciferase expression unit (TRE-UAS-P_{MIN}-Luc). Luciferase could be repressed by rtTR-NLS-KRAB-2SM2 which binds to 7 consecutive Tet-binding sites (Tet-responsive element; TRE) placed directly upstream UAS in the presence of doxycycline. TRE was PCR-amplified from pMF111 (5'-ggccggtaccCTCGAGTTTACCACTCCC-3', 5'-ggccgctagcGAGCTCGACTTTCACTTTTCTC-3') and cloned into the corresponding sites (KpnI/NheI) directly upstream UAS of pAS49.	This work
pAS53	Mammalian expression vector encoding UAS-P_{MIN}-driven GV16 expression unit (UAS-P_{MIN}-GV16). The construct is based on a positive feedback loop of an orthogonal transcriptional activator GV16, which amplifies its own transcription by binding UAS placed directly upstream P_{MIN}. GV16 was PCR amplified from pSGVP vector (5'-caggaagcttggcattccggtactgttggtaaagccaccATGAAGCTACTGTCTTCTATCGAACAAGC-3' and 5'-ggcctctagaaTTACCCACCGTACTCGTCAATTCCAAGGGC-3') and cloned into the corresponding sites (HindIII/XbaI) of pAS49, replacing the luciferase expression unit.	This work
pAS54	Mammalian expression vector encoding UAS-P_{MIN}-driven GV16-myc expression unit (UAS-P_{MIN}-GV16-myc). The construct is based on a positive feedback loop of an orthogonal transcriptional activator GV16, which amplifies its own transcription by binding UAS placed directly upstream P_{MIN}. GV16 was PCR amplified from pSGVP vector adding C-terminal myc-tag with the reverse primer (5'-caggaagcttggcattccggtactgttggtaaagccaccATGAAGCTACTGTCTTCTATCGAACAAGC-3' and 5'-ggcctctagaattacagatcctcttcagagatgagtttctgctcCCCACCGTACTCGTCAATTCCAAGGGC-3') and cloned into the corresponding sites (HindIII/XbaI) of pAS49, replacing the luciferase expression unit.	This work

pAS58	The inducible off-switch construct. Mammalian expression vector encoding constitutive CMV-promoter-driven rtTR-NLS-KRAB expression (P_{CMV}-rtTR-NLS-KRAB). rtTR-NLS-KRAB binds 7 consecutive Tet-binding sites (Tet-responsive element; TRE) and silences gene expression several kilobases upstream and downstream only in the presence of a doxycycline. rtTR-NLS-KRAB-2SM2 was PCR-amplified from pLVPT-rtTR-KRAB-2SM2 (5'-ggccggtaccGCCACCATGGCTAGACTGGACAAGAGCAAAGTCATAAACGGC-3', 5'-ccgggaattcTTAAACTGATGATTTGATTTCAAATGCAGTCTCTGAATCAGG-3') and cloned into the corresponding sites (KpnI/EcoRI) of pcDNA3.1.	This work
pAS60	The sensor construct. Mammalian expression vector encoding TRE-$P_{NF-κB2}$-P_{MIN}-driven GV16-myc expression unit (TRE-$P_{NF-κB2}$-P_{MIN}-GV16-myc). TRE was PCR-amplified from pMF111 (5'-ggccggtaccCTCGAGTTTACCACTCCC-3', 5'-ggccgctagcGAGCTCGACTTTCACTTTTCTC-3') and cloned into the corresponding sites (KpnI/NheI) directly upstream UAS of pAS44.	This work
pAS62	The amplifier construct. Mammalian expression vector encoding TRE-UAS-P_{MIN}-driven GV16-myc expression unit (TRE-UAS-P_{MIN}-GV16-myc). TRE was PCR-amplified from pMF111 (5'-ggccggtaccCTCGAGTTTACCACTCCC-3', 5'-ggccgctagcGAGCTCGACTTTCACTTTTCTC-3') and cloned into the corresponding sites (KpnI/NheI) directly upstream UAS of pAS54.	This work
pAS63	Mammalian expression vector encoding TRE-UAS-P_{MIN}-driven human IL-1RA expression unit (TRE-UAS-P_{MIN}-hIL-1RA). hIL-1RA was excised from pAS34 using HindIII/XbaI and cloned into the corresponding sites of pAS51 vector, replacing luciferase cassette.	This work
pAS67	The positive feedback "thresholder" construct. Mammalian expression vector encoding constitutive HSV-TK promoter-driven Gal4-myc expression unit (P_{HSV-TK}-G-myc). Gal4 was PCR amplified from pSGVP adding C-terminal myc-tag with the reverse primer (5'-caggaagcttggcattccggtactgttggtaaagccaccATGAAGCTACTGTCTTCTATCGAACAAGC-3', 5'-ggcctctagaattacagatcctcttcagagatgagtttctgctcCGATACAGTCAACTGTCTTTGACC-3') and cloned into the corresponding sites (HindIII/XbaI) of phRL-TK, replacing chimeric intron-renilla luciferase cassette.	This work
pAS72	Mammalian expression vector encoding TRE-UAS-P_{MIN}-driven secretory alkaline phosphatase (SEAP) expression unit (TRE-UAS-P_{MIN}-SEAP). SEAP was PCR-amplified from pMF208[4] vector (5'-	This work

	gtctaagcttggcattccggtactgttggtaaagccaccATGCTGCTGCTGCTGCTGCTGCTGGGCC-3', 5'-ggccactagtttatcaTGTCTGCTCGAAGCGGCCGGCC-3'), digested with HindIII/SpeI and cloned into the HindIII/XbaI digested pAS62, thereby giving SpeI/XbaI mixed site at 3', replacing GV16-myc.	
pAS75	Mammalian expression vector encoding CMV-driven secretory renilla luciferase (SR-Luc) expression unit (P_{CMV}-SR-Luc). Renilla luciferase was PCR-amplified from phRL-TK (5'-ggccaagcttGCTTCCAAGGTGTACGACCCCG-3', 5'-ccggtctagaaTTACTGCTCGTTCTTCAGC-3') and cloned into the corresponding sites (HindIII/XbaI) of pFLAG-CMV3, creating secretory form of renilla luciferase (preprotrypsin leader sequence).	This work
pAS97	Mammalian expression vector encoding TRE-$P_{NF\text{-}\kappa B2}$-P_{MIN}-driven GV16-myc-2A-mCitrine expression unit (TRE-$P_{NF\text{-}\kappa B2}$-P_{MIN}-GV16-myc-2A-mCit). 2A-mCit was PCR-amplified (5'-CATCTCTGAAGAGGATCTGggcgccggaagcggaGAGGGGAGAGGAAGTCTTCTGACC-3', 5'-CGGCCGGCCGCCCCGACTCTAGAATTAgcgcgcCTTGTACAGCTCGTCCATGCCG-3') from 10x[b]_l4_[CMV]_l2_TALA:KRAB:t2A:mCit[8] and pAS60 was PCR amplified (5'-CGGCATGGACGAGCTGTACAAGgcgcgcTAATTCTAGAGTCGGGGCGGCC-3', 5'-CCTCTCCCCTCtccgcttccggcgccCAGATCCTCTTCAGAGATGAGTTTCTGCTCC-3'). Both fragments were assembled using Gibson assembly method[9], introducing 2A-mCit cassette into the sensor construct downstream of GV16-myc. 2A amino acid sequence: GSGEGRGSLLTCGDVEENPGP[10].	This work
pAS98	Mammalian expression vector encoding TRE-UAS-P_{MIN}-driven GV16-myc-2A-tagBFP expression unit (TRE-UAS-P_{MIN}-GV16-myc-2A-tagBFP). First, 2A-TagBFP was PCR amplified (5'-atcgggcgccggaagcggaGAGGGGAGAGGAAGTCTTCTGACCTGCGG-3', 5'-cgatgcgcgcATTGAGCTTGTGCCCCAGTTTGCTAGGGAGG-3') from 10x[a]_l4_[CMV]_l2_TALB:KRAB:t2A:BFP[8] and ligated into the corresponding sites (KasI/BssHII) of pAS97. Then this construct was digested with EcoRI/XbaI and ligated into the corresponding sites of pAS62, introducing 2A-tagBFP cassette into the amplifier construct downstream of GV16-myc. 2A amino acid sequence: GSGEGRGSLLTCGDVEENPGP[10].	This work
pAS108	Mammalian expression vector for constitutive CMV promoter-driven luciferase expression	This work

	(P_{CMV}-Luc). CMV promoter was excised from pcDNA3.1 using BglII/HindIII and cloned into the corresponding sites of pAS51 vector, replacing P_{MIN}.	
pAS109	Mammalian expression vector for constitutive CMV promoter-driven SEAP expression (P_{CMV}-SEAP). CMV promoter was excised from pcDNA3.1 using BglII/HindIII and cloned into the corresponding sites of pAS72 vector, replacing P_{MIN}.	This work
pAS113	Mammalian expression vector encoding TRE-UAS-P_{MIN}-driven anti-hTNFα antibody expression unit (TRE-UAS-P_{MIN}-anti-hTNFα Ab). Anti-hTNFα antibody was excised from pAS117 using HindIII/XbaI and cloned into the corresponding sites of pAS51 vector, replacing luciferase cassette.	This work
pAS114	Mammalian expression vector encoding constitutive CMV promoter-driven anti-hTNFα antibody (P_{CMV}-anti-hTNFα Ab). Anti-hTNFα antibody was excised from pAS117 using HindIII/XbaI and cloned into the corresponding sites of pcDNA3.1 vector.	This work
pAS115	Mammalian expression vector encoding TRE-UAS-P_{MIN}-driven anti-hTNFα antibody-2A-tagBFP expression unit (TRE-UAS-P_{MIN}-GV16-myc-2A-anti-hTNFα Ab). Anti-hTNFα antibody was excised from pAS117 using HindIII/KasI and cloned into the corresponding sites of pAS98 vector, replacing GV16-myc cassette.	This work
pAS116	Mammalian expression vector encoding TRE-UAS-P_{MIN}-driven anti-hTNFα antibody-hIL-1RA-myc double effector expression unit (TRE-UAS-P_{MIN}-anti-hTNFα Ab-hIL-1RA; DE1). hIL-1RA was PCR amplified from pORF9-hIL1RNa (InvivoGen, commercially available vector) (5'-gtctggcgccggaagcggagaggggagaggaagtcttctgacctgcggagacgtcgaagagaatcctggacccATGGAAATCTGCAGAGGCCTCC-3', 5'-ggcctctagaattacagatcctcttcagagatgagtttctgctcCTCGTCCTCCTGGAAGTAGAATTTGGTGACC-3') adding N-terminal 2A peptide and C-terminal myc-tag and cloned into the corresponding sites of pAS115, replacing 2A-tagBFP (KasI/XbaI). Amino acid sequence with annotation: MGVKVLFALICIAVAEAEVQLVESGGGLVQPGRSLRLSCAASGFTFDDYAMHWVRQAPGKGLEWVSAITWNSGHIDYADSVEGRFTISRDNAKNSLYLQMNSLRAEDTAVYYCAKVSYLSTASSLDYWGQGTLVTVSSASTKGPSVFPLAPSSKSTSGGTAALGCLVKDYFPEPVTVSWNSGALTSGVHTFPAVLQSSGLYSLSSVVTVPSSSLGTQTYICNVNHKPSNTKVDKKVEPKSCDKTHTCPPCPAPELLGGPSVFLFPPKPKDTLMISRTPEVTCVVVDVSHEDPEVKFNWYVDGVEVHNAKTKPREEQYNSTYRVVSVLTVL	

	HQDWLNGKEYKCKVSNKALPAPIEKTISKAKGQPREPQVYTLPPSRDELTKNQVS LTCLVKGFYPSDIAVEWESNGQPENNYKTTPPVLDSDGSFFLYSKLTVDKSRWQQ GNVFSCSVMHEALHNHYTQKSLSLSPGKRAKRGSGEGRGSLLTCGDVEENPGPM GVKVLFALICIAVAEADIQMTQSPSSLSASVGDRVTITCRASQGIRNYLAWYQQKP GKAPKLLIYAASTLQSGVPSRFSGSGSGTDFTLTISSLQPEDVATYYCQRYNRAPYT FGQGTKVEIKTVAAPSVFIFPPSDEQLKSGTASVVCLLNNFYPREAKVQWKVDNA LQSGNSQESVTEQDSKDSTYSLSSTLTLSKADYEKHKVYACEVTHQGLSSPVTKSF NRGECRAKRGAGSGEGRGSLLTCGDVEENPGPMEICRGLRSHLITLLLFLFHSETIC RPSGRKSSKMQAFRIWDVNQKTFYLRNNQLVAGYLQGPNVNLEEKIDVVPIEPHA LFLGIHGGKMCLSCVKSGDETRLQLEAVNITDLSENRKQDKRFAFIRSDSGPTTSFE SAACPGWFLCTAMEADQPVSLTNMPDEGVMVTKFYFQEDEEQKLISEEDL Gaussia luciferase signal peptide[11] anti-hTNFα Ab heavy chain variable region[12] RAKR motif for cleavage by furine hIg gamma-1 chain constant region 2A peptide anti-hTNFα Ab light chain variable region[12] Ig kappa chain constant region hIL-1RA-myc tag	
pAS117	Synthetic gen, encoding anti-hTNFα antibody Adalimumab[12], (anti-hTNFα Ab). Nucleotide sequence: aagcttggcattccggtactgttggtaaagccaccATGGGCGTGAAGGTGCTGTTCGCCCTGATCTG TATCGCCGTGGCCGAGGCCGAAGTGCAGCTGGTGGAATCTGGCGGAGGACTG GTGCAGCCTGGCAGAAGCCTGAGACTGAGCTGTGCCGCCAGCGGCTTCACCTT CGACGACTACGCCATGCACTGGGTGCGCCAGGCCCCTGGAAAAGGCCTGGAAT GGGTGTCCGCCATCACCTGGAACAGCGGCCACATCGATTACGCCGACAGCGTG GAAGGCCGGTTCACCATCAGCCGGGACAACGCCAAGAACAGCCTGTACCTGC AGATGAACTCCCTGCGGGCCGAGGACACCGCCGTGTACTACTGTGCCAAGGTG TCCTACCTGAGCACCGCCAGCAGCCTGGATTATTGGGGCCAGGGCACACTCGT GACCGTGTCTAGCGCCAGCACAAAGGGCCCCAGCGTGTTCCCTCTGGCCCCTA GCAGCAAGAGCACAAGCGGAGGAACAGCCGCCCTGGGCTGCCTCGTGAAGGA CTACTTTCCCGAGCCCGTGACAGTGTCCTGGAATAGCGGAGCCCTGACCAGCG	This work

GCGTGCACACCTTTCCAGCTGTGCTGCAGAGCAGCGGCCTGTACAGCCTGAGC

AGCGTCGTGACTGTGCCCAGCAGCTCTCTGGGCACCCAGACCTACATCTGCAA

CGTGAACCACAAGCCCAGCAACACCAAGGTGGACAAGAAGGTGGAACCCAAG

AGCTGCGACAAGACCCACACCTGTCCCCCTTGTCCTGCCCCCGAACTGCTGGG

AGGCCCTTCCGTGTTCCTGTTCCCCCCAAAGCCCAAGGACACCCTGATGATCA

GCCGGACCCCCGAAGTGACCTGCGTGGTGGTGGATGTGTCCCACGAGGACCCT

GAAGTGAAGTTTAATTGGTACGTGGACGGCGTGGAAGTGCACAATGCCAAGA

CCAAGCCTAGAGAGGAACAGTACAACTCCACCTACCGGGTGGTGTCCGTGCTG

ACCGTGCTGCATCAGGACTGGCTGAACGGCAAAGAGTACAAGTGCAAAGTGT

CCAACAAGGCCCTGCCTGCCCCCATCGAGAAAACCATCAGCAAGGCCAAGGG

CCAGCCCCGCGAACCCCAGGTGTACACACTGCCCCCAAGCAGGGACGAGCTG

ACCAAGAACCAGGTGTCCCTGACCTGTCTCGTGAAAGGCTTCTACCCCAGCGA

CATTGCCGTGGAATGGGAGAGCAACGGCCAGCCCGAGAACAACTACAAGACC

ACCCCCCCTGTGCTGGACAGCGACGGCTCATTCTTCCTGTACTCCAAGCTGACA

GTGGACAAGTCCCGGTGGCAGCAGGGCAACGTGTTCAGCTGCAGCGTGATGCA

CGAGGCCCTGCACAACCACTACACCCAGAAGTCCCTGAGCCTGAGCCCCGGCA

AGAGAGCCAAGAGAGGATCTGGCGAGGGCAGAGGCAGCCTGCTGACATGTGG

CGACGTGGAAGAGAACCCAGGCCCTATGGGAGTGAAAGTGCTGTTTGCTCTGA

TCTGCATTGCTGTGGCTGAAGCCGACATCCAGATGACCCAGAGCCCCTCTAGC

CTGAGCGCCAGCGTGGGCGACAGAGTGACCATCACATGCAGAGCCAGCCAGG

GCATCCGGAACTACCTGGCCTGGTATCAGCAGAAGCCCGGCAAGGCCCCTAAG

CTGCTGATCTACGCCGCCTCCACACTGCAGAGCGGAGTGCCCTCCAGATTTTCC

GGCAGCGGCTCCGGCACCGACTTCACCCTGACAATCAGCTCCCTGCAGCCAGA

GGACGTGGCCACCTACTACTGCCAGCGGTACAACAGAGCCCCCTACACCTTCG

GACAGGGCACAAAGGTGGAAATCAAGACCGTGGCCGCTCCCTCCGTGTTCATC

TTCCCACCTAGCGACGAGCAGCTGAAGTCCGGCACAGCCTCTGTCGTGTGCCT

GCTGAACAACTTCTACCCTCGGGAAGCCAAGGTGCAGTGGAAAGTGGATAAC

GCCCTGCAGTCCGGCAACTCCCAGGAAAGCGTGACCGAGCAGGACAGCAAGG

ATAGCACCTACAGCCTGTCCTCCACCCTGACCCTGTCCAAGGCCGACTACGAG

AAGCACAAGGTGTACGCCTGTGAAGTGACCCACCAGGGCCTGTCCAGCCCCGT

GACCAAGAGCTTCAACCGGGGCGAGTGTAGGGCCAAGAGGGGCGCCtaattctaga).

Amino acid sequence with annotation:

MGVKVLFALICIAVAEAEVQLVESGGGLVQPGRSLRLSCAASGFTFDDYAMHWV

	RQAPGKGLEWVSAITWNSGHIDYADSVEGRFTISRDNAKNSLYLQMNSLRAEDTA VYYCAKVSYLSTASSLDYWGQGTLVTVSSASTKGPSVFPLAPSSKSTSGGTAALG CLVKDYFPEPVTVSWNSGALTSGVHTFPAVLQSSGLYSLSSVVTVPSSSLGTQTYI CNVNHKPSNTKVDKKVEPKSCDKTHTCPPCPAPELLGGPSVFLFPPKPKDTLMISR TPEVTCVVVDVSHEDPEVKFNWYVDGVEVHNAKTKPREEQYNSTYRVVSVLTVL HQDWLNGKEYKCKVSNKALPAPIEKTISKAKGQPREPQVYTLPPSRDELTKNQVS LTCLVKGFYPSDIAVEWESNGQPENNYKTTPPVLDSDGSFFLYSKLTVDKSRWQQ GNVFSCSVMHEALHNHYTQKSLSLSPGKRAKRGSGEGRGSLLTCGDVEENPGPM GVKVLFALICIAVAEADIQMTQSPSSLSASVGDRVTITCRASQGIRNYLAWYQQKP GKAPKLLIYAASTLQSGVPSRFSGSGSGTDFTLTISSLQPEDVATYYCQRYNRAPYT FGQGTKVEIKTVAAPSVFIFPPSDEQLKSGTASVVCLLNNFYPREAKVQWKVDNA LQSGNSQESVTEQDSKDSTYSLSSTLTLSKADYEKHKVYACEVTHQGLSSPVTKSF NRGECRAKRGA Gaussia luciferase signal peptide[11] anti-hTNFα Ab heavy chain variable region[12] RAKR motif for cleavage by furine hIg gamma-1 chain constant region 2A peptide anti-hTNFα Ab light chain variable region[12] Ig kappa chain constant region	
pAS132	The NF-κB-STAT3 hybrid sensor construct. Mammalian expression vector encoding TRE-$P_{NF\text{-}\kappa B2\text{-}STAT3}$-$P_{MIN}$-driven GV16-myc expression unit (TRE-$P_{NF\text{-}\kappa B2\text{-}STAT3}$-$P_{MIN}$-GV16-myc). NF-κB-STAT3 hybrid responsive element (sequence: GGGAATTTCCGGGGACTTTCCGGGAATTTCCGGGGACTTTCCGGGAATTTCCA ACGTTCATTTCCCGTAAATCGTCGAACGTTCATTTCCCGTAAATCGTCGAACGT TCATTTCCCGTAAATCGTCGAACGTTCATTTCCCGTAAATCGTCGAACGTTCAT TTCCCGTAAATCGTCGAACGTT) was cloned into the corresponding sites (NheI/BglII) of pAS60, replacing NF-κB2 responsive element.	This work
pAS133	Synthetic gen, encoding 2A-mouse IL-10-myc tag (mIL-10). Nucleotide sequence: GGCGCCGGAAGCGGAGAGGGGAGAGGAAGTCTTCTGACCTGCGGAGACGTCG AAGAGAATCCTGGACCCATGCCCGGCAGCGCCCTGCTGTGCTGCCTGCTGCTG CTGACAGGCATGAGGATCAGCAGGGGCCAGTACAGCAGGGAGGATAACAACT	This work

	GCACCCACTTCCCCGTGGGCCAAAGCCACATGCTGCTGGAACTGAGGACCGCC TTCTCCCAGGTGAAGACCTTCTTCCAGACCAAGGACCAGCTGGACAACATCCT GCTGACCGACAGCCTGATGCAGGACTTCAAGGGCTACCTGGGCTGCCAGGCCC TGAGCGAGATGATCCAGTTCTACCTGGTGGAGGTGATGCCCCAGGCTGAGAAG CACGGCCCCGAGATCAAGGAGCACCTGAACAGCCTGGGAGAGAAGCTGAAGA CCCTGAGGATGAGGCTGAGGAGATGCCACAGGTTCCTGCCCTGCGAGAACAA GTCCAAGGCCGTGGAGCAGGTGAAGAGCGACTTCAACAAGCTGCAGGACCAG GGCGTGTACAAGGCTATGAACGAGTTCGACATCTTCATCAACTGTATCGAGGC CTACATGATGATCAAGATGAAGAGCGAGCAGAAACTCATCTCTGAAGAGGAT CTGGCGCGCTAATTCTAGA. Amino acid sequence: GAGSGEGRGSLLTCGDVEENPGPMPGSALLCCLLLLTGMRISRGQYSREDNNCTH FPVGQSHMLLELRTAFSQVKTFFQTKDQLDNILLTDSLMQDFKGYLGCQALSEMI QFYLVEVMPQAEKHGPEIKEHLNSLGEKLKTLRMRLRRCHRFLPCENKSKAVEQV KSDFNKLQDQGVYKAMNEFDIFINCIEAYMMIKMKSEQKLISEEDLAR 2A peptide Mouse IL-10-myc tag	
pAS134	Mammalian expression vector encoding TRE-UAS-P_{MIN}-driven anti-hTNFα antibody-mIL-10-myc double effector expression unit (TRE-UAS-P_{MIN}-anti-hTNFα Ab-mIL-10; DE2). 2A-Mouse IL-10 was excised from pAS133 using (KasI/XbaI) and cloned into the corresponding sites of pAS115, replacing 2A-tagBFP. MGVKVLFALICIAVAEAEVQLVESGGGLVQPGRSLRLSCAASGFTFDDYAMHWV RQAPGKGLEWVSAITWNSGHIDYADSVEGRFTISRDNAKNSLYLQMNSLRAEDTA VYYCAKVSYLSTASSLDYWGQGTLVTVSSASTKGPSVFPLAPSSKSTSGGTAALG CLVKDYFPEPVTVSWNSGALTSGVHTFPAVLQSSGLYSLSSVVTVPSSSLGTQTYI CNVNHKPSNTKVDKKVEPKSCDKTHTCPPCPAPELLGGPSVFLFPPKPKDTLMISR TPEVTCVVVDVSHEDPEVKFNWYVDGVEVHNAKTKPREEQYNSTYRVVSVLTVL HQDWLNGKEYKCKVSNKALPAPIEKTISKAKGQPREPQVYTLPPSRDELTKNQVS LTCLVKGFYPSDIAVEWESNGQPENNYKTTPPVLDSDGSFFLYSKLTVDKSRWQQ GNVFSCSVMHEALHNHYTQKSLSLSPGKRAKRGSGEGRGSLLTCGDVEENPGPM GVKVLFALICIAVAEADIQMTQSPSSLSASVGDRVTITCRASQGIRNYLAWYQQKP GKAPKLLIYAASTLQSGVPSRFSGSGSGTDFTLTISSLQPEDVATYYCQRYNRAPYT FGQGTKVEIKTVAAPSVFIFPPSDEQLKSGTASVVCLLNNFYPREAKVQWKVDNA	This work

	LQSGNSQESVTEQDSKDSTYSLSSTLTLSKADYEKHKVYACEVTHQGLSSPVTKSF NRGECRAKRGAGSGEGRGSLLTCGDVEENPGPMPGSALLCCLLLLTGMRISRGQY SREDNNCTHFPVGQSHMLLELRTAFSQVKTFFQTKDQLDNILLTDSLMQDFKGYL GCQALSEMIQFYLVEVMPQAEKHGPEIKEHLNSLGEKLKTLRMRLRRCHRFLPCE NKSKAVEQVKSDFNKLQDQGVYKAMNEFDIFINCIEAYMMIKMKSEQKLISEEDL AR Gaussia luciferase signal peptide[11] anti-hTNFα Ab heavy chain variable region[12] RAKR motif for cleavage by furine hIg gamma-1 chain constant region 2A peptide anti-hTNFα Ab light chain variable region[12] Ig kappa chain constant region mIL-10-myc tag	

Supplementary Table 2. Amount of transfected plasmids used in different experiments

Experiment/type of plate	Plasmid (detailed description in Supplementary Table 1)	Amount (ng)
Fig. 2a left/CoStar White 96-well plates (Corning)	pAS49 phRL-TK pAS48	50 5 0/0.5/1/10
Fig. 2a middle/8-well tissue culture chambers (μ-Slide 8 well, Ibidi Integrated BioDiagnostics, Martinsried München, Germany)	pAS72 pA67 pAS58 pAS75 pmCherry-C1 pAS97	80 140 30 60 25 1.5
Fig. 2b left/CoStar White 96-well plates (Corning)	pAS49 phRL-TK pSGVP pAS53	50 5 1 0/0.5/1/10/50
Fig. 2b middle/8-well tissue culture chambers (μ-Slide 8 well, Ibidi Integrated BioDiagnostics, Martinsried München, Germany)	pAS72 pA67 pAS58 pAS75 pmCherry-C1 pAS98	80 140 30 60 25 0/20
Fig. 2c/CoStar White 96-well plates (Corning)	pAS51 phRL-TK pAS58 pAS60 pAS62	50 10 0/5 0/0.5/1/10 0/0.5/1/10
Fig. 3a/CoStar White 96-well plates (Corning)	pAS51 phRL-TK pAS58 pAS60 pAS62 pAS67	45 15 5 0.5 0.5 0/5/10/25/50/75/100

Fig. 3b and Supplementary Fig. 3a/CoStar White 96-well plates (Corning)	pAS72 pAS75 pAS67 pAS58 pAS60 pAS62	45 50 75 5 0.5 0/0.5
Fig. 4a/CoStar White 96-well plates (Corning)	pAS51 phRL-TK pAS67 pAS58 pAS60 pAS62	35 15 75 5 0.5 0.5
Fig. 4b, 4c and 4d/CoStar White 96-well plates (Corning)	pAS51 phRL-TK pAS67 pAS58 pAS60 pAS62	50 15 75 5 0.5 0.5
Fig. 4e The responsiveness of the synthetic anti-inflammatory device to an inflammatory signal *in vivo*/10 cm tissue culture petri dish (TPP)	pAS72 pAS75 pAS67 pAS58 pAS60 pAS62 or pcDNA3.1 (control group)	5000 2500 3000 600 30 20 11140
Fig. 4f The responsiveness of the synthetic anti-inflammatory device in a CLP model *in vivo*/10 cm tissue culture petri dish (TPP)	pAS72 pAS75 pAS67 pAS58 pAS60	6000 1000 3500 700 30

	pAS62	20
Fig. 5b Production of therapeutic anti-inflammatory proteins *in vitro* /10 cm tissue culture petri dish (TPP)	pAS116 or pAS134 pAS75 pAS67 pAS58 pAS60 pAS62	5000 2500 3500 700 30 20
Fig. 5c Production of therapeutic anti-inflammatory proteins *in vivo* /10 cm tissue culture petri dish (TPP)	pAS116 or pAS134 pAS75 pAS67 pAS58 pAS60 pAS62	8000 2500 3500 700 30 20
Fig. 5d, 6c-e and Supplementary Fig. 6c and d Production of therapeutic anti-inflammatory proteins *in vivo* and reversibility experiments with the anti-inflammatory proteins as an output *in vivo* /10 cm tissue culture petri dish (TPP)	pAS134 pAS75 pAS67 pAS58 pAS60 pAS62	8000 1000 3500 1000 35 20
Fig. 5e/6 wells tissue culture plate (TPP) for production cell line pr CoStar White 96-well plates for reporter cell line (Corning)	Production cell line: pAS35 or pAS114 Reporter cell line: pAS40 phRL-TK	 2000 50 5
Fig. 6a, Supplementary Fig. 6a and Supplementary Fig. 7a/10 cm tissue culture petri dish (TPP)	pAS72 pAS75 pAS67 pAS58 pAS60	5000 2500 3500 600 30

	pAS62	20
Fig. 6b Restraint *in vivo* and Supplementary Fig. 7c quantification of plasmid copy drop by real-time quantitative PCR/10 cm tissue culture petri dish (TPP)	pAS72 pAS75 pAS67 pAS58 pAS60 pAS62	5000 2500 3500 1000 30 20
Fig. 7a and Supplementary Fig. 5f, right Application of the anti-inflammatory device *in vivo* in acute murine colitis/10 cm tissue culture petri dish (TPP)	pAS134 or pcDNA3.1 (control group without an effector) pAS75 pAS67 pAS58 pAS60 pAS62	8000 2500 3500 700 30 20
Supplementary Fig. 1a/CoStar White 96-well plates (Corning)	pAS36 or pAS37 phRL-TK	100 5
Supplementary Fig. 1b/CoStar White 96-well plates (Corning)	pAS37 or pAS40 phRL-TK	100 5
Supplementary Fig. 1c left/CoStar White 96-well plates (Corning)	pAS51 phRL-TK pSGVP pAS58	50 10 20 0/5/20
Supplementary Fig. 1c middle/CoStar White 96-well plates (Corning)	pAS51 phRL-TK pAS58 pAS60 pAS62	50 10 5 1 1
Supplementary Fig. 1c right/CoStar White 96-well plates (Corning)	pAS51 phRL-TK pAS58 pSGVP pAS62	50 10 5 1 0/1

Supplementary Fig. 1d left/CoStar White 96-well plates (Corning)	pAS51 phRL-TK pAS58 pAS67 pAS97 or pAS60 (to compare to) pAS98 or pAS62 (to compare to) or pAS108 (as a constitutive control)	30 10 5 75 0.5 0.5 30
Supplementary Fig. 1d right/CoStar White 96-well plates (Corning)	pAS72 pAS75 pAS58 pAS67 pAS97 or pAS60 (to compare to) pAS98 or pAS62 (to compare to) or pAS109 (as a constitutive control)	40 30 5 75 0.5 0.5 40
Supplementary Fig. 3b/8-well tissue culture chambers (μ-Slide 8 well, Ibidi Integrated BioDiagnostics, Martinsried München, Germany)	pAS72 pA67 pAS58 pAS75 pmCherry-C1 pAS97 pAS98	80 140 30 60 25 1.5 2
Supplementary Fig. 3c/8-well tissue culture chambers (μ-Slide 8 well, Ibidi Integrated BioDiagnostics, Martinsried München, Germany)	pAS72 pA67 pAS58 pAS75 pmCherry-C1 pAS97	80 140 30 60 25 0/1.5

	pAS98	0/2
Supplementary Fig. 4e/CoStar White 96-well plates (Corning)	pAS51 phRL-TK pAS58 pAS67 pAS132 pAS62 pAS123	50 15 5 75 0.5 0.5 10
Supplementary Fig. 5/CoStar White 96-well plates (Corning)	Constitutive production: pAS35 pAS114 Inducible production: pAS60 pAS62 pAS58 pAS67 pAS63 or AS113 or pAS116	 50 50 0.5 0.5 5 75 50
Supplementary Fig. 5f, left Production of therapeutic anti-inflammatory proteins *in vitro* /10 cm tissue culture petri dish (TPP)	pAS113 pAS75 pAS67 pAS58 pAS60 pAS62	5000 2500 3500 700 25 20
Supplementary Fig. 5f Production of therapeutic anti-inflammatory proteins *in vitro* and *in vivo*/10 cm tissue culture petri dish (TPP)	pAS35	25000

MATHEMATICAL MODEL

Deterministic ODE model

To predict the responsiveness of the device to stimuli and determine the optimal transfection amounts, we constructed a simple deterministic model with ordinary differential equations (ODEs) using CellDesigner 4.4 software[13]. First we constructed a state transition diagram representing the genetic circuit (Supplementary Fig. 2). Next, we characterized the state transitions with the mass action kinetic law.

The formation of a complex between a transcription factor (TF) and its corresponding response element on DNA was expressed as:

$$\frac{d[TF\text{-}DNA]}{dt} = k_a \cdot [TF] \cdot [DNA] - k_d \cdot [TF\text{-}DNA]$$

where k_a represents the on-rate constant and k_d represents the off-rate constant.

For protein (P) production, we assumed first-order kinetics:

$$\frac{d[P]}{dt} = k_s \cdot [TF\text{-}DNA]$$

and

$$\frac{d[P]}{dt} = k_l \cdot [DNA]$$

The protein production rate constant is described with k_s. Parameter k_l corresponds to leaky protein production constant that represents the basal protein synthesis from transcribed genes under the control of an uninduced minimal promoter.

Proteins are degraded to amino acids (aa) according to the first order kinetics:

$$k_{deg} \cdot [P]$$

where k_{deg} corresponds to the protein degradation constant.

We also took into account the dilution of the device's genetic components due to cell division with dilution constant k_{dil}, which corresponds to the cell doubling time.

$$k_{dil} \cdot [DNA]$$

As protein turnover is faster than the typical cell doubling ($k_{dil} < k_{deg}$), we neglected the dilution of protein moieties.

Furthermore, we assumed the amount of amino acids remained constant over the course of simulation. Thus, the model species amino acids ("aa") served as a source and a sink for protein production and degradation, respectively. Conversely, the species "lost" represented a sink for the DNA constructs lost due to the dilution by cell division. These two model species were defined as boundary conditions in the CellDesigner state transition model (see Supplementary Table 3).

Simulations

The simulations were performed using the integrated SBML ODE Solver[14]. We were particularly interested in a behavior of the device in the two limiting cases: where there was no input signal (non-stimulated), i.e. the NF-κB protein complex particle number was set to zero, and where the input signal had maximal value (stimulated). The NF-κB particle number in simulations with stimulated genetic device was set to 24 000 by taking the mean nuclear NF-κB concentration of roughly 40 nM in persistently stimulated cells[15] and estimating the volume of a cell nucleus to be $1 \cdot 10^{-12}$ L.

$$N(NF\text{-}\kappa B) = c \cdot V \cdot N_A \approx 24\,000$$

The initial quantities of genetic constructs per individual cell were estimated by taking into account the efficiency of transient transfection with polyethylenimine (PEI) and the amount of DNA·PEI complexes that are successfully trafficked to the nucleus. We estimated that 90 % of the cells ($4 \cdot 10^4$ cells per well in a 96-well plate) receive the plasmids and that 0.07 % of the initial DNA quantity reach the nucleus[16,17].

$$N(DNA) = \frac{m(DNA) \cdot 7 \cdot 10^{-4}}{M(DNA) \cdot N(cells) \cdot 0.9} \cdot N_A$$

The time t = 0 in the simulations corresponds to the transfection of the cells with DNA constructs. In time course simulations, the particle number of NF-κB was held at 24 000 for the duration of stimulation (24 h post transfection to the end of the experiment at 48 h time point post transfection), similar to the experiments with cell cultures. In parameter scan experiments, the input signal for stimulated genetic device had maximal value for the duration of the simulation (24 h).

Supplementary Table 3. List of species included in the deterministic model exported from CellDesigner 4.4 software

Class	***id***	***Name***	***Initial quantity (particle number; N)***	***Boundary condition***	***Comment***
GENE	s1	sensor	2.2	false	The sensor construct (pAS60).
GENE	s19	amplifier	2.2	false	The amplifier construct (pAS62).
GENE	s28	effector	181.8	false	The luciferase effector construct (pAS51).
GENE	s15	repressor	8.1	false	The inducible OFF-switch construct (pAS58).
GENE	s29	thresholder	425.1	false	The "thresholder" construct (pAS67).
PROTEIN	s54	GV16	0.0	false	The Gal4-VP16 transcriptional activator.
PROTEIN	s11	rtTR-KRAB*	0.0	false	The doxycycline-induced active rtTR-KRAB transcriptional repressor.
PROTEIN	s45	NF-_kappa_B	0.0	false	The NF-κB represents the input signal for the device. In the non-stimulated setting, the initial quantity was 0. Conversely, in simulations of the induced genetic device, the initial quantity was set to 24 000 (estimated from ref.[15]).

PROTEIN	s57	EFFECTOR	0.0	false	In the model, the effector protein was set to be the firefly luciferase.
PROTEIN	s49	Gal4	0.0	false	The Gal4 regulatory protein from yeast.
PROTEIN	s8	rtTR-KRAB	0.0	false	The inactive rtTR-KRAB transcriptional repressor.
COMPLEX	s43	NF-_kappa_B RE-NF-_kappa_B (sensor)	0.0	false	NF-κB in complex with its corresponding response element in the sensor construct.
COMPLEX	s40	TRE-rtTR (sensor)	0.0	false	rtTR-KRAB in complex with its corresponding response element in the sensor construct.
COMPLEX	s39	TRE-rtTR_NF-_kappa_B RE-NF-_kappa_B (sensor)	0.0	false	NF-κB and rtTR-KRAB in complex with their corresponding response elements in the sensor construct.
COMPLEX	s32	UAS-Gal4 (effector)	0.0	false	Gal4 in complex with its corresponding response element in the effector construct.
COMPLEX	s34	UAS-GV16 (effector)	0.0	false	Gal4-VP16 in complex with its corresponding response element in the effector construct.
COMPLEX	s36	TRE-rtTR_UAS-Gal4 (effector)	0.0	false	Gal4 and rtTR-KRAB in complex with their corresponding response elements in the effector construct.
COMPLEX	s42	TRE-rtTR (effector)	0.0	false	rtTR-KRAB in complex with its corresponding response element in the effector construct.
COMPLEX	s38	TRE-rtTR_UAS-GV16 (effector)	0.0	false	Gal4-VP16 and rtTR-KRAB in complex with their

					corresponding response elements in the effector construct.
COMPLEX	s31	UAS-Gal4 (amplifier)	0.0	false	Gal4 in complex with its corresponding response element in the amplifier construct.
COMPLEX	s33	UAS-GV16 (amplifier)	0.0	false	Gal4 in complex with its corresponding response element in the amplifier construct.
COMPLEX	s35	TRE-rtTR_UAS-Gal4 (amplifier)	0.0	false	Gal4 and rtTR-KRAB in complex with their corresponding response elements in the amplifier construct.
COMPLEX	s41	TRE-rtTR (amplifier)	0.0	false	rtTR-KRAB in complex with its corresponding response element in the ampllifier construct.
COMPLEX	s37	TRE-rtTR_UAS-GV16 (amplifier)	0.0	false	Gal4-VP16 and rtTR-KRAB in complex with their corresponding response elements in the amplifier construct.
SIMPLE_MOLECULE	s58	Dox	0.0	true	Doxycycline (OFF-switch inducer) moiety.
DEGRADED	s30	aa	0.0	true	Amino acids (protein source and sink in the model).
DEGRADED	s16	lost	0.0	true	Lost DNA constructs due to dilution through cell division (sink in the model).

Supplementary Table 4. List of parameters included in the deterministic model exported from CellDesigner 4.4 software

id	*Name*	*Description*	*Value*	*Units*	*Comment*
ka_GV16	k_a^{GV16}	Gal4-VP16 - DNA on-rate binding constant.	$1.66 \cdot 10^{-6}$	$N^{-1} \cdot s^{-1}$	Value was calculated from $1 \cdot 10^6$ $M^{-1} \cdot s^{-1}$ (estimated from ref.[18]; $K_D \approx 10$ nM).
kd_GV16	k_d^{GV16}	Gal4-VP16 - DNA off-rate constant.	0.01	s^{-1}	Value was estimated from ref.[19].
k_l	k_l	Leaky protein production rate.	0.00125	s^{-1}	Estimated value represents 0.5 % of the maximal protein production rate.
k_deg	k_{deg}	Average protein degradation rate.	$2.79045 \cdot 10^{-5}$	s^{-1}	Value was calculated from estimated average protein half life in humans (6.9 h)[20].
ka_NFkB	$k_a^{NFκB}$	NF-κB - DNA on-rate binding constant.	$1.66 \cdot 10^{-6}$	$N^{-1} \cdot s^{-1}$	Value was calculated from $1 \cdot 10^{-6}$ $M^{-1} \cdot s^{-1}$[19].
kd_NFkB	$k_d^{NFκB}$	NF-κB - DNA off-rate constant.	0.01	s^{-1}	Value was estimated from ref.[18].
k_s	k_s	Protein production rate.	0.25	s^{-1}	Estimated.
k_dil	k_{dil}	Dilution rate.	$8.02254 \cdot 10^{-6}$	s^{-1}	Calculated from estimated cell generation time of 24 h.
k_dox	k^{dox}	Doxycycline – rtTR-KRAB association constant.	$1.66 \cdot 10^{-6}$	$N^{-1} \cdot s^{-1}$	Calculated from $1 \cdot 10^6$ $M^{-1} \cdot s^{-1}$ (estimated from ref.[21]).
ka_rtTR	k_a^{rtTR}	rtTR-KRAB - DNA on-rate binding constant.	$1.66 \cdot 10^{-6}$	$N^{-1} \cdot s^{-1}$	Estimated.
kd_rtTR	k_d^{rtTR}	rtTR-KRAB - DNA off-rate constant.	0.01	s^{-1}	Estimated.
k_deg_luc	k_{deg}^{luc}	Firefly luciferase degradation rate.	$9.62704 \cdot 10^{-5}$	s^{-1}	Value was calculated from luciferase half life in HEK 293T cells (2 h)[22].
k_deg_gal4	k_{deg}^{gal4}	Gal4 degradation rate.	$1.15525 \cdot 10^{-4}$	s^{-1}	Value was calculated from Gal4 half life in HeLa cells (100 min)[23].
k_deg_gv16	k_{deg}^{gv16}	Gal4-VP16 degradation rate.	$1.54033 \cdot 10^{-4}$	s^{-1}	Value was calculated from Gal4-VP16 half life in HeLa cells (75 min)[23].

Supplementary Table 5. List of reactions included in the deterministic model exported from CellDesigner 4.4 software

Type	*id*	*Reversible*	*Reaction*	*Trigger*	*Math*	*Comment*
HETERODIMER_ASSOCIATION	re1	true	$s45 + s1 \leftrightharpoons s43$		$\frac{d[s43]}{dt} = s45 \cdot s1 \cdot ka\_NFkB - s43 \cdot kd\_NFkB$	Binding and dissociation of NF-κB complex to its corresponding response element on the sensor construct.
STATE_TRANSITION	re2	false	$s30 \rightarrow s54$	s43	$\frac{d[s54]}{dt} = s43 \cdot k\_s$	Production of Gal4-VP16 from amino acids, triggered by NF-κB-induced transcription of the sensor construct expression unit.
STATE_TRANSITION	re3	false	$s30 \rightarrow s8$	s15	$\frac{d[s30]}{dt} = s15 \cdot k\_s$	Production of inactive rtTR-KRAB from amino acids, triggered by constitutive transcription from the repressor construct expression unit.
HETERODIMER_ASSOCIATION	re4	true	$s54 + s19 \rightleftharpoons s33$		$\frac{d[s33]}{dt} = s54 \cdot s19 \cdot ka\_GV16 - s33 \cdot kd\_GV16$	Binding and dissociation of Gal4-VP16 to its corresponding response

						element on the amplifier construct.
STATE_TRANSITION	re5	false	$s8 \rightarrow s30$		$\frac{d[s30]}{dt} = s8 \cdot k\_deg$	Inactive rtTR-KRAB degradation.
HETERODIMER_ASSOCIATION	re6	true	$s54 + s28 \rightleftharpoons s34$		$\frac{d[s34]}{dt} = s54 \cdot s28 \cdot ka\_GV16 - s34 \cdot kd\_GV16$	Binding and dissociation of Gal4-VP16 to its corresponding response element on the effector construct.
STATE_TRANSITION	re7	false	$s30 \rightarrow s57$	s34	$\frac{d[s57]}{dt} = s34 \cdot k\_s$	Production of luciferase reporter from amino acids, triggered by Gal4-VP16-induced transcription of the effector construct expression unit.
STATE_TRANSITION	re8	false	$s54 \rightarrow s30$		$\frac{d[s30]}{dt} = s54 \cdot k\_deg\_gv16$	Gal4-VP16 degradation to amino acids.
STATE_TRANSITION	re9	false	$s30 \rightarrow s49$	s29	$\frac{d[s49]}{dt} = s29 \cdot k\_s \cdot 0.01$	Production of Gal4 from amino acids, triggered by constitutive transcription from the “thresholder” construct

						expression unit. The production rate was set to 1 % of the estimated maximal protein production rate (k_s).
HETERODIMER_ASSOCIATION	re10	true	$s49 + s19 \rightleftharpoons s31$		$\frac{d[s31]}{dt} = s49 \cdot s19 \cdot ka\_GV16 - s31 \cdot kd\_GV16$	Binding and dissociation of Gal4 to its corresponding response element on the amplifier construct.
HETERODIMER_ASSOCIATION	re11	true	$s49 + s28 \rightleftharpoons s32$		$\frac{d[s32]}{dt} = s49 \cdot s28 \cdot ka\_GV16 - s32 \cdot kd\_GV16$	Binding and dissociation of Gal4 to its corresponding response element on the effector construct.
STATE_TRANSITION	re12	false	$s49 \rightarrow s30$		$\frac{d[s30]}{dt} = s49 \cdot k\_deg\_gal4$	Gal4 degradation to amino acids.
STATE_TRANSITION	re13	false	$s30 \rightarrow s54$	s1	$\frac{d[s54]}{dt} = s1 \cdot k\_l$	Production of Gal4-VP16 from amino acids, triggered by leaky transcription of the sensor construct expression unit.
STATE_TRANSITION	re14	false	$s30 \rightarrow s54$	s33	$\frac{d[s54]}{dt} = s33 \cdot k\_s$	Production of

						Gal4-VP16 from amino acids, triggered by Gal4-VP16-induced transcription of the amplifier construct expression unit.
STATE_TRANSITION	re15	false	s30 → s54	s19	$\frac{d[s54]}{dt} = s19 \cdot k\_l$	Production of Gal4-VP16 from amino acids, triggered by leaky transcription of the amplifier construct expression unit.
STATE_TRANSITION	re16	false	s30 → s57	s28	$\frac{d[s57]}{dt} = s28 \cdot k\_l$	Production of luciferase reporter from amino acids, triggered by leaky transcription of the effector construct expression unit.
STATE_TRANSITION	re17	false	s57 → s30		$\frac{d[s30]}{dt} = s57 \cdot k\_deg\_luc$	Luciferase reporter degradation to amino acids.
STATE_TRANSITION	re18	false	s30 → s54	s31	$\frac{d[s54]}{dt} = s31 \cdot k\_l \cdot 0.01$	Production of Gal4-VP16 from amino acids, triggered by leaky

						transcription of the Gal4-bound amplifier construct expression unit. The repressed leaky production rate was set to 1 % of the unrepressed leaky production rate.
STATE_TRANSITION	re19	false	s30 → s57	s32	$\frac{d[s57]}{dt} = s32 \cdot k\_l \cdot 0.01$	Production of luciferase effector from amino acids, triggered by leaky transcription of the Gal4-bound effector construct expression unit. The repressed leaky production rate was set to 1 % of the unrepressed leaky production rate.
STATE_TRANSITION	re20	false	s1 → s16		$\frac{d[s16]}{dt} = s1 \cdot k\_dil$	Dilution of the sensor construct due to cell division.
STATE_TRANSITION	re21	false	s29 → s16		$\frac{d[s16]}{dt} = s29 \cdot k\_dil$	Dilution of the “thresholder” construct due to

						cell division.
STATE_TRANSITION	re22	false	$s15 \rightarrow s16$		$\frac{d[s16]}{dt} = s15 \cdot k\_dil$	Dilution of the repressor construct due to cell division.
STATE_TRANSITION	re23	false	$s19 \rightarrow s16$		$\frac{d[s16]}{dt} = s19 \cdot k\_dil$	Dilution of the amplifier construct due to cell division.
STATE_TRANSITION	re24	false	$s28 \rightarrow s16$		$\frac{d[s16]}{dt} = s28 \cdot k\_dil$	Dilution of the effector construct due to cell division.
STATE_TRANSITION	re25	false	$s8 \rightarrow s11$	s58	$\frac{d[s11]}{dt} = s8 \cdot s58 \cdot k\_dox$	Binding of doxycycline to an inactive rtTR-KRAB, producing an active rtTR-KRAB.
HETERODIMER_ASSOCIATION	re26	true	$s11 + s34 \rightleftharpoons s38$		$\frac{d[s38]}{dt} = s11 \cdot s34 \cdot ka\_rtTR - s38 \cdot kd\_rtTR$	Binding and dissociation of rtTR-KRAB to its corresponding response element on the Gal4-VP16-bound effector construct.
HETERODIMER_ASSOCIATION	re27	true	$s11 + s28 \rightleftharpoons s42$		$\frac{d[s42]}{dt} = s11 \cdot s28 \cdot ka\_rtTR - s42 \cdot kd\_rtTR$	Binding and dissociation of rtTR-KRAB to its corresponding response element on the

						effector construct.
HETERODIMER_ASSOCIATION	re28	true	$s11 + s32 \rightleftharpoons s36$		$\frac{d[s36]}{dt} = s11 \cdot s32 \cdot ka\_rtTR - s36 \cdot kd\_rtTR$	Binding and dissociation of rtTR-KRAB to its corresponding response element on the Gal4-bound effector construct.
HETERODIMER_ASSOCIATION	re29	true	$s11 + s33 \rightleftharpoons s37$		$\frac{d[s37]}{dt} = s11 \cdot s33 \cdot ka\_rtTR - s37 \cdot kd\_rtTR$	Binding and dissociation of rtTR-KRAB to its corresponding response element on the Gal4-VP16-bound amplifier construct.
HETERODIMER_ASSOCIATION	re30	true	$s11 + s19 \rightleftharpoons s41$		$\frac{d[s41]}{dt} = s11 \cdot s19 \cdot ka\_rtTR - s41 \cdot kd\_rtTR$	Binding and dissociation of rtTR-KRAB to its corresponding response element on the amplifier construct.
HETERODIMER_ASSOCIATION	re31	true	$s11 + s31 \rightleftharpoons s35$		$\frac{d[s35]}{dt} = s11 \cdot s31 \cdot ka\_rtTR - s35 \cdot kd\_rtTR$	Binding and dissociation of rtTR-KRAB to its corresponding response

						element on the Gal4-bound amplifier construct.
HETERODIMER_ASSOCIATION	re32	true	$s11 + s1 \rightleftharpoons s40$		$\frac{d[s40]}{dt} = s11 \cdot s1 \cdot ka\_rtTR - s40 \cdot kd\_rtTR$	Binding and dissociation of rtTR-KRAB to its corresponding response element on the sensor construct.
HETERODIMER_ASSOCIATION	re33	true	$s11 + s43 \rightleftharpoons s39$		$\frac{d[s39]}{dt} = s11 \cdot s43 \cdot ka\_rtTR - s39 \cdot kd\_rtTR$	Binding and dissociation of rtTR-KRAB to its corresponding response element on the NF-κB-bound sensor construct.
STATE_TRANSITION	re34	false	$s43 \rightarrow s16$		$\frac{d[s16]}{dt} = s43 \cdot k\_dil$	Dilution of the NF-κB-bound sensor construct due to cell division.
STATE_TRANSITION	re35	false	$s40 \rightarrow s16$		$\frac{d[s16]}{dt} = s40 \cdot k\_dil$	Dilution of the rtTR-KRAB-bound sensor construct due to cell division.
STATE_TRANSITION	re36	false	$s39 \rightarrow s16$		$\frac{d[s16]}{dt} = s39 \cdot k\_dil$	Dilution of the NF-κB and rtTR-KRAB-bound sensor construct due to cell division.

STATE_TRANSITION	re39	false	$s31 \rightarrow s16$		$\frac{d[s16]}{dt} = s31 \cdot k\_dil$	Dilution of the Gal4-bound amplifier construct due to cell division.
STATE_TRANSITION	re40	false	$s33 \rightarrow s16$		$\frac{d[s16]}{dt} = s33 \cdot k\_dil$	Dilution of the Gal4-VP16-bound amplifier construct due to cell division.
STATE_TRANSITION	re42	false	$s11 \rightarrow s30$		$\frac{d[s30]}{dt} = s11 \cdot k\_deg$	Active rtTR-KRAB degradation.
STATE_TRANSITION	re44	false	$s35 \rightarrow s16$		$\frac{d[s16]}{dt} = s35 \cdot k\_dil$	Dilution of the Gal4 and rtTR-KRAB-bound amplifier construct due to cell division.
STATE_TRANSITION	re45	false	$s41 \rightarrow s16$		$\frac{d[s16]}{dt} = s41 \cdot k\_dil$	Dilution of the rtTR-KRAB-bound amplifier construct due to cell division.
STATE_TRANSITION	re46	false	$s37 \rightarrow s16$		$\frac{d[s16]}{dt} = s37 \cdot k\_dil$	Dilution of the Gal4-VP16 and rtTR-KRAB-bound amplifier construct due to cell division.
STATE_TRANSITION	re47	false	$s32 \rightarrow s16$		$\frac{d[s16]}{dt} = s32 \cdot k\_dil$	Dilution of the Gal4-bound effector construct due to cell division.
STATE_TRANSITION	re48	false	$s34 \rightarrow s16$		$\frac{d[s16]}{dt} = s34 \cdot k\_dil$	Dilution of the Gal4-VP16-

						bound amplifier construct due to cell division.
STATE_TRANSITION	re49	false	s36 → s16		$\frac{d[s16]}{dt} = s36 \cdot k\_dil$	Dilution of the Gal4 and rtTR-KRAB-bound effector construct due to cell division.
STATE_TRANSITION	re50	false	s42 → s16		$\frac{d[s16]}{dt} = s42 \cdot k\_dil$	Dilution of the rtTR-KRAB-bound effector construct due to cell division.
STATE_TRANSITION	re51	false	s38 → s16		$\frac{d[s16]}{dt} = s38 \cdot k\_dil$	Dilution of the Gal4-VP16 and rtTR-KRAB-bound effector construct due to cell division.

SUPPLEMENTARY REFERENCES

1. King, GA, Daugulis, AJ, Faulkner, P and Goosen, MFA. (1987). Alginate-Polylysine Microcapsules of Controlled Membrane Molecular Weight Cutoff for Mammalian Cell Culture Engineering. *Biotechnol. Prog.* **3**: 231–240.
2. Dubrot, J, Portero, A, Orive, G, Hernández, RM, Palazón, A, Rouzaut, A, *et al.* (2010). Delivery of immunostimulatory monoclonal antibodies by encapsulated hybridoma cells. *Cancer Immunol. Immunother.* **59**: 1621–1631.
3. Wirtz, S, Neufert, C, Weigmann, B and Neurath, MF (2007). Chemically induced mouse models of intestinal inflammation. *Nat. Protoc.* **2**: 541–546.
4. Fussenegger, M, Morris, RP, Fux, C, Rimann, M, von Stockar, B, Thompson, CJ, *et al.* (2000). Streptogramin-based gene regulation systems for mammalian cells. *Nat. Biotechnol.* **18**: 1203–1208.
5. Sadowski, I, Ma, J, Triezenberg, S and Ptashne, M (1988). GAL4-VP16 unusualy potent transcription activator. *Nature* **335**: 563–564.
6. Szulc, J, Wiznerowicz, M, Sauvain, M, Trono, D and Aebischer, P (2006). A versatile tool for conditional gene expression and knockdown. *Nat. Methods* **3**.
7. Fussenegger, M, Mazur, X and Bailey, JE (1997). A Novel Cytostatic Process Enhances the Ovary Cells. *Biotechnol Bioeng*. **20**:927-939.
8. Lebar, T, Straz, M, Bezeljak, U, Golob, A, Jerala, M, Kadunc, L, *et al.* (2014). A bistable genetic switch based on designable DNA-binding domains. **29**: 5007
9. Gibson, DG, Young, L, Chuang, R-Y, Venter, JC, Hutchison, CA and Smith, HO (2009). Enzymatic assembly of DNA molecules up to several hundred kilobases. *Nat. Methods* **6**: 343–345.
10. Kim, JH, Lee, SR, Li, LH, Park, HJ, Park, JH, Lee, KY, *et al.* (2011). High cleavage efficiency of a 2A peptide derived from porcine teschovirus-1 in human cell lines, zebrafish and mice. *PLoS One* **6**: 1–8.
11. Stern, B, Olsen, LC, Tröße, C, Ravneberg, H and Pryme, IF (2007). Improving mammalian cell factories : The selection of signal peptide has a major impact on recombinant protein synthesis and secretion in mammalian cells. *Trends Cell Mol. Biol.* **2**: 1–17.
12. Abbott Biotechnology Ltd. Human antibodies that bind human TNFα. US Patent 6,090,382 filed 9 Feb. 1996, and issued 18 Jul. 2000.
13. Funahashi, A, Morohashi, M, Kitano, H and Tanimura, N (2003). CellDesigner: a process diagram editor for gene-regulatory and biochemical networks. *Biosilico* **1**: 159–162.
14. Machné, R, Finney, A, Müller, S, Lu, J, Widder, S and Flamm, C (2006). The SBML ODE Solver Library: A native API for symbolic and fast numerical analysis of reaction networks. *Bioinformatics* **22**: 1406–1407.
15. Hoffmann, A, Levchenko, A, Scott, ML and Baltimore, D (2002). The IkappaB-NF-kappaB signaling module: temporal control and selective gene activation. *Science* **298**: 1241–1245.
16. Kichler, A, Leborgne, C, Coeytaux, E and Danos, O (2001). Polyethylenimine-mediated gene delivery: A mechanistic study. *J. Gene Med.* **3**: 135–144.

17. Pollard, H, Remy, JS, Loussouarn, G, Demolombe, S, Behr, JP and Escande, D (1998). Polyethylenimine but not cationic lipids promotes transgene delivery to the nucleus in mammalian cells. *J. Biol. Chem.* **273**: 7507–7511.

18. Hong, M, Fitzgerald, MX, Harper, S, Luo, C, Speicher, DW and Marmorstein, R (2008). Structural Basis for Dimerization in DNA Recognition by Gal4. *Structure* **16**: 1019–1026.

19. Bergqvist, S, Alverdi, V, Mengel, B, Hoffmann, A, Ghosh, G and Komives, E a (2009). Kinetic enhancement of NF-kB - DNA dissociation by IkBa. **2009**: 1–6.

20. Eden, E, Geva-Zatorsky, N, Issaeva, I, Cohen, A, Dekel, E, Danon, T, *et al.* (2011). Proteome half-life dynamics in living human cells. *Science* **331**: 764–768.

21. Sotiropoulos, V and Kaznessis, YN (2007). Synthetic tetracycline-inducible regulatory networks: computer-aided design of dynamic phenotypes. *BMC Syst. Biol.* **1**: 7.

22. Ignowski, JM and Schaffer, D V. (2004). Kinetic analysis and modeling of firefly luciferase as a quantitative reporter gene in live mammalian cells. *Biotechnol. Bioeng.* **86**: 827–834.

23. Salghetti, SE, Muratani, M, Wijnen, H, Futcher, B and Tansey, WP (2000). Functional overlap of sequences that activate transcription and signal ubiquitin-mediated proteolysis. *Proc. Natl. Acad. Sci. U. S. A.* **97**: 3118–3123.